PEG-DERIVATIZED FTS-BASED MICELLES FOR COMBINATION CANCER THERAPY

by

Xiaolan Zhang

B. Eng. in Pharmaceutical Engineering, Wuhan Institute of Technology, 2008

M. Eng. in Chemical Technology, Wuhan University of Technology, 2011

Submitted to the Graduate Faculty of

School of Pharmacy in partial fulfillment

of the requirements for the degree of

Doctor of Philosophy

University of Pittsburgh

2016

UNIVERSITY OF PITTSBURGH

SCHOOL OF PHARMACY

This dissertation was presented

by

Xiaolan Zhang

It was defended on

March 29, 2016

and approved by

Paul A. Johnston, Ph.D., Research Associate Professor
Department of Pharmaceutical Sciences, School of Pharmacy University of Pittsburgh

Raman Venkataramanan, Ph.D., Professor
Director of the Clinical Pharmacokinetics Laboratory, Department of Pharmaceutical Sciences, School of Pharmacy
Director of Therapy Drug Monitoring, Department of Pathology, School of Medicine
University of Pittsburgh

Xiaochao Ma, Ph.D., Associate Professor
Center for Pharmacogenetics, Department of Pharmaceutical Sciences, School of Pharmacy
University of Pittsburgh

Lin Zhang, Ph.D., Professor
Department of Pharmacology and Chemical Biology, University of Pittsburgh

Dissertation Advisor: **Song Li**, M.D., Ph.D., Professor
Center for Pharmacogenetics, Department of Pharmaceutical Sciences, School of Pharmacy
University of Pittsburgh Cancer Institute
University of Pittsburgh

PEG-DERIVATIZED FTS-BASED MICELLES FOR COMBINATION CANCER THERAPY

Xiaolan Zhang, Ph.D.

University of Pittsburgh, 2016

Polymeric micelles represent a promising drug carrier system that has gained considerable attention due to its simplicity, small sizes, and ability to solubilize water-insoluble drugs and accumulate specifically in the tumors. However, most of them do not possess any biological activity by themselves. One interesting approach in the design of a carrier is to incorporate components in the carrier system itself that exhibit favorable biological activity, either counteracting the side effects caused by the loaded anticancer drugs, or promoting synergistic effect with the incorporated drug.

We first developed a dual function carrier that is based on PEG-derivatized S-trans, trans-farnesylthiosalicylic acid (FTS) (PEG_{5k}-FTS_2). FTS is a synthetic farnesylcysteine mimetic that acts as a potent and especially nontoxic Ras antagonist. In addition to retention of anti-Ras activity, PEG_{5k}-FTS_2 forms small-sized micelles that are capable of synergistic delivery of various hydrophobic agents. A further structure activity relationship (SAR) study was conducted in four PEG-FTS conjugates that vary in the molecular weight of PEG (PEG_{2K} vs PEG_{5K}) and the molar ratio of PEG/FTS (1/2 vs 1/4). We demonstrated that PEG_{5k}-FTS_4 formed the most stable mixed micelles with PTX among the four PEG-FTS conjugates.

Next, we examined whether the performance of PEG_{5k}-FTS_2 can be further improved via incorporation of Fmoc, based on our recent discovery of Fmoc as a novel and potent drug-interactive motif. Our data showed that introduction of an Fmoc at the interfacial region of

PEG_{5k}-FTS_2 led to a significant improvement in the drug loading capacity for a number of anticancer agents including paclitaxel (PTX), doxorubicin (DOX), curcumin, and etoposide. Finally, we established a reduction-sensitive delivery system by incorporation of an additional cleavable linkage (disulfide bond) into PEG_{5k}-FTS_2. We demonstrated that the incorporation of a disulfide linkage led to an enhanced release of FTS inside tumor cells, which was associated with an improved cytotoxicity against tumor cells.

In summary, our data demonstrated that PEG-derivatized FTS can serve as dual functional carrier for the targeted delivery of therapeutic agents and contribute additional effects with the loaded anticancer drug. Our improved dual function carrier represents a simple and effective targeted drug delivery system for cancer.

TABLE OF CONTENTS

LIST OF TABLES

LIST OF FIGURES

PREFACE

This Ph.D. dissertation described herein is comprised of the research undertaken at the Center for Pharmacogenetics, Department of Pharmaceutical Sciences, in University of Pittsburgh under the supervision of my mentor, Dr. Song Li.

I would like to thank the people who made this achievement possible. The most important person that I must acknowledge is my advisor Dr. Song Li for his extremely valuable guidance and endless support in the completion of this dissertation. I have been very fortunate to join his lab and work under his supervision. Truly, Dr. Li has been an incredible advisor, dedicated scientist and very professional mentor who cares about his students in both scientific and personal levels. It is his enormous direction and unconditional support that made me where I am today.

I would like to extend my gratitude to my committee members, Dr. Paul A. Johnston, Dr. Raman Venkataramanan, Dr. Xiaochao Ma, Dr. Lin Zhang, for their valuable suggestions and comments along the way. A special thank goes to Dr. Jiang Li for always being happy to share his profound knowledge in biology, and also for providing valuable advices when something that upsets me. Many thanks to Dr. Xiang Gao for teaching me how to make my first ever micellar formulation; to Dr. Yixian Huang for his direction on the organic chemistry synthesis; and other labmates (Yifei Zhang, Mohammed Ghazwani, Jianqin Lu, Peng Zhang, Jilong Li, Yichao Chen,

Jieni Xu, Yuan Wei, Min Zhao, Tianqun Lang, Yifei He, Yukun Huang, Jingjing Sun, Qiongfeng Liao, Lei Liang, Yanhua Liu, Zuojun Li, Qianyu Zhai). Without their company, the research would be much less enjoyable.

I would like to express my appreciation to the Center for Pharmacogenetics and the School of Pharmacy at the University of Pittsburgh. Specially, to Dr. Barry Gold, Dr. Xie Wen, Dr. Yang Da, Dr. Robert B Gibbs, Dr. Maggie Folan, Lori Schmotzer and William C. Smith for their endless support and help all these years.

This dissertation is dedicated to my father Jianping Zhang, and my mother Ruihua Sui for their endless love and support. I also dedicate this success to my dear and loving husband Xiaoke Huang. His company made my journey much more enjoyable.

1.0 INTRODUCTION

1.1 NANOMEDICINE IN CANCER THERAPY

Cancer is the leading cause of death in U.S., accounting for nearly 1 out of every 4 deaths. There were an estimated 14.1 million new global cancer incidences in 2012. This number is expected to increase to as many as 24 million within the next two decades [1]. Chemotherapy is a major therapeutic approach for the treatment of various types of cancers [2]. Nevertheless, clinical application of anticancer drugs is beleaguered by problems such as poor water solubility, short-term physical stability, non-specificity, and high toxicity. First, administration of poorly water soluble drugs results in poor absorption and low bioavailability [3]. Second, the aggregation of water insoluble drugs could cause local toxicity. Third, anticancer drugs are usually small molecule drugs and are rapidly eliminated by liver and kidneys. Furthermore, nonspecific permeation into the entire body will lead to serious systemic toxicity. Currently, Cremophor EL/ethanol (1:1, v/v) and certain surfactants are used to improve the aqueous solubility of anticancer drugs [4]. However, Cremophor EL can cause hypersensitivity reactions, neuropathy, and other serious side effects. In addition, the utility of some commonly used surfactants is limited by their high critical micelle concentrations (CMCs), which raises the concern of drug precipitation or burst release of drug upon dilution in the blood [5]. The advent of nanotechnology brings promising alternatives in delivery of anticancer drugs [6]. A number of

macromolecular delivery systems such as polymeric micelles, liposomes, dendrimers and nanoparticles are under investigation to circumvent the limitations of current chemotherapies and improve the potential of the anticancer drugs [7]. These vehicles can carry various types of drugs, protect them from degradation, and prevent undesirable side effect on normal cells. Among the many studied delivery systems, polymeric micelles have gained considerable attention owing to their ease in preparation, small size (10-100 nm), and the ability to solubilize water-insoluble anticancer drugs and accumulate specifically at the targeted sites [8]. Currently, several polymeric micelles incorporated with anticancer agents, NK012, NK105, NK911, NC-6004, SP1049C and Genexol-PM are under clinical evaluation [9], of which Genexol-PM has been approved by FDA for use in patients with breast cancer [10].

1.2 POLYMERIC MICELLES DELIVERY SYSTEM IN ONCOLOGY

1.2.1 Polymeric micelle system

Polymeric micelles usually have the unique core-shell architecture composed of distinct hydrophilic and hydrophobic domains, with the structure of the copolymer usually being a di-block, tri-block, or graft copolymer [5]. The hydrophobic core provides a loading space for poorly water-soluble drugs and the hydrophilic shell allows polymeric micelle gain the stability in aqueous environment [11]. The hydrophobic block should have good biodegradability and provide excellent compatibility with the loaded drugs. Most commonly used polymers for hydrophobic core formation are polyesters and polyamides. The polyesters used include polycaprolactone (PCL), poly(lactic acid) (PLA), poly(glycolic acid) (PGA), and poly(lactide-

co-glycolide) (PLGA), all of which have been approved by the FDA for use in various clinical conditions [12-14]. Polyamides used include poly(L-histidine) (pHis), poly(L-aspartic acid) derivatives (pAsp) and poly(L-glutamic acid) derivatives (pGlu). These biocompatible polyesters and polyamides display gradual degradation kinetics inside the body with the degradation time ranging from days to weeks. Polymeric micelles generally possesse a very low CMC, ranging between 10^{-6}-10^{-7} M, which is 1,000 times lower than those of low molecular weight surfactants. The stability (CMC) of polymeric micelles varies depending on the type and molecular weight of the hydrophobic block. Generally, the higher the molecular weight of a hydrophobic block is, the lower the CMC of the polymer will be.

One unique type of polymeric micelles composed of cholic acid (CA) dendrimers as the hydrophobic block and poly (ethylene glycol) (PEG) as the hydrophilic domain have been developed by Lam's group [15-17]. One such amphiphilic linear-dendritic copolymer PEG5K-CA8 was composed of PEG, CA and lysine. They prepared paclitaxel (PTX) loaded PEG5K-CA8 micelles with a tunable size of 20-60 nm. The most impressive properties of these micelles were excellent PTX loading capacity (35%, w/w of drug polymer ratio) and superior stability (longer than six months). This is due to the planar structure and the facial amphiphilicity of CA and the dendritic configuration of the hydrophobic core. These PTX loaded PEG-CA micelles showed preferential tumor accumulation and superior toxicity profiles and antitumor effects compared to Taxol (paclitaxel dissolved in Cremophor EL/ethanol (1:1, v/v) mixture) and Abraxane (Albumin-bound paclitaxel) that are two FDA approved formulations. [15]. This system has also been successfully applied to the delivery of doxorubicin (DOX) to tumor [18].

Lipid-core micellar systems are another special type of polymeric micelles composed of lipid moieties as a hydrophobic block capped with a hydrophilic segment such as PEG. One

unique feature of lipid-core micelles is that they can be readily developed. In addition, the lipid-core micelles have a relatively low CMC and demonstrate better stability compared to some commonly used lipid surfactants. Torchilin's group first developed one such micellar system that is based on a PEG-phosphatidylethanolamine (PE) conjugate [19, 20]. These PEG-PE micelles had a CMC value that was at least a 100-fold lower than conventional surfactants. The presence of two fatty acyls contributes to an enhanced interaction between the lipid chains in the micelle core, which contributes to the high stability of drugs [19]. This system has been used for delivery of several hydrophobic drugs such as PTX, and camptothecin [20].

Most micellar systems utilize PEG as the hydrophilic segment of the micelles. PEG is not biodegradable and does not form toxic metabolites. At the same time, PEG is commercially available in a variety of molecular weights from 1,000 to 20,000 Da. A prominent advantage of PEG modification is to impart *in vivo* longevity to drug carriers. First, PEG can reduce unwanted aggregation due to secondary interactions between polymeric particles. Second, the surface modification of a polymeric carrier with PEG can reduce the binding of plasma proteins and minimize nonspecific uptake by the reticuloendothelial system (RES), allowing the carrier to circulate in the blood for a long period of time. For example, amphiphilic diblock copolymers of PEG-b-poly(D,L-lactide–co-glycolide) (PEG-b-PLGA) showed prolonged blood circulation times compared to the conventional PLGA nanoparticles [14]. In addition to PEG, several other biocompatible hydrophilic polymers have been developed as steric protectors, such as poly (acryloyl morpholine) (PAM), phosphatidyl polyglycerols and polyvinyl alcohol (PVA). PAM is a non-ionic hydrophilic polymer with similar properties to PEG, which has good polymerization efficiency, low toxicity and minimal immunological reactions *in vivo* [21]. PAM-modified

liposomes showed prolonged circulation *in vivo* [22]. Similarly, phosphatidyl polyglycerols or PVA coated liposomes showed prolonged circulating time *in vivo* [23].

1.2.2 Passive and active targeting via micellar system

Targeted delivery of anticancer agents to tumor tissues not only increases the therapeutic effect of the drugs, but also reduces the toxic effects on normal tissue [24]. It is well known that tumor blood vessels have a high proportion of proliferating endothelial cells and that capillaries of tumor blood vessels become much more permeable than the capillaries of normal tissues [25]. In addition, tumor tissues generally have a defective lymphatic drainage system, leading to enhanced accumulation and retention of the macromolecules in tumors [26]. Therefore, given the long circulation times in blood, macromolecules and particles ranging from 10 to 500 nm are preferentially and passively accumulated at tumor and inflammatory tissues [27]. Since the passive targeting phenomenon was first discovered by Maeda et al. [28], numerous studies have substantiated that a nanocarrier with the size of 20-100 nm preferentially extravasates into solid tumor tissues owing to the leaky tumor vasculature [29, 30]. Besides, the effect of size on the biodistribution of polymeric micelles is organ- and tumor-type-dependent [31]. A recent study from Lam's group compared the passive targeting of nanoparticles of different sizes in a subcutaneous model of human ovarian cancer xenograft. It was shown that particles with a size of 154 nm were significantly taken up by liver and lungs with limited accumulation at tumor sites. In contrast, particles of 17 and 64 nm were much more effective in passive targeting to the solid tumor [17]. Cabral and colleagues compared the targeting efficiency of polymeric micelles of different sizes (30, 50, 70, and 100 nm) in both highly and poorly permeable tumors. While all of the tested polymeric micelles penetrated highly permeable tumors in mice, only the 30 nm

micelles could penetrate poorly permeable pancreatic tumors to achieve an antitumor effect [32]. Thus, size optimization of polymeric micelles is one of the keys to successful passive targeting to different types of tumors [33].

The further development of the targeted polymeric micelles involves attempting to add an active targeting moiety capable of recognizing receptors on the tumors, which will facilitate the specific interaction with the tumor cells and the subsequent intracellular delivery. Various types of ligands have been examined for active targeting including antibody, peptide, and small molecule ligands [34, 35]. Antibodies have been widely applied in terms of diversity of targets and specificity of interaction [35]. The accumulation of PEG-PE micelles can be enhanced in tumors through modification with anti-nucleosome monoclonal antibody 2C5 [36]. The use of small molecule ligands has the advantages of low cost and minimal immunogenicity. Folate receptor has been shown to be overexpressed in various types of cancers and folate-decorated delivery systems have been widely used for targeted delivery of various types of therapeutics to cancers [37]. Small molecules specific for prostate-specific membrane antigen (PSMA) is another promising ligand for active targeting of prostate cancers that overexpress PSMA [38]. Recently, there also has been an interest in exploring sigma receptor ligands for tumor imaging and targeted therapy. Sigma receptors are overexpressed in a variety of human tumors including non-small cell lung carcinoma (NSCLC), prostate cancer, melanoma, and breast cancer [39]. OA02-peptide was also used to prepare paclitaxel-loaded micelle targeted to α-3 integrin receptor to improve specific tumor-targeting to ovarian cancer cells [40]. Another interesting approach involves simultaneous incorporation of dual ligands into a nanomicellar system. It is reported that incorporation of dual ligands can enhance targeting efficiency and cytotoxicity *in vitro* and *in vivo* to A2780 ovarian carcinoma compared to single ligand-targeted micelles [41].

1.2.3 Environmentally responsive micellar system

In addition to targeted delivery, another important consideration in the design of an optimal delivery system is controlled or triggered drug release upon reaching the tumor tissues or intracellular delivery to tumor cells. Ideally, polymeric micelles should be designed such that they are stable in the circulation or in normal tissues, but, able to disintegrate and release the entrapped drugs in selective areas with unique environments such as in tumors and sites of inflammation. Tumors and inflammation sites usually exhibit mildly acidic pH. Acid-cleavable links such as acetal [42], orthoesters [43] and hydrazones [44] are stable at pH around 7.5 but are hydrolyzed rapidly at pH values of 6 and below [45]. Thus, pH-sensitive polymeric micelles with acid-labile linkages are prone to disintegration and release of loaded drugs at the tumor sites [46]. For example, Kataoka's group reported that anticancer drugs, adriamycin (ADR), conjugated to the core forming block through a pH-sensitive hydrazone bond and the micelles released ADR both time- and pH-dependently as the pH value decreased from pH 7.4 to 3.0 [47]. Another interesting example of pH-sensitive micelle was shown by Bae's group. They demonstrated that the cationic micelle was shielded by pH-sensitive anionic block copolymer to endow stability of micelle at pH 7.4. After the endocytosis of the micelle, the core was protonated in the acidic environment, which led to dissociation of the micelle and enhanced the delivery of drugs to the cytosol [48]. Redox-potential is another significant difference between the extra- and intra-cellular environments. It has been found that the disulfide bond linkages, though sufficiently stable in low glutathione (GSH) concentrations (2-20 μM) in the body, show a rapid cleavage (over a time scale of a minutes to hours) under the reducing conditions of high intracellular GSH concentrations of 0.5-10mM [49]. Generally, the concentration of GSH in tumor tissues is several times higher than those of normal tissues. As a result, polymers containing disulfide

bonds show unique advantages of reduction-sensitive cleavage in the intracellular tumor environment via thiol-disulfide exchange reactions. The disulfide linkages in these reducible polymers are located in the main or side chains, and act as cross-linkers [50]. Other environmentally responsive systems such as temperature-sensitive, magnet-sensitive and ultrasound-sensitive system have also attracted increased attention recently.

1.2.4 PEG-derivatized FTS-based dual functional micellar system

S-trans, trans-farnesylthiosalicylic acid (FTS) is a synthetic farnesylcysteine mimetic that acts as a potent and especially nontoxic Ras antagonist [51]. Constitutively active Ras caused by mutation in the Ras family of proto-oncogenes is present in one-third of human cancers, with the highest incidence of mutational activation of Ras being detected in pancreatic (90%) and colon (50%) cancers [52]. Ras is also activated in cancer cells by other mechanisms. In particular, hyper activation of the epidermal growth factor receptor (EGFR) tyrosine kinase activity causes persistent activation of Ras and Ras-mediated signaling [53]. The activated form of Ras constitutively activates its downstream effectors, contributing to cell transformation [54]. FTS can inhibit both oncogenically activated Ras and growth factor receptor-mediated Ras activation, resulting in the inhibition of Ras-dependent tumor growth [55]. FTS can inhibit Ras transforming activity and reverse the transformed phenotype of Ras-transformed fibroblasts [56]. FTS has demonstrated significant reduction of Ras levels in a wide array of established cancer models and inhibition of tumor growth in animals with no adverse toxicity [57]. One major mechanism involves disrupting Ras membrane interactions by competing with Ras for binding to Ras-escort proteins, facilitating its degradation, and thus disrupting Ras protein signaling in the plasma membrane [58].

The major application of FTS in cancer treatment is in combination with other drugs of different mechanisms of action [59, 60]. The combined treatment of FTS and gemcitabine showed synergistic effects in inhibiting the growth of Panc-1 tumors, resulting in 81% reduction in tumor volume, which compared favorably to the individual drug treatments. In a clinical study, the combination of gemcitabine and FTS appeared to be well tolerated and exerted clinical and pharmacodynamics (PD) activity in pancreatic adenocarcinoma (PDA) [59]. The combination of FTS and a glycolysis inhibitor 2-deoxy-D-glucose (2-DG) had an effect on inhibition of cancer cell proliferation [60]. The combined application of histone deacetylase inhibitors, such as valproic acid (VPA) and FTS could synergistically inhibit the proliferation of cancer cells that express oncogenic K-Ras through down regulation of Ras and blocking the expression of survivin and aurora-A [61]. Kloog's group demonstrated that FTS could chemosensitize Panc-1 pancreatic cancer cells and SW 480 colon cancer cells to cytotoxic drugs without developing drug resistance [62]. FTS also exhibits anti-inflammatory activity. It can induce an increase in regulatory T cells in mouse splenocytes [63]. The combination of Celecoxib and FTS enhanced the anti-inflammatory activity on T cells independent of prostaglandin E2 production [64]. We have recently shown that FTS synergizes with curcumin in various types of cancers including breast and prostate cancer [65].

FTS is poorly water soluble and also has limited oral bioavailability. Formulations for FTS have been rarely reported. One example is FTS-eluting fibers that exhibited controlled release characteristics and effectively led to brain tumor growth inhibition [66]. We have recently shown that coupling of the hydrophobic FTS to PEG leads to a significant increase in water solubility [67]. Similar to PEG-embelin conjugates, PEG-FTS conjugates self-assemble to form micelles that are effective in solubilizing hydrophobic drugs. Again, this suggests that the

embelin conjugates with PEG_{5K} work more effectively than the $PEG_{3.5K}$ counterparts and the PEG-FTS_2 conjugates performed better than the PEG-FTS conjugates.

1.2.5 Dual-functional micellar systems with drug-interactive domains

Despite the various differences among the reported micellar systems, essentially all of them are designed to load drugs through the principle of hydrophobic/hydrophobic interactions. However, most of the existing drugs or drug candidates are only moderately hydrophobic agents. Carrier/drug incompatibility may contribute to limited drug loading capacity and decreased formulation stability. Park's group has shown that inclusion of less hydrophobic and hydrogen bond-forming "hydrotropic motifs" into the hydrophobic domain of polymeric micelles significantly improved the compatibility of the core-forming blocks with the drugs that were not entirely hydrophobic/lipophilic, leading to significant improvement in both drug loading capacity and the colloidal stability of drug-loaded micelles [68]. However, this concept has not been tested in lipidic systems. Interestingly, pegylated surfactants with Vitamin E, embelin, or FTS as a hydrophobic domain, work significantly better than those with simple lipids as micellar formulations. The lipid core of our system is extremely hydrophobic due to the presence of two lipids, which might contribute considerably to an increase in hydrophobic interactions between the lipid chains. Further, Vitamin E, embelin, and FTS all have an interfacial aromatic ring linked to an acyl chain. Hydrophobic π-π interactions further elevated the hydrophobic interactions in the micelle's core, which may contribute significantly to the improved formulation properties over surfactants with simple lipid chains. These studies highlight the benefit of introducing additional structural variables to traditional lipid-based excipients. We recently hypothesized that incorporation of a drug-interactive motif into a surfactant at the

interfacial region will introduce additional carrier/drug interaction mechanisms, which shall lead to improvement in both drug-loading capacity and formulation stability. This concept was tested with JP4-039, a mitochondria-targeted antioxidant and also a poorly water-soluble agent. We have developed a simple screening process to identify agents that have potential drug-interactive activities based on their ability to prevent the formation of JP4-039 crystals in aqueous solution [69]. Among several motifs screened, 9-Fluorenylmethoxycarbony (Fmoc) moiety, a functional group that is routinely used for amino acid protection, was the most potent one identified. We designed and synthesized a micelle-forming PEG-lipopeptide conjugate with a lysine branching segment and two Fmoc groups located at the interfacial region, and two oleoyl chains as the hydrophobic core. We found that incorporation of Fmoc motifs into a PEG-lipopeptide conjugate led to a significantly improved formulation with respect to both JP4-039 loading capacity and the stability of JP4-039-loaded micelles. We then demonstrated that this micellar formulation can also be effectively used in formulating 7 drugs of diverse structures including probucol, niclosamide, JP4-039, progesterone, cyclosporin A, nifedipine, and griseofulvin [70]. These data strongly suggest that α-Fmoc behaves as a "formulation chemophor" or a structural unit capable of interacting with many pharmaceutical agents. This has led us to testing whether incorporation of a Fmoc motif can further improve the performance of the PEG_{5K}-FTS_2 micellar system. Indeed, this approach has led to a 3.9- and 3-fold increase in drug loading capacity for PTX and DOX, respectively. In addition, the stability of drug-loaded formulations was significantly improved [71]. More studies on the *in vitro* and *in vivo* characterization of the improved dual-functional carrier are ongoing in our laboratory.

2.0 PEG-FARNESYLTHIOSALICYLATE CONJUGATE AS A NANOMICELLAR CARRIER FOR DELIVERY OF PACLITAXEL DELIVERY

2.1 ABSTRACT

S-trans, trans-farnesylthiosalicylic acid (FTS) is a synthetic small molecule that acts as a potent and especially nontoxic Ras antagonist. It inhibits both oncogenically activated Ras and growth factor receptor-mediated Ras activation, resulting in the inhibition of Ras-dependent tumor growth. In this work, an FTS conjugate with poly(ethylene glycol) (PEG) through a labile ester linkage, PEG_{5K}-FTS_2(L), was developed. PEG_{5K}-FTS_2 conjugate readily forms micelles in aqueous solutions with a critical micelle concentration of 0.68 μM, and hydrophobic drugs such as paclitaxel (PTX) could be effectively loaded into these particles. Both drug-free and PTX-loaded micelles were spherical in shape with a uniform size of 20−30 nm. The release of PTX from PTX-loaded PEG_{5K}-FTS_2 micelles was significantly slower than that from Taxol formulation. In vitro cytotoxicity studies with several tumor cell lines showed that PEG_{5K}-FTS_2 (L) was comparable to FTS in antitumor activity. Western immunoblotting showed that total Ras levels were downregulated in several cancer cell lines treated with FTS or PEG_{5K}-FTS_2 (L). The micellar formulation of PTX exhibited more in vitro cytotoxic activity against several tumor cell lines compared with free PTX, suggesting a possible synergistic effect between the carrier and the codelivered drug. The antitumor activity of the PTX loaded PEG_{5K}-FTS_2 (L) micelles in a

syngeneic murine breast cancer model was found to be significantly higher than that of Taxol, which may be attributed to their preferential tumor accumulation and a possible synergistic effect between PEG_{5K}-FTS_2 carrier and loaded PTX.

2.2 BACKGROUND

Clinical application of PTX in cancer therapy is limited by problems such as low water solubility, lack of tissue-specificity and high toxicity [72, 73]. A number of macromolecular delivery systems are under investigation to circumvent these limitations and improve the potential of the anticancer drug [5, 7]. However, it remains a challenge to design a vehicle that can carry sufficient amount of drugs and efficiently overcome various physiological barriers to reach the tumor tissues [74]. Micelles with a nanoscopic supramolecular core-shell structure, are one such carrier of choice. It has been established that a nanocarrier with the size of 20-100 nm preferentially extravasates into solid tumor tissues owing to the leaky tumor vasculature [29, 30]. Additionally, a hydrophilic polymer (PEG) grafted onto the surface prolongs blood circulation times of the micelles due to the inhibition of nonspecific uptake by the reticuloendothelial system (RES) [33, 75]. However, for most delivery systems, the vehicles themselves rarely possess pharmacological activity. The use of "inert" excipients that lack therapeutic activity not only adds to the cost but also potentially imposes safety issues [76].

An interesting strategy to the design of multifunctional nanocarriers is to use the highly water-insoluble drug itself as the hydrophobic region of polymeric micelles. One example is pegylated vitamin E, D-α-tocopheryl poly(ethylene glycol) succinate (Vitamin E TPGS or TPGS) [77-79]. Vitamin E itself shows antitumor effect against different types of cancers and

vitamin E TPGS is effective in solubilizing various hydrophobic drugs. Synergistic effects between the TPGS-based carriers and delivered anti-cancer drugs have been demonstrated [8].

Recently our group reported another dual-functional carrier that is based on PEG-derivatized embelin [80]. Embelin shows antitumor activity in various types of cancers through various mechanisms such as the inhibition of the activity of X-linked inhibitor of apoptosis protein (XIAP) [81]. PEG-modified embelin shows significantly increased solubility (> 200 mg/mL) in aqueous solution. More importantly, PEG-embelin forms micelles that effectively solubilize various types of hydrophobic drugs such as PTX. Significantly improved antitumor activities were demonstrated for PTX formulated in PEG-embelin micelles both *in vitro* and *in vivo* [80].

In this study, we design a self-assembling nanomicellar system that is based on PEG-derivatized farnesylthiosalicylic acid (FTS) for targeted delivery of PTX. FTS is a first-in-class direct Ras antagonist designed to inhibit overactive cell growth in cancers caused by various Ras proteins [51]. Permanently active Ras caused by mutation in the Ras family of proto-oncogenes, is present in one-third of human cancers, with the highest incidence of mutational activation of Ras being detected in pancreatic (90%) and colon (50%) cancers [82, 83]. FTS has demonstrated significant reduction of Ras levels in a wide array of established cancer models without observable side effects [62]. One major mechanism involves affecting membrane interaction by inducing dislodgement of Ras protein from its anchorage domains, facilitating its degradation, and thus disrupting Ras protein signaling in the plasma membrane [55, 84]. FTS is poorly water-soluble [66] and PEGylation is designed to improve its solubility. At the same time, the PEG-FTS conjugate forms micelles, which could be applied as an ideal carrier for hydrophobic drugs to improve their efficiency and safety profiles. Additionally, the carrier materials can potentially

promote synergistic effects with the co-delivered anti-cancer drug. The PEG_{5K}-FTS_2 conjugate was synthesized and characterized for its structure and molecular weight. We further characterized the biophysical properties of drug-loaded micelles including particle size, loading capacity, and *in vitro* drug release kinetics. Finally, the *in vitro* and *in vivo* antitumor activity of PTX/PEG-FTS was investigated.

2.3 EXPERIMENTAL PROCEDURES

2.3.1 Materials

Paclitaxel (98%) was purchased from AK Scientific Inc. (CA, USA). FTS was synthesized and purified following a published literature [85]. Pan Ras Ab (Ab-3) was purchased from Calbiochem (La Jolla, CA). HRP-labeled goat anti-mouse IgG and the ECL chemiluminescence kit were purchased from Amersham Biosciences (Piscataway, NJ, USA). Dulbecco's phosphate buffered saline (DPBS) was purchased from Lonza (MD, USA). Poly(ethylene glycol) methyl ether (MeO-PEG-OH, Mw=5000 kDa), dimethyl sulfoxide (DMSO), 3-(4,5-dimethylthiazol-2-yl)-2,5-diphenyl tetrazolium bromide (MTT), trypsin-EDTA solution, Triton X-100, and Dulbecco's Modified Eagle's Medium (DMEM) were all purchased from Sigma-Aldrich (MO, USA). Fetal bovine serum (FBS) and penicillin-streptomycin solution were from Invitrogen (NY, USA).

2.3.2 Synthesis of PEG_{5K}-FTS_2(L) and PEG_{5K}-FTS_2(S) conjugate

PEG_{5K}-FTS_2(L) conjugates with a labile linkage were prepared via solution phase condensation reactions from MeO-PEG-OH with a molecular weight of 5000 (**Figure 1**). We started with synthesizing carboxyl terminated PEG monomethyl ether (MeO-PEG_{5k}-COOH) from MeO-PEG_{5k}-OH (1 eq.) by a facile chemical reaction with succinic anhydride (5 eq.) and 4-(dimethylamino) pyridine (DMAP 5 eq.) in pyridine according to a reported method [80]. To obtain two hydroxyl group terminated PEG monomethyl ether (MeO-PEG_{5k}-$(OH)_2$), diethanolamine (3 eq.) was coupled onto the carboxylic group of MeO-PEG_{5k}-COOH (1 eq.) using *N*-hydroxysuccinimide (NHS 3.6 eq.)/dicyclohexylcarbodiimide (DCC 3.6 eq.) as coupling agent in chloroform overnight. The polymer was precipitated and washed by ice-cold ether three times, and concentrated under vacuum. MeO-PEG_{5k}-$(OH)_2$, FTS, DCC and DMAP were then dissolved in chloroform with a molar ratio of 1: 6: 3: 0.3 and allowed to react overnight at room temperature. The solution was filtered and precipitated in ice-cold diethyl ether and ethanol twice respectively, and concentrated under vacuum. The powder was then dissolved in water and filtered through a filter with a pore size of 0.2 μm. The final product was obtained by lyophilizing the filtrate. At the same time, we also prepared a PEG_{5K}-FTS_2(S) conjugate (**Figure 2**) with a stable amide linkage. MeO-PEG_{5k}-OH and (S)-2,6-Bis-tert-butoxycarbonylaminohexanoic acid (Boc-Lys(Boc)-OH) were dissolved in chloroform together with DCC and DMAP with a molar ratio of 1:3:1.5:0.3 and the mixture was left to react overnight at room temperature. PEGylated molecules were recovered from the mixture through three cycles of dissolution/reprecipitation with chloroform and ether, respectively. Boc groups were removed via the treatment with 50% (v/v) trifluoroacetic acid (TFA) in chloroform, and PEGylated molecules were precipitated and washed with ice-cold ether. Finally, FTS was

coupled onto the N terminal group of MeO-PEG_{5k}-Lys-$(NH_2)_2$ (1 eq.) via NHS (3.6 eq.)/DCC (3.6 eq.) as described above. After the reaction was completed, the solution was precipitated in cold ether. PEG_{5K}-FTS_2(S) was similarly purified as that for PEG_{5K}-FTS_2(L).

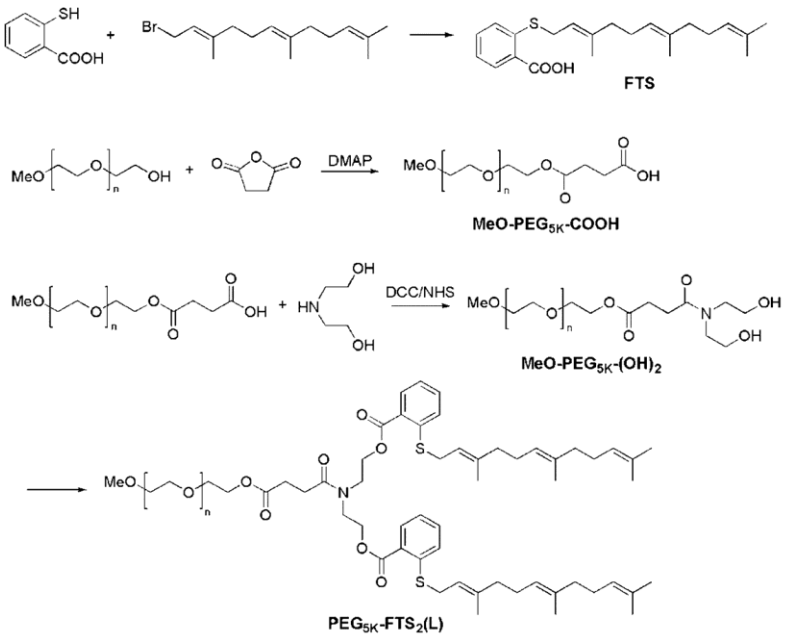

Figure 1. Synthesis scheme of PEG_{5K}-FTS_2 (L) conjugate

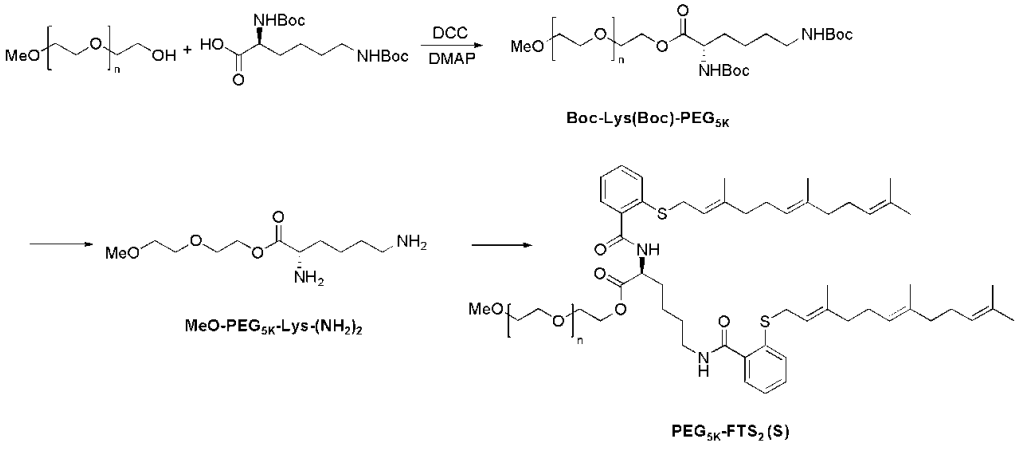

Figure 2. Synthesis scheme of PEG_{5K}-FTS_2 (L) conjugate

2.3.3 Preparation of PTX loaded and drug-free micelles

PTX (10 mM in chloroform) and PEG_{5K}-FTS_2 (10 mM in chloroform) were mixed with various carrier/drug ratios. The organic solvent was removed by nitrogen flow to form a thin film of drug/carrier mixture. The film was dried under vacuum for 1 h to remove the remaining solvent. DPBS was added to hydrate the thin film and the drug-loaded micelles were formed. The drug-free micelles were similarly prepared as described above.

2.3.4 Characterizations of PTX loaded and drug-free micelles

The particle size and zeta potential of micelles were measured by a Zetasizer (DLS) (Zetasizer Nano ZS instrument, Malvern, Worcedtershire, UK). The micelle concentrations were kept at 1 mg/mL. The morphology and size distribution of drug-free or PTX-loaded PEG_{5K}-FTS_2 micelles were observed using transmission electron microscopy (TEM). A copper grid with Formvar was used. The copper grid was immersed in a drop of sample solution and stained with 1% uranyl acetate. Imaging was performed at room temperature on JEOL JEM-1011.

The critical micelle concentration (CMC) of PEG_{5K}-FTS_2 was determined using pyrene as a fluorescence probe [13]. PEG_{5K}-FTS_2 was prepared in chloroform at 1.2 mg/mL and various amounts were added to 9 separate vials, respectively. Then 10 μl of 1.8×10^{-4} M of pyrene in chloroform was added to each vial and the solution was mixed well. The organic solvent was removed by nitrogen flow to form a thin film. Finally, 3 ml Milli-Q water was added to each vial and the final pyrene concentration was 6×10^{-7} M with PEG_{5K}-FTS_2 concentrations ranging from 0.0001 to 0.5 mg/mL. The vials were kept on a shaker at 37℃ for 24 h to reach equilibrium prior to fluorescence measurement. The excitation spectra were scanned from 310 to 350 nm at a fixed

emission wavelength of 390 nm by Synergy H1 Hybrid Multi-Mode Microplate Reader (Winooski, VT). The pyrene fluorescence intensity ratio I_{338}/I_{334} in the excitation spectra was analyzed for calculation of CMC.

The drug loading efficiency was quantified by high performance liquid chromatography (HPLC) (Alliance 2695-2998 system). The reverse phase Lichrospher® 100 RP-18 (5 μm） column was used and the mobile phase consisted of methanol/water (80: 20 v/v). The flow rate was set at 0.8 mL/min and the column effluent was detected at 227 nm with a UV/Vis detector. Drug loading capacity (DLC) and drug loading efficiency (DLE) were calculated according to the following equation:

DLC (%) = [weight of drug used/(weight of polymer + drug used)] ×100%

DLE (%) = (weight of loaded drug/weight of input drug) ×100%

2.3.5 *In vitro* drug release study

Release of PTX from PTX-loaded PEG_{5K}-FTS_2 micelles was performed following a method described previously [80]. Briefly, 3 mL of PTX-loaded PEG_{5K}-FTS_2 micelles or Taxol (1 mg PTX/mL) solution was placed in a dialysis bag (MWCO = 12 KDa, Spectrum Laboratories) that was incubated in 200 mL DPBS (PH = 7.4) containing 0.5% (w/v) Tween 80 at 37 ℃ with gentle shaking. The concentration of PTX remaining in the dialysis tubes at designated time points was measured by HPLC with the detection wavelength at 227 nm. Values were reported as the means from triplicate samples.

2.3.6 Hemolytic effect of PEG_{5K}-FTS_2 micelles

A hemolysis was assessed using fresh blood collected through cardiac puncture from rats. The red blood cells (RBCs) were collected by centrifugation at 1500 rpm for 10 min at 4 ℃. After washing three times with PBS, RBCs were diluted to a final concentration of 2% w/v in PBS. One mL of diluted RBC suspension was mixed with various concentrations (0.2 and 1.0 mg/mL) of PEG_{5k}-FTS_2 and PEI, respectively, and then incubated at 37 ℃ in an incubator shaker for 4 h. The mixtures were centrifuged at 1500 rpm for 10 min at 4 ℃, and 100 μL of supernatant from each sample was transferred into a 96-well plate. The release of hemoglobin was determined by absorbance at 540 nm using a microplate reader. RBCs incubated with Triton X-100 (2%) and PBS were used as the positive and negative controls, respectively. The percentage of hemolysis of RBCs was calculated as $(OD_{sample}-OD_{negative\ control})/ (OD_{positive\ control}-OD_{negative\ control}) \times 100\%$

2.3.7 Cell culture

DU145 and PC-3 are two androgen-independent human prostate cancer cell lines. 4T1.2 is a mouse metastatic breast cancer cell line. HCT-116 is a human colon carcinoma cell line. All cell lines were cultured in DMEM containing 5% FBS and 1% penicillin-streptomycin at 37 ℃ in a humidified 5 % CO_2 atmosphere.

2.3.8 *In vitro* cell cytotoxicity

For cytotoxicity measurement, DU145 (2000 cells/well), PC-3 (2000 cells/well), 4T1.2 (1000 cells/ell) or HCT-116 (1000 cells/well) were seeded in 96-well plates. After 24 h of incubation in

DMEM with 5% FBS and 1% streptomycin-penicillin, the old medium was removed and the cells were incubated for 72 h in the presence of indicated concentrations of PTX (free or formulated in PEG_{5K}-FTS_2 micelles). Twenty μL of 3-(4, 5-dimethylthiazol-2-yl)-2,5-diphenyltetrazoliumbromide (MTT) in DPBS (5 mg/mL) was added to each well and cells were further incubated for 4 h. MTT formazan was solubilized by DMSO. The absorbance in each well was measured by a microplate reader at a wavelength of 550 nm with a reference wavelength at 630 nm. Untreated groups were used as controls. Cell viability was calculated as $[(OD_{treat}-OD_{blank})/ (OD_{control}-OD_{blank}) \times 100\%]$. The cytotoxicity of PEG_{5K}-FTS_2(L) or PEG_{5K}-FTS_2(S) alone was similarly examined.

2.3.9 Western immunoblotting

Cells were grown in dishes in medium containing 5 % FBS, in the presence of 0.1 % DMSO (control) or indicated concentrations of FTS, PEG_{5K}-FTS_2(L), and PEG_{5K}-FTS_2(S) respectively. Following treatment for 48 h, cells were washed with ice-cold PBS twice and solubilized in lysis buffer. The lysates were centrifuged at 14000 for 10 min after a 10-min incubation on ice. Samples with equal amounts of total cellular proteins were subjected to 15% sodium dodecylsulfate polyacryl amide gel electrophoresis (SDS-PAGE) before proteins were transferred to nitrocellulose membranes. The membranes were incubated with primary antibody in 5% non fat dry milk dissolved in DPBS with 0.1% Tween 20 (PBST) overnight at 4℃. After washing three times with PBST, the membranes were incubated with secondary antibody at a final dilution of 1:10,000 in PBST for 1 h at room temperature. After washing three times with PBST, bound antibodies were detected by chemiluminescence. β-actin was used as a loading control.

2.3.10 Animals

Female BALB/c mice, 10-12 weeks in age, were purchased from Charles River (Davis, CA). All animals were housed under pathogen-free conditions according to AAALAC guidelines. All animal-related experiments were performed in full compliance with institutional guidelines and approved by the Animal Use and Care Administrative Advisory Committee at the University of Pittsburgh.

2.3.11 *In vivo* therapeutic study

A syngeneic murine breast cancer model (4T1.2) was used to examine the therapeutic effect of different formulations of PTX. 1 x 10^5 4T1.2 cells in 200 μL PBS were inoculated subcutaneously (s.c) at the right flank of female BALB/c mice. Treatments were started when tumors in the mice reached a tumor volume of ~50 mm^3 and this day was designated as day 1. On day 1, these mice were randomly divided into six groups (n=5) and administered i.v. with PBS (control), free PEG_{5K}-FTS_2(S) micelles, Taxol (10 mg PTX/kg), PTX-loaded PEG_{5K}-FTS_2(L) (10 and 20 mg PTX/kg), and PTX-loaded PEG_{5K}-FTS_2(S) (10 mg PTX/kg), respectively on days 1, 4, 6, 8, 11 and 13. Free PEG_{5K}-FTS_2(L) micelles were given at the equivalent dosage of the carrier in the group of PTX-loaded PEG_{5K}-FTS_2(L) micelles (10 mg PTX/kg). Tumor sizes were measured with digital caliper three times a week and calculated by the formula: $(L \times W^2)/2$, where L is the longest, W is the shortest in tumor diameters (mm). To compare between groups, relative tumor volume (RTV) was calculated at each measurement time point (where RTV equals to the tumor volume at a given time point divided by the tumor volume prior to first treatment). Mice were sacrificed when tumor volume reached 2000 mm^3.

2.3.12 Statistical analysis

In all statistical analysis, the significance level was set at a probability of $P < 0.05$. All results were reported as the mean ± standard error (SEM) unless otherwise indicated. Statistical analysis was performed by Student's t-test for two groups, and one-way ANOVA for multiple groups, followed by Newman-Keuls test with a $P < 0.05$.

2.4 RESULTS

2.4.1 Synthesis of PEG_{5K}-FTS_2(L) and PEG_{5K}-FTS_2(S) conjugates

PEG_{5K}-FTS_2(L) conjugates, containing two molecules of FTS coupled to one molecule of PEG via a labile ester linkage, were developed by solution phase condensation reactions. ^{1}H NMR spectra of PEG_{5K}-FTS_2(L) conjugate are shown in **Figure 3**, with signals at 3.63 ppm attributable to the methylene protons of PEG. Carbon chain signals and benzene ring signals of FTS were located at 1.5-2.2 ppm and 7-8 ppm, respectively. A peak appearing at δ 4.5 from a $–CH_2CH_2N$ group confirmed the conjugation of FTS with PEG. The signal ratio of the protons on PEG chain to the protons on -C=C(CH_3)$_2$ group of FTS is around 1:8 (**Figure 3**), which suggested that two FTS molecules were attached onto the PEG chain. The molecular weight of the PEG_{5K}-FTS_2(L) conjugate measured by MALDI-TOF Mass Spectra is close to the theoretical value (5867) (**Figure 4**), further confirming that two FTS molecules were conjugated to one molecule of PEG. We also synthesized a PEG_{5K}-FTS_2(S) conjugate in which FTS was coupled onto PEG chain via a stable amide linkage.

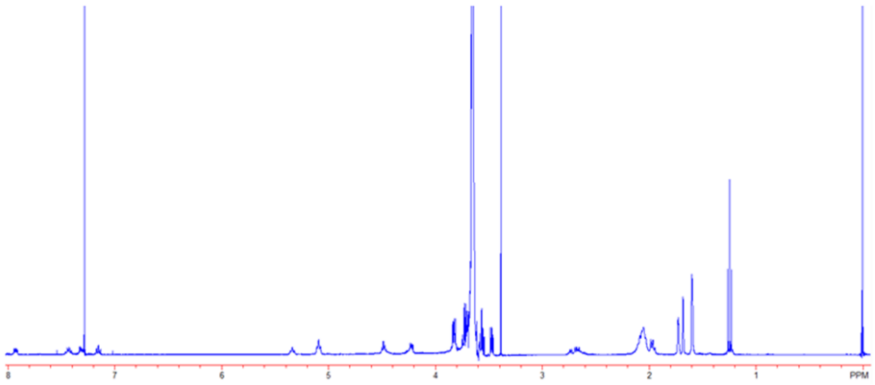

Figure 3. ^{1}H NMR spectra of PEG_{5K}-FTS_2(L) conjugate

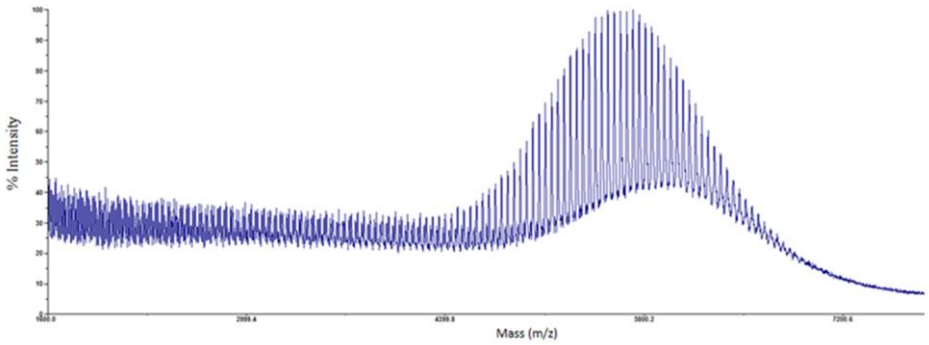

Figure 4. MALDI-TOF mass spectra of PEG_{5K}-FTS_2(L) conjugate

2.4.2 Characterizations of micelles

The PEG_{5K}-FTS_2 conjugates readily formed micelles in aqueous solution. Dynamic light scattering (DLS) measurements showed that these micelles had hydrodynamic sizes around 22 nm at the concentration of 20 mg/mL (**Figure 5A**). TEM revealed spherical particles with uniform size distribution (**Figure 5B**). The size observed by TEM shows good agreement with

that determined by DLS. PTX could be effectively loaded into PEG_{5K}-FTS_2 micelles. The size and size distribution were not significantly affected when PTX was loaded into micelles at a drug concentration of 1 mg/mL and a carrier/drug ratio of 5/1 (m/m) (**Figures 5C and D**).

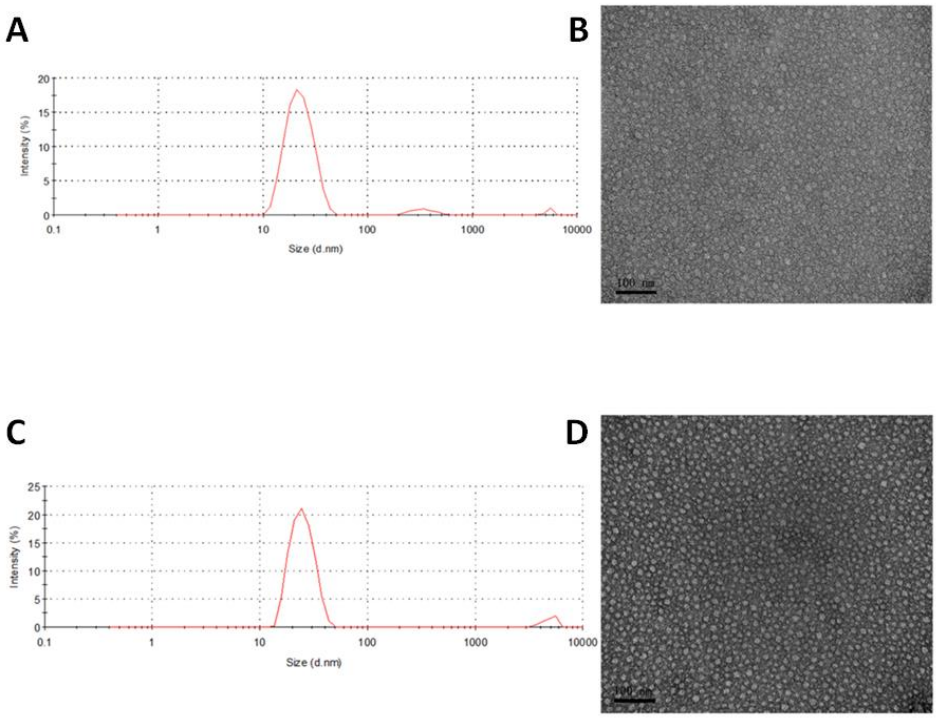

Figure 5. Particle size distribution of free drug PEG_{5K}-FTS_2 (A) and PTX/PEG_{5K}-FTS_2 micelles (C). TEM images of free drug PEG_{5K}-FTS_2 (B) and PTX/PEG_{5K}-FTS_2 micelles (D).

The CMC of PEG_{5K}-FTS_2 micelles was measured using pyrene as a fluorescence probe. When the concentration of the PEG_{5K}-FTS_2 reached the CMC, there is a major change for the I_{338}/I_{334} value due to the transfer of pyrene from polar micro-environment to non-polar micro-environment caused by the formation of micelles. The CMC of the PEG_{5K}-FTS_2 micelles was determined to be 0.68 μM (**Figure 6**).

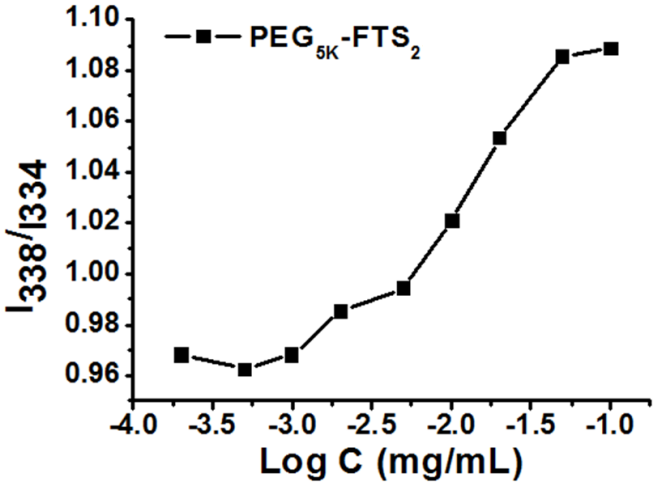

Figure 6. Plot of the ratio of I_{338}/I_{334} from fluorescence spectra as a function of logarithm concentration of PEG_{5K}-FTS_2 micelles.
Pyrene was used as molecular probe ([Pyrene]=6.0×10^{-7} M).

Table 1 shows the size of PTX-loaded micelles at different carrier/drug molar ratios. All of them had small size of around 20 nm. With increases in the input molar ratio of PEG_{5K}-FTS_2/PTX, the sizes of the PTX-loaded micelles were more close to that of drug-free micelles. The drug loading efficiency of PEG_{5K}-FTS_2 micelles was over 90% at various carrier/drug ratios examined (**Table 1)**.

Table 1. Physicochemical characterization of free drug and PTX-loaded PEG_{5K}-FTS_2 micelles

Micelles	Molar ratio	Conc. of PTX[a] (mg/mL)	Size[b] (nm)	PDI[c]	DLE[d] (%)	DLC[e] (%)
PEG_{5K}-FTS_2	-	-	17.61 ± 0.9	0.201	-	-
PEG_{5K}-FTS_2 :PTX	3.75 :1	1	24.93 ± 1.2	0.354	90.6	3.73
PEG_{5K}-FTS_2 :PTX	5 :1	1	25.63 ± 3.4	0.234	97.6	2.82
PEG_{5K}-FTS_2 :PTX	7.5 :1	1	22.27 ± 0.6	0.268	98.0	1.90
PEG_{5K}-FTS_2 :PTX	10 :1	1	20.17 ± 0.2	0.189	96.2	1.43

[a]PTX concentration in micelle was kept at 1 mg/mL. Blank micelle concentration was 20 mg/mL. Values repotted are the mean ± SD for triplicate samples.
[b]Measured by dynamic light scattering particle sizer.
[c]PDI = polydispersity index.
[d]DLC = drug loading capacity. [e]DLE = drug loading efficiency.

2.4.3 *In vitro* drug release study

The profile of PTX release was examined by a dialysis method and compared to that of Taxol. For the initial 8 h, about 41.2 % of PTX was released from the Taxol formulation while only 16.7 % of PTX was released from the PTX-loaded PEG_{5K}-FTS_2 micelles (**Figure 7**). PTX release from PEG_{5K}-FTS_2 micelle formulation was significantly slower compared to Taxol formulation during the entire experimental period. The $T_{1/2}$ of PTX release is 95.4 h for PEG_{5K}-FTS_2 formulation, which is significantly longer than that for Taxol formulation (17.6 h).

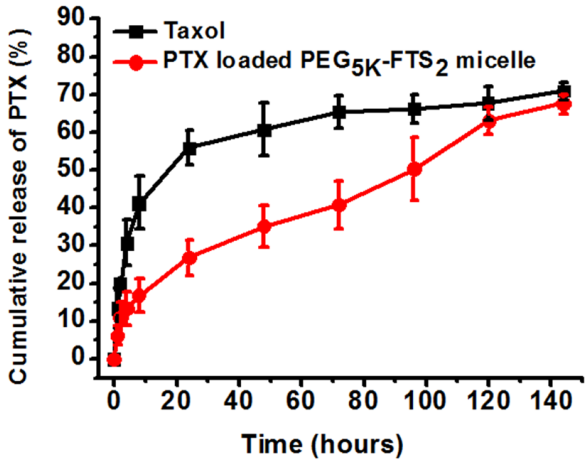

Figure 7. Cumulative PTX release profile from Taxol and PEG_{5K}-FTS_2 micelles.

2.4.4 Hemolytic effect of PEG_{5K}-FTS_2 micelles

Detrimental interaction of micelles with blood constituents such as RBCs must be avoided when these micelles are injected into the blood circulation as a carrier for drug delivery [86]. **Figure 8** shows the hemolytic activities of drug free PEG_{5K}-FTS_2 micelles and polyethylenimine (PEI), a cationic polymer known to have significant hemolytic effect [86]. PEI induced hemolysis in a dose-dependent manner. In contrast, free PEG_{5K}-FTS_2 micelles did not show any detectable

hemolytic activities at the same experimental concentrations, suggesting that is safe to administer the product intravenously without concern for hemolysis.

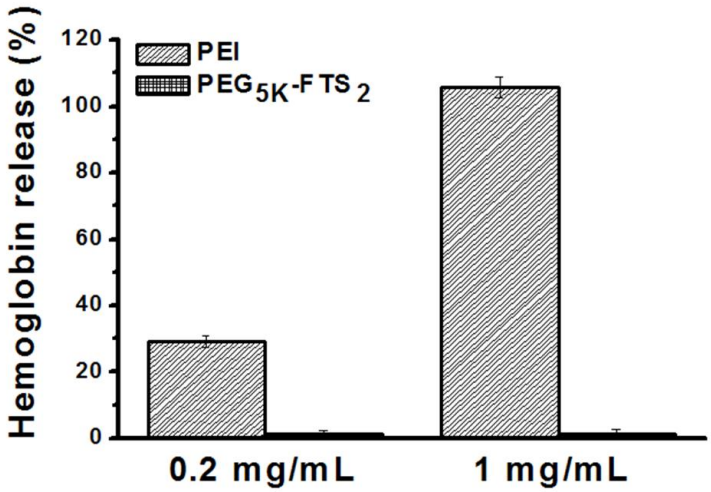

Figure 8. *In vitro* hemolysis assay of empty PEG_{5K}-FTS_2 micelles.
Compared with PEL with two different concentrations (0.2, 1 mg/mL). Value reported are the mean ± SD for triplicate samples.

2.4.5 Western immunoblotting

We incubated HCT-116 or 4T1.2 cells with various concentrations of FTS, PEG_{5K}-FTS_2(L) and PEG_{5K}-FTS_2(S) for 48 h, respectively, and the protein expression levels of Ras in the cells were examined by Western immunoblotting with pan anti-Ras Ab. As shown in **Figure 9**, FTS treatment caused a reduction in the total amount of cellular Ras in both cell lines. These results are consistent with the known action of FTS as a Ras inhibitor. PEG_{5K}-FTS_2(L) was comparable to free FTS in reducing the protein levels of Ras in the treated cells. In contrast, PEG_{5K}-FTS_2(S) showed minimal effect at the same FTS concentration.

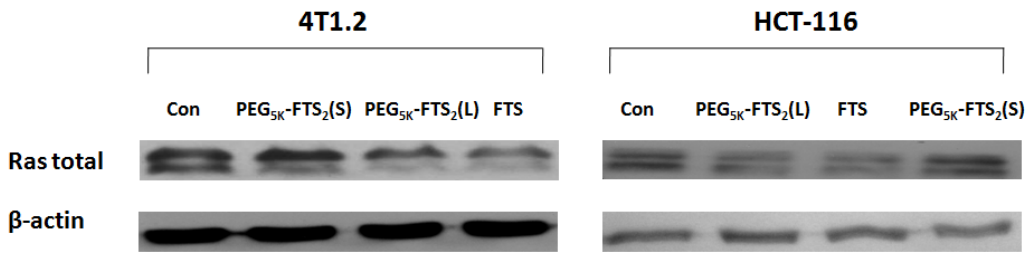

Figure 9. Effect of FTS, PEG_{5K}-FTS_2(L) and PEG_{5K}-FTS_2(S) on total Ras expression analyzed by Western blot.
Cells grown in dishes in medium containing 5% FBS, in the presence of 0.1% DMSO (control) or in the presence of 5 μM of PEG_{5K}-FTS_2(L), PEG_{5K}-FTS_2(S) and 10 μM of FTS for 48 h. Total cell lysate was subjected to Western blot analysis. β-actin was used as a loading control.

2.4.6 *In vitro* cytotoxicity

Several cancer cell lines were included in the cytotoxicity studies including murine breast cancer cells 4T1.2, human colon carcinoma cell line HCT-116, and two human prostate cancer cell lines PC-3 and DU145. **Figure 10A** shows the cytotoxicity of two PTX-free micelles, PEG_{5K}-FTS_2(L) and PEG_{5K}-FTS_2(S), in comparison with free FTS in 4T1.2 tumor cells. Free FTS inhibited the tumor cell growth in a concentration-dependent manner. Conjugation of FTS to PEG via a labile ester linkage resulted in only a slight decrease in antitumor activity. In contrast, a similar conjugate with a stable amide linkage [PEG_{5K}-FTS_2(S)] was significantly less active compared to both free FTS and PEG_{5K}-FTS_2 (L). A similar result was obtained in human colon cancer cells, HCT-116 (**Figure 10B**).

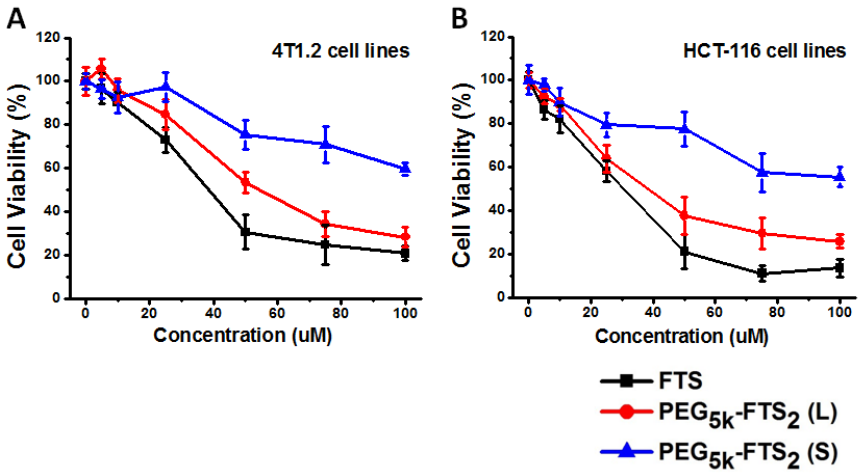

Figure 10. Cytotoxicity of free FTS, PEG_{5K}-FTS_2(L) and PEG_{5K}-FTS_2(S) in 4T1.2 mouse breast cancer cell line (A) and HCT-116 human colon carcinoma cell line (B).

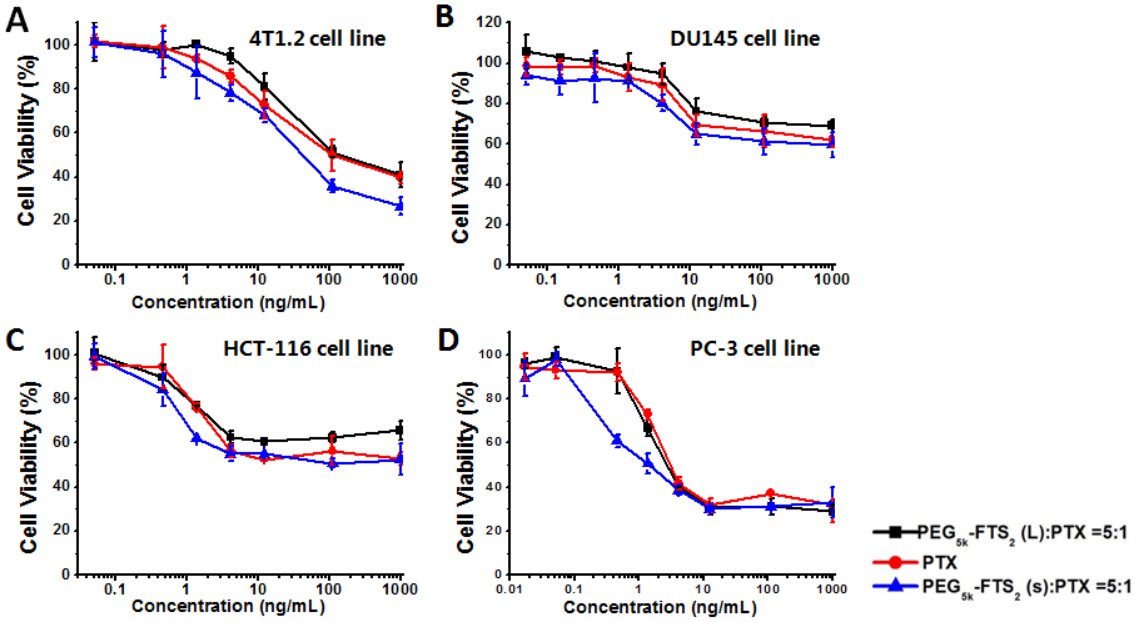

Figure 11. Cytotoxicity of free PTX, free PEG_{5K}-FTS_2(L) and PTX/PEG_{5K}-FTS_2(L) micelles against different cancer cell lines.
Including the 4T1.2 mouse breast cancer cell line (A), two androgen-independent human prostate cancer cell lines DU145 (B) and PC-3 (D), and human colon carcinoma HCT-116 cell line (C). Cells were treated for 72 h and cytotoxicity was determined by MTT assay. Values reported are the means ± SD for triplicate samples.

Figure 11A shows the cytotoxicity of free PTX (in DMSO) and PTX formulated in PEG_{5K}-FTS_2(L) or PEG_{5K}-FTS_2(S) micelles in 4T1.2 tumor cells. Free PTX inhibited the tumor cell growth in a concentration dependent manner. Delivery of PTX via PEG_{5K}-FTS_2(L) micelles led to a significant increase in the cytotoxicity. Interestingly, PTX formulated in PEG_{5K}-FTS_2(S) was less active than free PTX. Similar results were obtained in other tumor cell lines including DU145 (**Figure 11B**), PC-3 (**Figure 11C**), and HCT-116 (**Figure 11D**).

2.4.7 *In vivo* therapeutic study

The *in vivo* therapeutic activity of PTX formulated in PEG_{5K}-FTS_2 micelles was investigated in a syngeneic murine breast cancer model (4T1.2). As shown in **Figure 12A**, free PEG_{5K}-FTS_2 micelles alone showed no effects in inhibiting the tumor growth at the concentration used. The other groups treated with different PTX formulations showed varied levels of antitumor effects and they were ranked as PTX/PEG_{5K}-FTS_2(L) > PTX/PEG_{5K}-FTS_2(S) > Taxol at the same dose of 10 mg PTX/kg. By day 13, the relative tumor volume (RTV) was 15.1 for Taxol, while the RTVs for PTX/PEG_{5K}-FTS_2(S) and PTX/PEG_{5K}-FTS_2(L) were 13.3 and 9.6, respectively. Increasing the PTX dosage to 20 mg/kg in PTX-loaded PEG_{5K}-FTS_2(L) formulation resulted in a further improvement in antitumor activity with a RTV of 5.2. No significant changes in body weight were noted in all treatment groups compared to PBS control group (**Figure 12**).

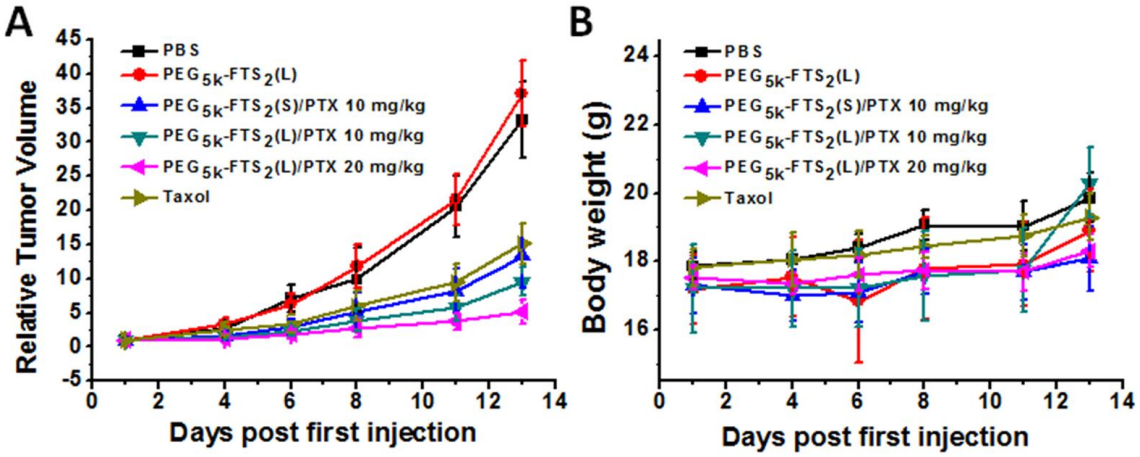

Figure 12. Enhanced antitumor activity of PTX formulated in PEG_{5K}-FTS_2(L) and PEG_{5K}-FTS(S) micelles.
BABL/c mice were inoculated s.c. with 4T1.2 cells (1 x 10^5 cells/mouse). Five days later, mice received various treatments twice a week and tumor growth was monitored and plotted as relative tumor volume (mm^3). (A) The changes of relative tumor volume. (B) Body weight after administration. $P < 0.001$ (PTX/PEG_{5K}-FTS_2 (L) vs. Taxol). N = 5.

2.5 DISCUSSION

In this study, we developed a micellar system that is based on PEG-derivatized FTS. FTS is an antagonist of Ras and is currently being evaluated as a new therapy for the treatment of various types of cancers that are associated with Ras mutations and elevated levels of Ras activity. A major feature with FTS is its excellent safety profile compared to other chemotherapeutic agents [58, 83, 87]. This will render PEG-FTS micelles a safe delivery system for *in vivo* delivery of various types of anticancer agents including FTS itself.

One major advantage of PEG-FTS micellar system is its very small size (~20 nm). It is generally regarded that particles in the size range of 10 ~ 200 nm can be passively targeted to tumors via the leaky tumor vasculature [28, 88, 89]. However, recent studies have shown that the size of the particles needs to be below 50 ~ 60 nm for them to effectively reach poorly

vascularized tumors [17, 32]. The small size of PEG-FTS micelles will allow effective passive targeting to various types of cancers including those with poorly developed tumor vasculature.

In vitro release study showed significantly slower release kinetics for PTX formulated in PEG_{5K}-FTS_2 micelles compared to Taxol formulation (**Figure 7**). This might be due to a more effective drug/carrier interaction for PTX/PEG_{5K}-FTS_2 mixed micelles. FTS has a benzene ring and an acyl chain. In addition to hydrophobic interaction with PTX, the π-π stacking and the hydrogen bonding also contribute to the overall carrier/PTX interaction. The close proximity of two FTS molecules in PEG_{5K}-FTS_2 conjugate shall enhance the interaction of the carrier with PTX. Indeed, a PEG-FTS conjugate of 1:1 molar ratio was much less active than PEG_{5K}-FTS_2 in forming stable mixed micelles with PTX (data not shown). More studies are needed to better define the mechanism of drug/carrier interactions for PTX/PEG_{5K}-FTS_2 mixed micelles.

PEG_{5K}-FTS_2(L) alone was much more active than PEG_{5K}-FTS_2(S) in antitumor activity in both 4T1.2 and HCT-116 cell lines (**Figure 10**). It is unlikely that this is attributed to differences in the surface activity of the two conjugates as both showed minimal hemolytic activity at the concentrations that were much higher than those used in the cytotoxicity study. It is likely that FTS is much more readily released from PEG_{5K}-FTS_2(L) by esterases following intracellular delivery. The cytotoxicity data agree with Western blotting in which PEG_{5K}-FTS_2(L) was more active than PEG_{5K}-FTS_2(S) in reducing the protein expression levels of Ras in treated tumor cells (**Figure 9**).

In addition to more potent antitumor activity by itself, PEG_{5K}-FTS_2(L) was also more active than PEG_{5K}-FTS_2(S) in mediating PTX cytotoxicity to tumor cells (**Figure 11**). At the concentrations used for PTX delivery, both PEG_{5K}-FTS_2(L) and PEG_{5K}-FTS_2(S) were not active in killing tumor cells by themselves. This is consistent with published works [56, 90, 91] and our

own data (**Figure 10**) that FTS works at high μM concentrations. It remains to be determined if, at suboptimal concentrations as those in cells treated with PEG_{5K}-FTS_2(L), the released FTS could synergize with PTX in the overall antitumor activity. It is also possible that PTX is more readily released from PEG_{5K}-FTS_2(L) micelles due to the disintegration of the micellar system following the cleavage and release of FTS from PEG_{5K}-FTS_2(L) conjugate. More studies are needed to better understand the mechanism by which PTX/PEG_{5K}-FTS_2(L) mediated the cytotoxicity to tumor cells *in vitro*.

In vivo, PTX formulated in both PEG_{5K}-FTS_2(L) and PEG_{5K}-FTS_2(S) micelles showed better antitumor activity than Taxol formulation although it is not statistically significant between Taxol and PTX/PEG_{5K}-FTS_2(S). This is likely due to a better stability of PEG_{5K}-FTS_2(L) micellar formulation as demonstrated in release study (**Figure 7**). Again, PTX/PEG_{5K}-FTS_2(L) was more effective than PTX/PEG_{5K}-FTS_2(S) in antitumor activity *in vivo*. It remains to be determined if similar mechanisms are involved in the improved antitumor activity for PTX/PEG_{5K}-FTS_2(L) both *in vitro* and *in vivo*.

In summary, a conjugate of PEG with two molecules of FTS forms small-sized micelles that effectively solubilize PTX. PTX formulated in this micellar system shows a PTX release kinetics that is significantly slower than that of Taxol. PEG_{5K}-FTS_2(L) conjugate well retains the biological activity of FTS and PTX formulated in PEG_{5K}-FTS_2(L) micelles is more active in cytotoxicity than free PTX *in vitro*. *In vivo*, PTX/PEG_{5K}-FTS_2(L) shows an antitumor activity that is more potent than that of Taxol or PTX/PEG_{5K}-FTS_2(S). PEG_{5K}-FTS_2(L) may represent a promising micellar system that could effectively deliver anticancer agents to tumors. Furthermore it may potentially synergize with co-delivered drugs in the overall antitumor activity.

3.0 PEG-FARNESYL THIOSALICYLIC ACID TELODENDRIMER MICELLES AS AN IMPROVED FORMULATION FOR TARGETED DELIVERY OF PACLITAXEL

3.1 ABSTRACT

We have recently designed and developed a dual-functional drug carrier that is based on poly(ethylene glycol) (PEG)-derivatized farnesylthiosalicylate (FTS, a nontoxic Ras antagonist). PEG_{5K}-FTS_2 readily form micelles (20-30 nm) and hydrophobic drugs such as paclitaxel (PTX) could be effectively loaded into these micelles. PTX formulated in PEG_{5K}-FTS_2 micelles showed an antitumor activity that was more efficacious than Taxol in a syngeneic mouse model of breast cancer (4T1.2). In order to further improve our PEG-FTS micellar system, four PEG-FTS conjugates were developed that vary in the molecular weight of PEG (PEG_{2K} vs PEG_{5K}) and the molar ratio of PEG/FTS (1/2 vs 1/4) in the conjugates. These conjugates were characterized including CMC, drug loading capacity, stability, and their efficacy in delivery of anticancer drug PTX to tumor cells in vitro and in vivo. Our data showed that the conjugates with four FTS molecules were more effective than the conjugates with two molecules of FTS and that FTS conjugates with PEG_{5K} were more effective than the counterparts with PEG_{2K} in forming stable mixed micelles. PTX formulated in PEG_{5K}-FTS_4 micelles was the most effective formulation in inhibiting the tumor growth in vivo.

3.2 BACKGROUND

Paclitaxel (PTX) is one of the first-line chemotherapeutic agents used in the treatment of patients with breast, ovarian, non-small cell lung cancer and advanced forms of Kaposi's sarcoma. The mechanism involves interfering with the normal breakdown of microtubules during cell division [92]. Successful application of PTX in the clinic has been limited by its poor water solubility and the systemic toxicity. Taxol is a Cremophor EL/ethanol formulation of PTX that has been used in the clinic. However, Cremophor EL can cause hypersensitivity reactions, neuropathy, and other serious side effects [93]. Thus there is a need to develop an alternative delivery system for PTX. Various macromolecular delivery systems such as liposomes, dendrimers, and nanoparticles are under investigation, among which polymeric micelles have gained considerable attention owing to their ease of preparation and very small sizes (10-100 nm) [94, 95]. Recent studies have substantiated that sub-100 nm micelle sizes are critical for a delivery system to achieve effective tumor targeting [29, 32, 96-98].

Our group has previously developed PEG-FTS as a dual-functional carrier for the delivery of poorly water soluble anticancer drugs [67]. This system was constructed by coupling two molecules of S-trans, trans-farnesylthiosalicylic acid (FTS) to polyethylene glycol (PEG, M_W = 5000) through an ester linkage (PEG_{5K}-FTS_2). Different from most reported delivery systems that use "inert" excipients, our system employ a water-insoluble drug FTS as the hydrophobic region of the polymeric micelles. FTS is a nontoxic Ras antagonist [99]. It can inhibit both oncogenically activated Ras and growth factor receptor-mediated Ras activation, resulting in the inhibition of Ras-dependent tumor growth [55, 56]. A preliminary study showed that the antitumor activity of FTS was well retained following coupling to PEG_{5K}. Furthermore, PEG_{5K}-FTS_2 readily formed small-sized micelles (20-30 nm) that are effective in loading and

delivering PTX. The *in vivo* study demonstrated that the antitumor activity of the PTX-loaded PEG_{5K}-FTS_2 micelles was significantly higher than that of Taxol [67].

Recent studies have shown that the Vitamin E-based micellar system could be significantly improved via modulating the PEG motifs and the molar ratio of PEG/Vitamin E [100, 101]. In another study with PEG-embelin system, we have shown that a conjugate with two embelin molecules linked to PEG was significantly more effective than the conjugate with one embelin molecule coupled to PEG. This has prompted us to carry out a similar study with the PEG-FTS system [102]. Four PEG-FTS conjugates that vary in the molecular weight of PEG (PEG_{2K} vs PEG_{5K}) and the molar ratio of PEG/FTS (1/2 vs 1/4) have been developed. We demonstrated that PEG_{5K}-FTS_4 formed the most stable mixed micelles with PTX among the four PEG-FTS conjugates evaluated. Furthermore, PTX formulated in PEG_{5K}-FTS_4 micelles was the most effective formulation in inhibiting the tumor growth *in vivo*.

3.3 EXPERIMENTAL PROCEDURES

3.3.1 Materials

Paclitaxel (98%) was purchased from AK Scientific Inc. (CA, USA). FTS was synthesized and purified following a published literature [103]. Dulbecco's phosphate buffered saline (DPBS) was purchased from Lonza (MD, USA). Poly(ethylene glycol) methyl ether (MeO-PEG-OH, MW=2000, 5000 kDa), dimethyl sulfoxide (DMSO), succinate anhydride, diethanolamine, 3-(4,5-dimethylthiazol-2-yl)-2,5-diphenyl tetrazolium bromide (MTT), trypsin-EDTA solution,

Triton X-100, and Dulbecco's Modified Eagle's Medium (DMEM) were all purchased from Sigma-Aldrich (MO, USA). Fetal bovine serum (FBS) and penicillin-streptomycin solution were purchased from Invitrogen (NY, USA). *N*-hydroxysuccinimide (NHS) and dicyclohexylcarbodiimide (DCC) were purchased from Alfa Aesar (MA, USA). 4-(dimethylamino) pyridine (DMAP) was purchased from Calbiochem-Novabiochem Corporation (CA, USA). All solvents used in this study were HPLC grade.

3.3.2 Cell culture

MCF-7 is a human breast carcinoma cell line. 4T1.2 is a mouse metastatic breast cancer cell line. HCT-116 is a human colon carcinoma cell line. All cell lines were cultured in DMEM containing 5% FBS and 1% penicillin-streptomycin at 37 ℃ in a humidified 5% CO_2 atmosphere.

3.3.3 Synthesis of PEG_{2K}-FTS_2, PEG_{2K}-FTS_4, PEG_{5K}-FTS_2 and PEG_{5K}-FTS_4

PEG_{5K}-FTS_4 was prepared via solution phase condensation reactions (**Figure 13**). We started to synthesize two hydroxyl group terminated PEG monomethyl ether (MeO-PEG_{5k}-OH_2) by following a published procedure [17]. Carboxyl terminated PEG monomethyl ether (MeO-PEG_{5k}-$COOH_2$) was synthesized from MeO-PEG_{5k}-$(OH)_2$ by a facile chemical reaction with succinic anhydride and DMAP. To obtain four hydroxyl groups terminated PEG monomethyl ether (MeO-PEG_{5k}-OH_4), diethanolamine was coupled onto the carboxylic group of MeO-PEG_{5k}-$COOH_2$ using NHS/DCC as coupling agent in chloroform overnight. The polymer was precipitated and washed by ice-cold diethyl ether and ethanol twice respectively, and concentrated under vacuum. MeO-PEG_{5k}-OH_4, FTS, DCC and DMAP were then dissolved in

chloroform and allowed to react overnight at room temperature. The solution was filtered and precipitated in ice-cold diethyl ether and ethanol twice respectively, and concentrated under vacuum. The powder was then dissolved in water and filtered through a filter with a pore size of 0.22 μm. The final product was obtained by lyophilizing the filtrate. PEG_{2K}-FTS_4 was similarly synthesized as PEG_{5K}-FTS_4. PEG_{5K}-FTS_2 and PEG_{2K}-FTS_2 were synthesized following the literature [104].

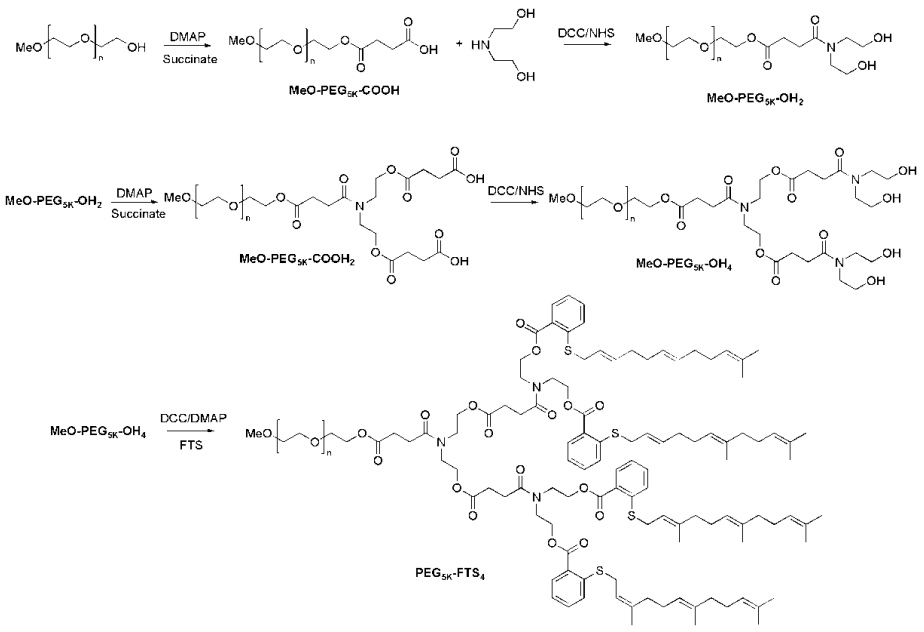

Figure 13. Synthesis scheme of PEG_{5K}-FTS_4 conjugate

3.3.4 Preparation of drug-loaded and drug-free micelles

PTX (10 mM in chloroform) and four PEG-FTS conjugates (10 mM in chloroform) were mixed at various carrier/drug ratios. The organic solvent was removed by nitrogen flow to form a thin film of drug/carrier mixture. The film was dried under vacuum for 1 h to remove the remaining

solvent. DPBS was added to hydrate the thin film and the drug-loaded micelles were formed. Unincorporated PTX (precipitate) was removed by filtering through a syringe filter (pore size: 0.22 μm). The drug-free micelles were similarly prepared as described above.

3.3.5 Characterizations of drug-loaded and drug-free micelles

The particle size and zeta potential of micelles were measured by a Zetasizer (DLS) (Zetasizer Nano ZS instrument, Malvern, Worcestershire, UK). The morphology and size distribution of drug-free or drug-loaded PEG_{2K}-FTS_2, PEG_{2K}-FTS_4, PEG_{5K}-FTS_2 and PEG_{5K}-FTS_4 micelles were observed using transmission electron microscopy (TEM). A copper grid with Formvar was used. The copper grid was immersed in a drop of sample solution and stained with 1% uranyl acetate. Imaging was performed at room temperature on JEOL JEM-1011.

The critical micelle concentrations (CMC) of four PEG-FTS micelles were determined by using pyrene as a fluorescence probe [13]. Four PEG-FTS conjugates, PEG_{2K}-FTS_2, PEG_{2K}-FTS_4, PEG_{5K}-FTS_2 and PEG_{5K}-FTS_4, were prepared in chloroform at 1.2 mg/mL, and various amounts were added to 9 separate vials. Then 10 μl of 1.8×10^{-4} M of pyrene in chloroform was added to each vial and the solution was mixed well. The organic solvent was removed by oil pump, and then 3 mL Milli-Q water was added to each vial. The final pyrene concentration was 6×10^{-7} M with the four PEG-FTS conjugate concentrations ranging from 0.0001 to 0.5 mg/mL. The vials were kept on a shaker for 24 h at 37℃ to reach equilibrium before fluorescence measurement. The fluorescence intensities of samples were measured at the excitation wavelength of 334 nm and emission wavelength of 390 nm by Synergy H1 Hybrid Multi-Mode Microplate Reader (Winooski, VT). The CMC is determined from the threshold concentration, where the sharp increase in pyrene fluorescence intensity is observed.

The PTX loading efficiency was quantified by high performance liquid chromatography (HPLC) (Alliance 2695-2998 system) as described previously [104]. Drug loading capacity (DLC) and drug loading efficiency (DLE) were calculated according to the following equation:

DLC (%) = [weight of drug loaded/(weight of polymer + drug used)] ×100%

DLE (%) = (weight of loaded drug/weight of input drug) ×100%

3.3.6 *In vitro* PTX release study

The *in vitro* PTX release kinetics for the four PEG-FTS micelles was determined by a dialysis method according to our published protocol [67]. Briefly, PTX loaded PEG-FTS micelles at a concentration of 0.5 mg PTX/mL were placed into a dialysis bag (MW cutoff 14000). The dialysis bag was incubated in 200 mL PBS containing 0.5% (w/v) Tween 80 with gentle shaking at 37 ℃. The concentrations of PTX remaining in the dialysis bag at designated time points were measured by HPLC.

3.3.7 Hemolytic effect of PEG-FTS micelles

Hemolysis assay was performed using fresh blood collected through cardiac puncture from rats [105]. Red blood cells (RBCs) were collected by centrifugation and washed with PBS three times. Then RBCs were diluted in PBS to a final concentration of 2% w/v. One mL of diluted RBC suspension was mixed with different concentrations (0.2 and 1.0 mg/mL) of four PEG-FTS micelles and PEI, respectively, and then incubated at 37 ℃ in an incubator shaker for 4 h. The mixtures were centrifuged and supernatants were transferred into a 96-well plate. The release of hemoglobin was determined at 540 nm absorbance using a microplate reader. RBCs incubated

with PBS and Triton X-100 (2%) were used as the negative and positive controls, respectively. The percentage of hemolysis of RBCs was calculated as $(OD_{sample}\text{-}OD_{negative\ control})/(OD_{positive\ control}\text{-}OD_{negative\ control}) \times 100\%$.

3.3.8 *In vitro* cytotoxicity study

The cytotoxicity of PTX formulated in PEG_{2K}-FTS_2, PEG_{2K}-FTS_4, PEG_{5K}-FTS_2 and PEG_{5K}-FTS_4 micelles was assessed with several cancer cell lines and compared to free PTX in DMSO respectively. Briefly, 4T1.2 (1000 cells/well) cell lines were seeded in 96-well plates. After 24 h of incubation in DMEM with 5% FBS and 1% streptomycin-penicillin, the old medium was removed and the cells were incubated for 72 h in the presence of indicated concentrations of PTX (free or formulated in four PEG-FTS micelles). 100 μL of 3-(4, 5-dimethylthiazol-2-yl)-2,5-diphenyltetrazoliumbromide (MTT) in DPBS (0.5 mg/mL) was added to each well and cells were further incubated for 2 h. MTT formazan was solubilized by DMSO. The absorbance in each well was measured by a microplate reader at a wavelength of 550 nm and a reference wavelength of 630 nm. Untreated groups were used as controls. Cell viability was calculated as $[(OD_{treat}\text{-}OD_{blank})/(OD_{control}\text{-}OD_{blank}) \times 100\%]$. The cytotoxicity of PEG_{2K}-FTS_2, PEG_{2K}-FTS_4, PEG_{5K}-FTS_2 and PEG_{5K}-FTS_4 micelles alone was similarly tested in 4T1.2, MCF-7 and HCT-116 cell line as described above.

3.3.9 Western blotting

Ras protein expression level in HCT-116 cells was evaluated by Western blotting following our published method [102]. Briefly, HCT-116 cells with 60-70% confluency in a 6-well plate were

treated with four PEG-FTS conjugates for 20 h at a FTS concentration of 40 μM. The antibodies used for Western blotting included those against Ras and β-actin. Bound antibodies were detected by chemiluminescence.

3.3.10 Animals

Female BALB/c mice, 4-6 weeks in age, were purchased from Charles River (Davis, CA). All animals were housed under pathogen-free conditions according to AAALAC guidelines. All animal-related experiments were performed in full compliance with institutional guidelines and approved by the Animal Use and Care Administrative Advisory Committee at the University of Pittsburgh.

3.3.11 *In vivo* therapeutic study

A syngeneic murine breast cancer model (4T1.2) was used to examine the therapeutic effect of different formulations of PTX. 2 x 10^5 4T1.2 cells in 200 μL PBS were inoculated s.c. at the right flank of female BALB/c mice. Treatments were started when tumors in the mice reached a tumor volume of ~ 50 mm^3 and this day was designated as day 1. On day 1, these mice were randomly divided into six groups (n=5) and administered i.v. with PBS (control), Taxol (10 mg PTX/kg), PTX-loaded PEG_{2K}-FTS_2, PEG_{2K}-FTS_4, PEG_{5K}-FTS_2, and PEG_{5K}-FTS_4 micelles (10 mg PTX/kg), respectively on days 1, 3, 5, 8, 10 and 12. Tumor sizes were measured with digital caliper three times a week and calculated by the formula: $(L \times W^2)/2$, where L is the longest, and W is the shortest in tumor diameters (mm). To compare between groups, relative tumor volume

(RTV) was calculated at each measurement time point (where RTV equals to the tumor volume at a given time point divided by the tumor volume prior to first treatment). Mice were sacrificed before tumor reached 2000 mm^3.

To monitor the potential toxicity, the body weights of all mice from different groups were measured every three days. In addition, serum levels of transaminases (AST, ALT) in the mice with different treatments were investigated at the completion of the study.

3.3.12 Statistical analysis

In all statistical analysis, the significance level was set at a probability of $P < 0.05$. All results were reported as the mean ± standard deviation (SD), unless otherwise indicated. Statistical analysis was performed by Student's t-test for two groups, and one-way ANOVA for multiple groups, followed by Newman-Keuls test with a $P < 0.05$.

3.4 RESULTS

3.4.1 Synthesis of four PEG-FTS conjugates

PEG_{5K}-FTS_4 conjugate, containing four molecules of FTS coupled to one molecule of PEG_{5K} via a labile ester linkage, was developed by solution phase condensation reactions. The synthetic scheme is presented in **Figure 13**. ^1H NMR spectra of PEG_{5K}-FTS_4 conjugate are shown in **Figure 14**. The intense peak at 3.66 ppm was attributable to the methylene protons of PEG. Carbon chain signals and benzene ring signals of FTS were located at 1.5-2.2 ppm and 7-8 ppm,

respectively. MALDI-TOF suggested that four FTS were successfully attached to PEG_{5K} (**Figure 15**). We also synthesized PEG_{2K}-FTS_2, PEG_{2K}-FTS_4, and PEG_{5K}-FTS_2 conjugates, which were confirmed by ^1H NMR spectra and MALDI-TOF mass spectra (**Figures 14 & 15**).

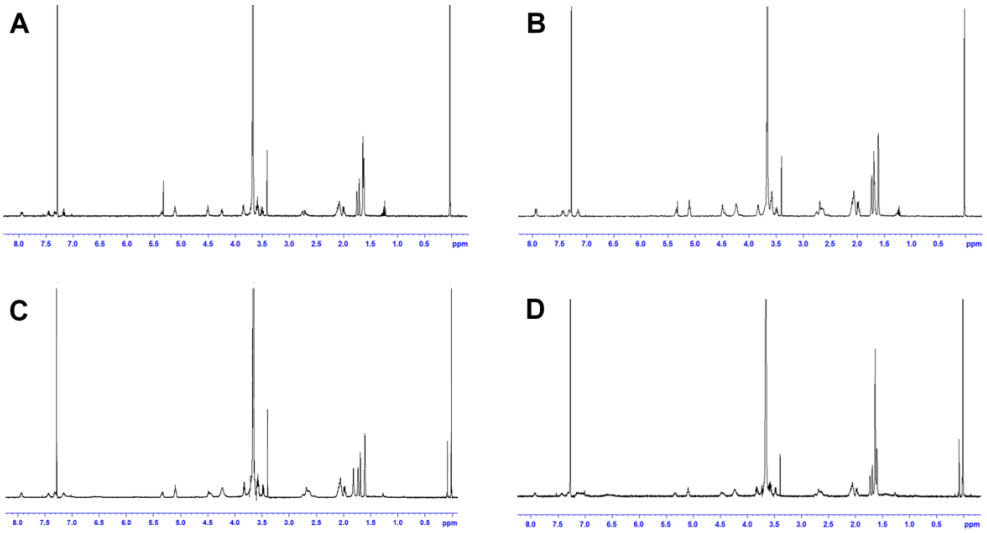

Figure 14. ^1H NMR spectra (400MHz) of PEG_{2K}-FTS_2 (A), PEG_{2K}-FTS_4 (B), PEG_{5K}-FTS_2 (C) and PEG_{5K}-FTS_4 (D) conjugates in $CDCl_3$.

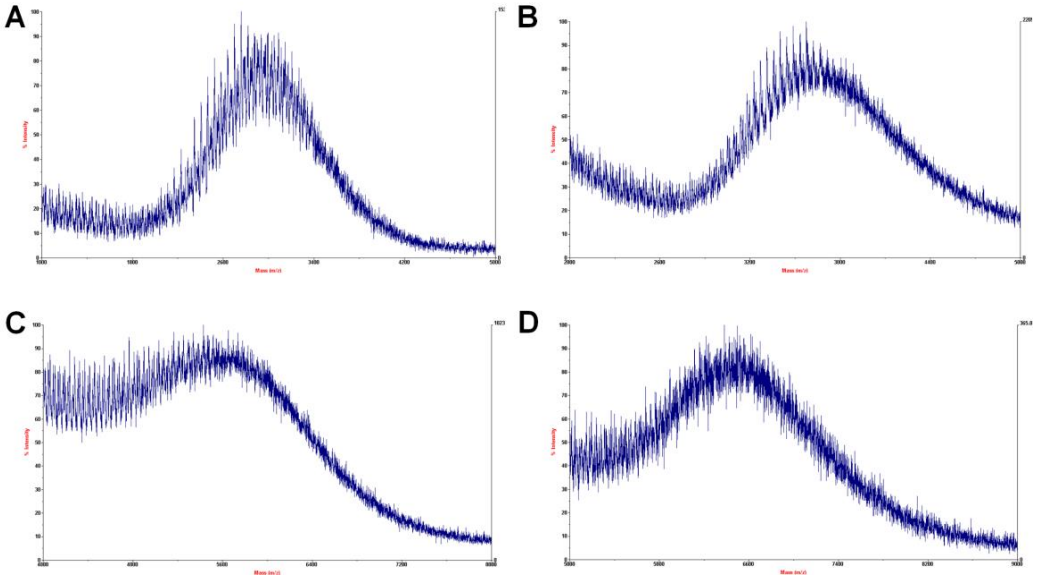

Figure 15. MADLI-TOF of PEG_{2K}-FTS_2 (A), PEG_{2K}-FTS_4 (B), PEG_{5K}-FTS_2 (C) and PEG_{5K}-FTS_4 (D) conjugates.

3.4.2 Size and size distribution of micelles

The four PEG-FTS conjugates readily formed micelles in aqueous solution with the particle sizes of 20-30 nm (**Table 2**). Dynamic light scattering (DLS) measurements showed that PEG_{5K}-FTS_4 micelles had hydrodynamic sizes around 27 nm at the concentration of 20 mg/mL (**Figure 16A**). TEM revealed spherical particles with uniform size distribution (**Figure 16B**). The size observed by TEM shows good agreement with that determined by DLS (**Figures 17 & 18**). PTX could be effectively loaded into PEG_{5K}-FTS_4 micelles. The spherical shape and size distribution were well retained when PTX was loaded into micelles at a drug concentration of 1 mg/mL and a carrier/drug ratio of 2.5/1 (m/m) (**Figure 16C & D**). Similar results were shown for the other three micelles (**Figures 17 & 18**).

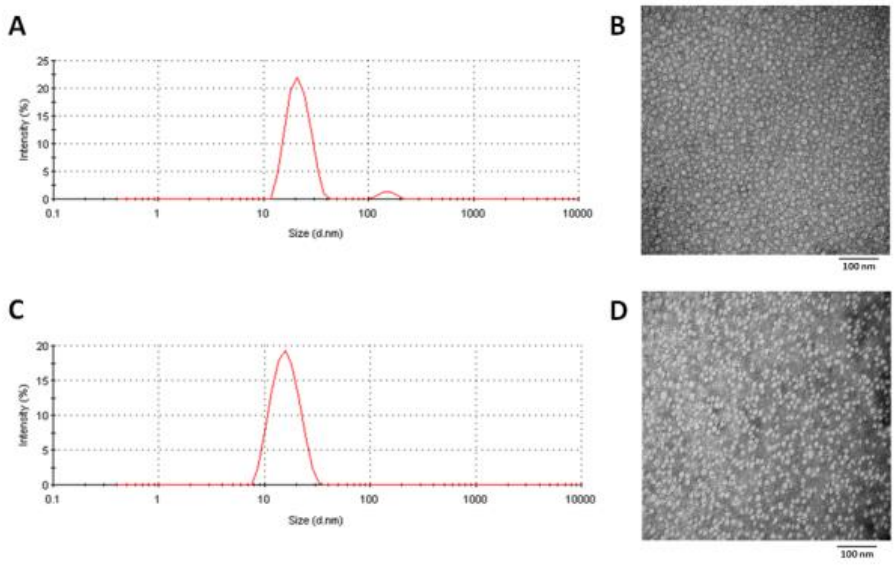

Figure 16. Particle size distribution and morphology of drug-free and PTX-loaded PEG_{5K}-FTS_4 micelles.
The size and size distribution of drug-free PEG_{5K}-FTS_4 micelles (A) and PTX-loaded PEG_{5K}-FTS_4 micelles (C) were evaluated by DLS. The morphology of drug-free PEG_{5K}-FTS_4 micelles (B) and PTX-loaded PEG_{5K}-FTS_4 micelles (D) was examined by TEM. The PTX concentration was kept at 1 mg/mL.

Table 2. Size and CMC of four PEG-FTS conjugates

Conjugates	Size[a]	PDI[b]	CMC[c] (μM)
PEG_{2K}-FTS_2	25.75	0.09	1.22
PEG_{2K}-FTS_4	26.12	0.15	1.43
PEG_{5K}-FTS_2	17.61	0.13	0.34
PEG_{5K}-FTS_4	26.80	0.12	0.29

[a]Measured by dynamic light scattering particle sizer. [b]PDI = polydispersity index. [c]CMC = critical micelle concentration.

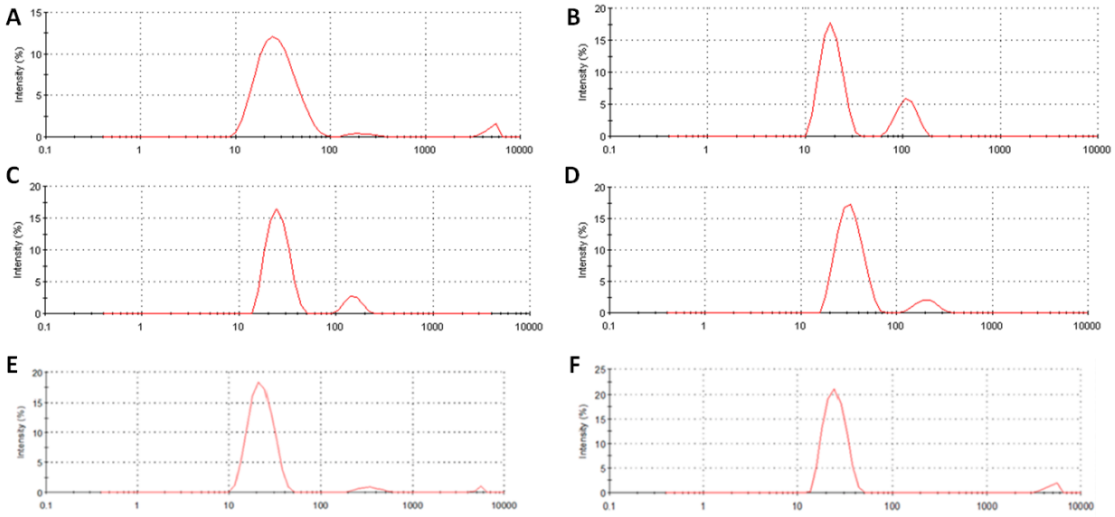

Figure 17. The size distribution of free PEG_{2K}-FTS_2 (A), PEG_{2K}-FTS_4 (C), PEG_{5K}-FTS_2 (E) micelles and PTX-loaded PEG_{2K}-FTS_2 (B), PEG_{2K}-FTS_4 (D), PEG_{5K}-FTS_2 (F) micelles in PBS measured by dynamic light scattering (DLS).

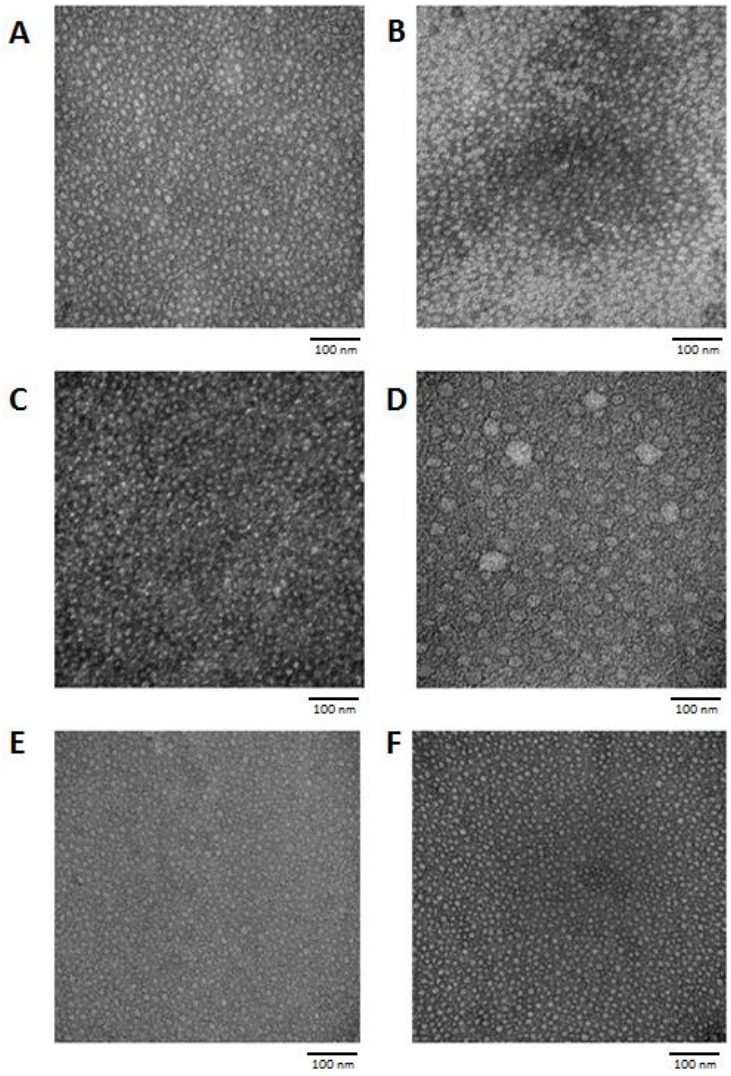

Figure 18. Transmission electron microscopy (TEM) of free PEG_{2K}-FTS_2 (A), PEG_{2K}-FTS_4 (C), PEG_{5K}-FTS_2 (E) micelles and PTX-loaded PEG_{2K}-FTS_2 (B), PEG_{2K}-FTS_4 (D), PEG_{5K}-FTS_2 (F) micelles.

3.4.3 Critical micelle concentration (CMC)

The CMC of PEG_{2K}-FTS_2, PEG_{2K}-FTS_4, PEG_{5K}-FTS_2 and PEG_{5K}-FTS_4 micelles were measured using pyrene as a fluorescence probe (**Table 2**). When the concentration of the PEG-FTS reached the CMC, the fluorescence intensity of pyrene would change dramatically due to the transfer of pyrene from polar micro-environment to non-polar surroundings caused by the formation of

micelles. The CMCs of PEG_{5K}-FTS_2 and PEG_{5K}-FTS_4 conjugates were determined to be 0.34 μM and 0.29 μM, respectively, which were lower than those of PEG_{2K}-FTS_2 (1.22 μM) and PEG_{2K}-FTS_4 (1.43 μM) (**Figure 19**). The lower CMCs of PEG_{5K}-FTS micelles may be attributed to the longer PEG hydrophilic chain and more effective stabilizing effect for the micelles.

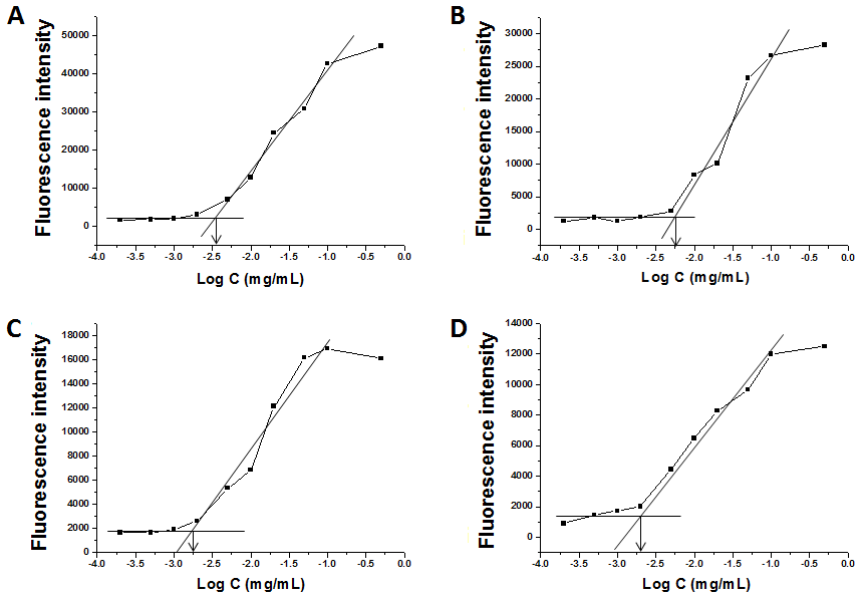

Figure 19. Critical micelle concentration (CMC) of PEG_{2K}-FTS_2 (A), PEG_{2K}-FTS_4 (B), PEG_{5K}-FTS_2 (C) and PEG_{5K}-FTS_4 (D) micelles.

3.4.4 Drug loading

The PTX loading of PEG_{2K}-FTS_2, PEG_{2K}-FTS_4, PEG_{5K}-FTS_2 and PEG_{5K}-FTS_4 micelles with different carrier to drug molar ratios was determined by HPLC (**Table 3**). The sizes of these PTX loaded PEG-FTS micelles were also evaluated under corresponding conditions. PEG_{5K}-FTS_4 micelles could effectively solubilize PTX in aqueous solution at a molar ratio as low as 1:1 (m/m) with particle size around 50 nm (**Table 3**). However, these PTX-loaded PEG_{5K}-FTS_4 micelles were only stable for 2.5 h. With an increase in carrier/drug ratio to 2.5/1, they formed mixed micelles with PTX that were stable for about one day. For the other three micelles, a

minimal carrier/drug ratio of 2.5/1 was required to solubilize PTX. Overall, the conjugates with four molecules of FTS worked better than the conjugates with two molecules of FTS and PEG_{5K} conjugates were more effective than the PEG_{2K} counterparts in forming stable drug loaded micelles. The four conjugates were ranked as PEG_{5K}-FTS_4 > PEG_{2K}-FTS_4 > PEG_{5K}-FTS_2 > PEG_{2K}- FTS_2 with respect to their efficiency in forming stable mixed micelles with PTX.

Table 3. Serum levels of transaminases in mice of different treatment groups

Groups	ALT (U/L)	AST (U/L)
PBS	37.3 ± 1.0	94.3 ± 20.4
Taxol (10 mg/kg)	22.2 ± 4.1	97.6 ± 1.4
PEG_{2K}-FTS_2/PTX (10 mg/kg)	23.2 ± 1.7	102.6 ± 15.9
PEG_{2K}-FTS_4/PTX (10 mg/kg)	26.4 ± 1.0	94.3 ± 36.4
PEG_{5K}-FTS_2/PTX (10 mg/kg)	22.2 ± 0.7	86.3 ± 11.5
PEG_{5K}-FTS_4/PTX (10 mg/kg)	24.0 ± 2.8	130.3 ± 28.8

ALT = alanine aminotransferase
AST = aspartate aminotransferase

3.4.5 *In vitro* PTX release study

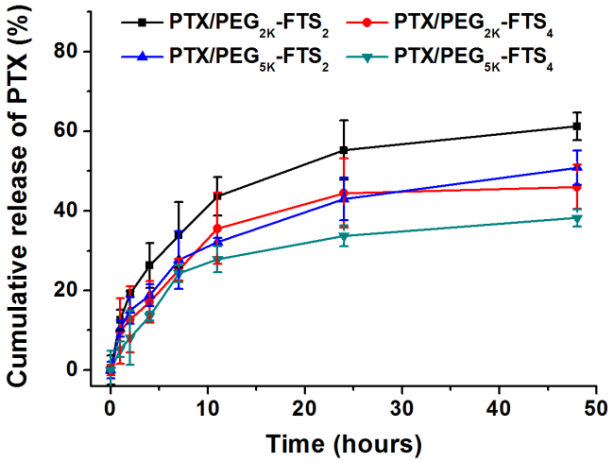

Figure 20. Cumulative PTX release profile from four PTX-loaded PEG-FTS micelles. PBS containing 0.5% (w/v) Tween 80 was used as the release medium. PTX concentration was fixed at 0.5 mg PTX/mL. Values reported are the means ± SD for triplicate samples.

The profile of PTX release from the four PEG-FTS micelles was examined by a dialysis method. As shown in **Figure 20**, PEG_{5K}-FTS_4/PTX mixed micelles showed relatively slower kinetics of PTX release compared to other PTX-loaded PEG-FTS micelles.

3.4.6 Hemolytic effect of PEG-FTS micelles

As a delivery system for intravenous application, the potential detrimental interaction of PEG-FTS-based micellar system with blood components should be minimized. **Figure 21** shows the hemolytic activities of drug-free PEG_{2K}-FTS_2, PEG_{2K}-FTS_4, PEG_{5K}-FTS_2 and PEG_{5K}-FTS_4 micelles. Polyethylenimine (PEI), a cationic polymer known to have significant hemolytic effect [86], was included as a positive control. PEI induced hemolysis in a concentration-dependent manner. In contrast, all of the four drug-free PEG-FTS micelles displayed only negligible levels of hemolytic activities, suggesting that PEG-FTS micelles are mild surfactants suitable for *in vivo* delivery of hydrophobic anticancer drugs.

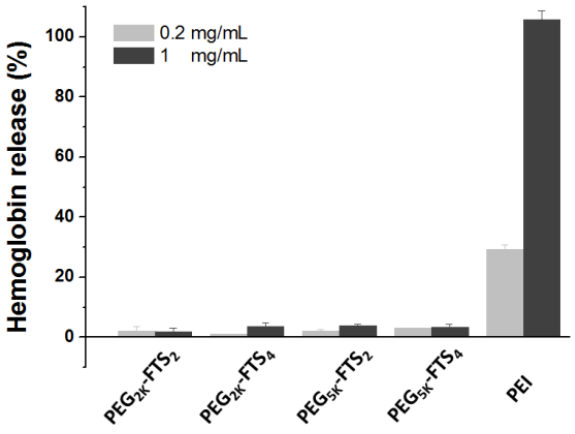

Figure 21. *In vitro* hemolysis assay of four PEG-FTS micelles compared with PEI.
Rat RBCs were treated with the 4 different PEG-FTS micelles or PET at 0.2 and 1 mg/mL, respectively. The lysis of RBCs was determined by measuring the release of hemoglobin spectrophotometrically (λ = 540 nm). RBCs incubated with PBS and Triton X-100 (2%) were used as the negative and positive controls. Values reported are the means ± SD for triplicate samples.

3.4.7 *In vitro* cytotoxicity

Figure 22A shows the cytotoxicity of 4 carriers alone in MCF-7 cells. The FTS_2 conjugates (PEG_{2K}-FTS_2 and PEG_{5K}-FTS_2) were more effective than FTS_4 conjugates (PEG_{2K}- FTS_4 and PEG_{5K}-FTS_4) in inhibiting the tumor cell proliferation. Similar results were found when the four conjugates were examined in HCT-116 (**Figure 22B**) and 4T1.2 cells (**Figure 22C**).

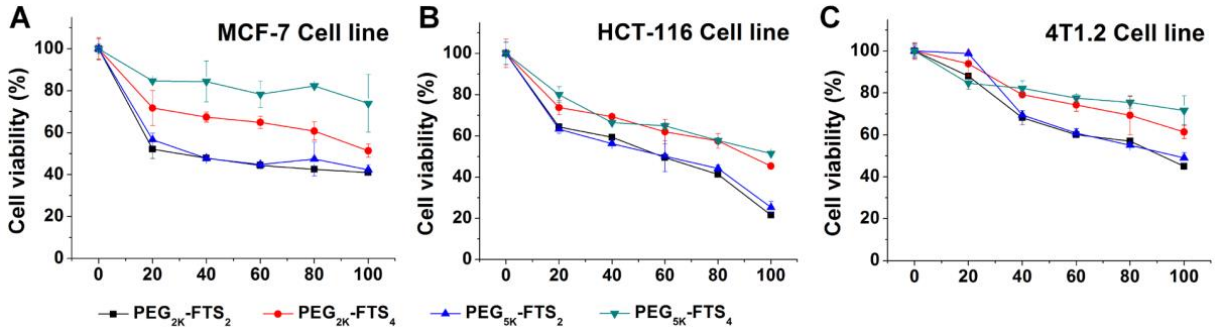

Figure 22. Cytotoxicity of four drug-free PEG-FTS micelles in MCF-7 human breast carcinoma cell line (A), HCT-116 human colon carcinoma cell line (B) and 4T1.2 mouse breast cancer cell line (C).
Cells were treated with different micelles for 72 h and cytotoxicity was determined by MTT assay. Values reported are the means ± SD for triplicate samples.

3.4.8 Western blotting

Figure 23 shows the protein expression level of total Ras 20 h following treatment of HCT-116 cells with the four different conjugates at a FTS concentration of 40 μM. Downregulation of Ras protein expression was seen in all treatment groups. However, the conjugates with two FTS molecules were more active than the counterparts with four FTS molecules in reducing the protein expression levels of Ras in HCT-116 cells.

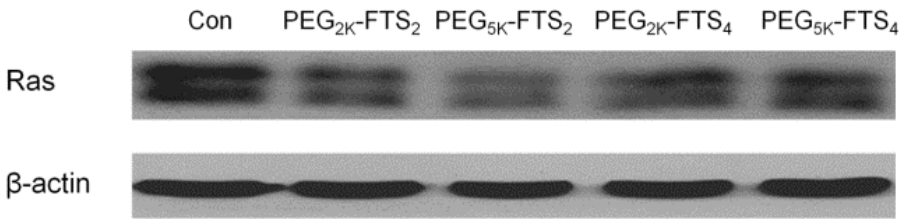

Figure 23. Effects of PEG-FTS micelles on total Ras protein expression in HCT-116 cells. HCT-116 cells were treated with four different PEG-FTS micelles for 20 h (at a FTS concentration of 40 μM). The protein expression level of total Ras was examined by Western blotting.

3.4.9 *In vitro* cytotoxicity of PTX-loaded micelles

Figure 24 shows the cytotoxicity of free PTX (in DMSO) and PTX formulated in PEG_{2K}-FTS_2, PEG_{2K}-FTS_4, PEG_{5K}-FTS_2 and PEG_{5K}-FTS_4 micelles in 4T1.2 cell line. Free PTX inhibited the cell growth in a dose-dependent manner. Delivery of PTX via the four different PEG-FTS micelles led to varied levels of improvement. Nonetheless, PTX-loaded PEG_{5K}-FTS_4 micelles were more potent than PTX formulated in the other micellar formulations (PEG_{2K}-FTS_2, PEG_{2K}-FTS_4 and PEG_{5K}-FTS_2) in inhibiting the tumor cell growth. The IC_{50} of free PTX and the four micellar formulations of PTX are summarized in **Table 4**.

Table 4. IC_{50} of PTX-loaded PEG-FTS micelles compared to free PTX in 4T1.2 mouse breast cancer cell line.

IC_{50} (ng/mL)				
PTX	PEG_{2K}-FTS_2/PTX	PEG_{2K}-FTS_4/PTX	PEG_{5K}-FTS_2/PTX	PEG_{5K}-FTS_4/PTX
202.0	72.8	181.8	59.3	33.2

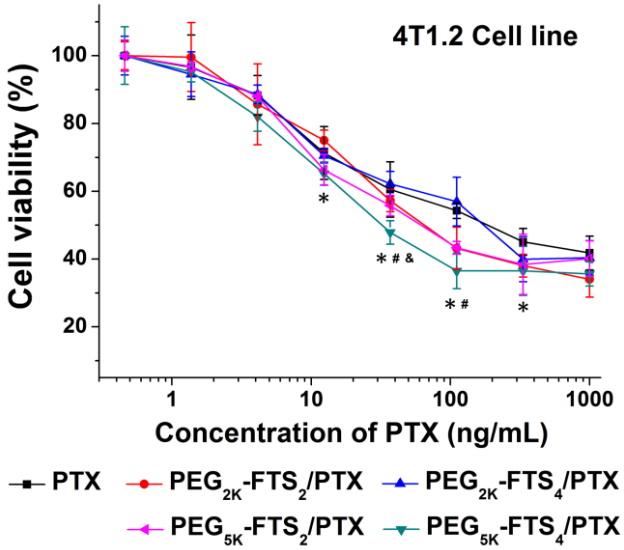

Figure 24. Cytotoxicity of PTX-loaded PEG-FTS micelles in 4T1.2 mouse breast cancer cell line.
Cells were treated with free PTX or different micellar formulations of PTX for 72 h and cytotoxicity was determined by MTT assay. PTX-loaded PEG_{5K}-FTS_4 micelles showed an improvement in cell growth inhibition compared with other formulations. *P<0.05 (PTX/PEG_{5K}-FTS_4 vs PTX), $^{\#}$P<0.05 (PTX/PEG_{5K}-FTS_4 vs PTX/PEG_{5K}-FTS_2 or PTX/PEG_{2K}-FTS_4), $^{\&}$P<0.05 (PTX/PEG_{5K}-FTS_4 vs PTX/PEG_{2K}-FTS_2, PTX/PEG_{5K}-FTS_2 or PTX/PEG_{2K}-FTS_4). Values reported are the means ± SD for triplicate samples.

3.4.10 *In vivo* therapeutic study

The *in vivo* therapeutic effectiveness of PTX formulated in PEG_{2K}-FTS_2, PEG_{2K}-FTS_4, PEG_{5K}-FTS_2, and PEG_{5K}-FTS_4 micelles was evaluated, respectively, in a syngeneic murine breast cancer model (4T1.2), and compared to Taxol. As shown in **Figure 25A**, PTX-loaded PEG_{2K}-FTS_2 micelles exhibited a similar tumor growth inhibitory effect compared to Taxol treatment group. In contrast, PTX formulated in PEG_{5K}-FTS_2 and PEG_{5K}-FTS_4 micelles demonstrated a significantly enhanced antitumor activity compared to Taxol (P < 0.01). Furthermore, PTX formulated in PEG_{5K}-FTS_4 showed a trend of improvement in antitumor activity compared with PTX formulated in PEG_{5K}-FTS_2 (P = 0.09). No significant changes in body weight were noticed in all treatment groups compared to PBS control group (**Figure 25B**). In addition, serum levels

of transaminases in the mice with different treatments were comparable to those in PBS control group (**Table 5**).

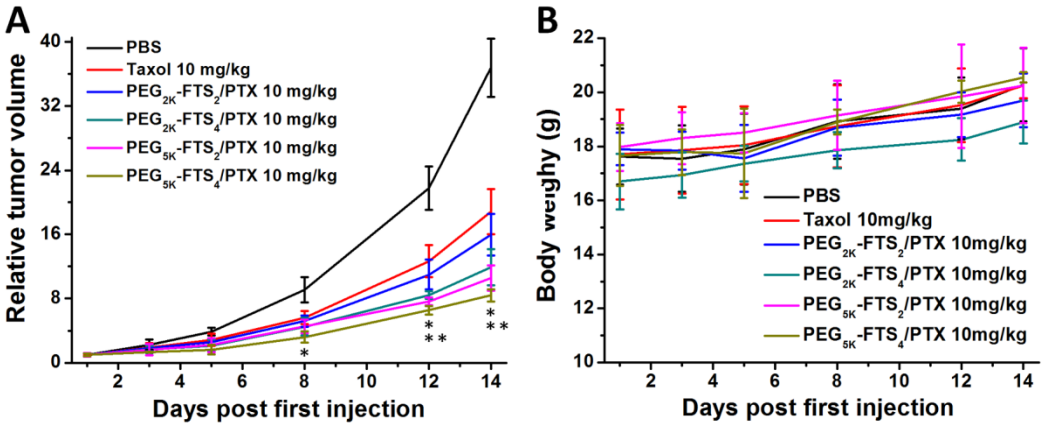

Figure 25. Enhanced anti-tumor efficacy of PTX loaded in PEG_{5K}-FTS_4 micelles. BABL/c mice were inoculated s.c. with 4T1.2 cells (2×10^5 cells/mouse). Six days later, mice received various treatments twice a week and tumor growth was monitored and plotted as relative tumor volume (A). Significant improvement in antitumor activity was found for the PTX-loaded PEG_{5K}-FTS_4 group compared with the Taxol group (**P<0.01; N=5) and the group of PTX-loaded PEG_{2K}-FTS_2 (*P<0.05; N=5). Changes in body weights of mice in different treatment groups were also monitored (B).

Table 5. Serum levels of transaminases in mice of different treatment groups

Groups	ALT[a] (U/L)	AST[b] (U/L)
PBS	37.3 ± 1.0	94.3 ± 20.4
Taxol (10 mg/kg)	22.2 ± 4.1	97.6 ± 1.4
PEG_{2K}-FTS_2/PTX (10 mg/kg)	23.2 ± 1.7	102.6 ± 15.9
PEG_{2K}-FTS_4/PTX (10 mg/kg)	26.4 ± 1.0	94.3 ± 36.4
PEG_{5K}-FTS_2/PTX (10 mg/kg)	22.2 ± 0.7	86.3 ± 11.5
PEG_{5K}-FTS_4/PTX (10 mg/kg)	24.0 ± 2.8	130.3 ± 28.8

ALT[a] = alanine aminotransferase
AST[b] = aspartate aminotransferase

3.5 DISCUSSION

We have systematically compared the physicochemical property and the *in vitro* and *in vivo* PTX delivery efficiency of four PEG-FTS conjugates that vary in the length of PEG motif (PEG_{2K} vs PEG_{5K}) and the molar ratio of PEG/FTS (1/2 vs 1/4). All of the four PEG-FTS micelles possessed very small sizes of 20-30 nm. After drug loading, micelles retained small size of 20-60 nm. Doxil (doxorubicin HCl liposome) and Abraxane (albumin-bound paclitaxel) are two FDA-approved formulations. The particle sizes of Doxil and Abraxane are ~150 and 130 nm, respectively. Their relatively large sizes may limit the diffusion in the tumor, and thus limit their therapeutic effectiveness [106]. It has been reported that nanoparticles need to be smaller than 100 nm in order to circumvent macrophage clearance in the lungs [15] and that particles of further reduced size (≤ 64 nm) are needed for effective penetration through neovasculatures to reach tumor cells [17, 32]. The small sizes of our PEG-FTS micelles shall ensure efficient passive targeting to the solid tumors.

In addition to size, drug loading capacity and formulation stability are two other important features for an effective micellar system. Our data showed that the PEG-FTS conjugates with four FTS molecules were significantly more effective than the conjugates with two molecules of FTS in forming stable drug-loaded micelles. Previous studies have shown that increasing the ratio of hydrophobic/hydrophilic blocks is associated with increased drug loading capacity and enhanced formulation stability [32]. The improved performance of PEG-FTS conjugates with an increased number of core forming units may be attributed to a similar mechanism. FTS, as a hydrophobic core of micelles, has a lipid chain and benzene ring structure. The lipid chain of FTS contributes to the loading of hydrophobic drug through hydrophobic interaction. At the same time, the benzene ring of FTS is capable of forming π-π interaction with

drug carrying aromatic ring structure. In PEG-FTS micellar system, π-π stacking and hydrophobic interaction are likely to work cooperatively to promote both drug/carrier and carrier/carrier interactions. Such interactions are also expected to be further enhanced with an increase in the number of FTS molecules in PEG-FTS conjugates.

PEG is widely used as a polymeric steric stabilizer. A prominent advantage of PEG modification is to impart the *in vivo* longevity to drug carriers. Torchilin's group [20] has reported that the PEG/core ratio affected the performance of the micelles. Furthermore, the length of PEG also acted on the CMC, which in turn influenced the performance of the micelles, particularly *in vivo* [8, 102]. Our data showed that PEG_{5K}-conjugates had a lower CMC and were more effective than PEG_{2K}-conjugates in forming stable micelles with PTX.

One unique feature for PEG-FTS micellar delivery system is its intrinsic antitumor activity. The four different PEG-FTS conjugates showed varied levels of antitumor activity by themselves in three cancer cell lines. The conjugates with two FTS molecules showed higher levels of cytotoxicity compared to the counterparts with four FTS molecules. The higher levels of cytotoxicity for the conjugates with two FTS molecules are unlikely due to a more active surface activity of the double chain conjugates as all of the four conjugates showed minimal hemolytic activity (**Figure 21**). It is likely that active FTS is more readily cleaved from the conjugates with two FTS than the ones with four FTS molecules due to less steric hindrance to intracellular esterases. We also compared the *in vitro* cytotoxicity of the four PTX-loaded PEG-FTS micelles (**Figure 24**). PTX-loaded PEG_{5K}-FTS_4 micelles showed better cytotoxicity than free PTX and PTX formulated in other three micelles in 4T1.2 cells. This is likely due to a more efficient intracellular delivery of PTX via PEG_{5K}-FTS_4 micelles because PEG_{5K}-FTS_4 formed the most stable micelles with PTX among the four micellar systems tested.

In vivo therapy study clearly showed a significantly higher level of antitumor activity for PTX formulated in PEG_{5K}-FTS_4 micelles compared to either Taxol or PTX formulated in PEG_{2K}-FTS_2 (**Figure 25A**). This is likely due to the significantly improved stability for PEG_{5K}-FTS_4 micelles, which contributes to more effective delivery of PTX to tumor tissue *in vivo*.

4.0 TARGETED DELIVERY OF ANTICANCER AGENTS VIA A DUAL FUNCTION NANOCARRIER WITH AN INTERFACIAL DRUG-INTERACTIVE MOTIF

4.1 ABSTRACT

We have developed a dual-function drug carrier, polyethylene glycol (PEG)-derivatized farnesylthiosalicylate (FTS). Here we report that incorporation of a drug-interactive motif (Fmoc) into PEG_{5k}-FTS_2 led to further improvement in both drug loading capacity and formulation stability. Doxorubicin (DOX) formulated in PEG_{5k}−Fmoc−FTS_2 showed sustained release kinetics slower than those of DOX loaded in PEG_{5k}-FTS_2. The maximum tolerated dose of DOX- or paclitaxel (PTX)-loaded PEG_{5k}-Fmoc-FTS_2 was significantly higher than that of the free drug. Pharmacokinetics and biodistribution studies showed that DOX/PEG_{5k}-Fmoc-FTS_2 mixed micelles were able to retain DOX in the bloodstream for a significant amount of time and efficiently deliver the drug to tumor sites. More importantly, drug (DOX or PTX)-loaded PEG_{5k}-Fmoc-FTS_2 led to superior antitumor activity over other treatments including drugs formulated in PEG_{5k}-FTS_2 in breast cancer and prostate cancer models. Our improved dual function carrier with a built-in drug-interactive motif represents a simple and effective system for targeted delivery of anticancer agents.

4.2 BACKGROUD

Formulations represent an important strategy to improve the therapeutic index of anticancer agents via improving their solubility, bioavailability, and pharmacokinetic and biodistribution profiles [97, 107]. Taxol® is a FDA-approved clinical formulation of paclitaxel (PTX) in which Cremophor EL/ethanol (1:1, v/v) mixture is used to solubilize PTX. However, Taxol® can cause hyperactivity reactions, neuropathy, and other serious side effects [93]. PEGylated liposomal doxorubicin (DOX) (Doxil®) is the first nanoformulation of DOX approved by the FDA. Although Doxil® has demonstrated decreased cardiotoxicity, it shows limited improvement over free DOX in therapeutic efficacy. In addition, Doxil is associated with other side effects such as hand-foot syndrome [108]. Over the last 2-3 decades, micelles with a nanoscopic supramolecular core-shell structure have gained increasing attention [5, 109] due to their easy preparation, small sizes, and their ability to improve the pharmacokinetics and efficacy of anticancer drugs [13, 18, 40, 110, 111]. However, most delivery systems involve the use of “inert” materials that do not possess any favourable biological activity. One interesting approach is the development of dual function carriers that have both a delivery function and an antitumor activity [65, 67, 97, 100, 102, 112, 113].

We have recently reported a new self-assembling nanomicellar system that is based on pegylated S-trans, trans-farnesylthiosalicylic acid (FTS) [67]. FTS, a synthetic farnesylcysteine mimetic, is a potent and especially nontoxic Ras antagonist [82, 114]. Constitutively active Ras caused by mutation in the Ras family of proto-oncogenes is present in one-third of human cancers [53, 115]. FTS can inhibit Ras-dependent tumor growth with no adverse toxicity [57]. One major mechanism involves affecting membrane interaction of Ras by competing with Ras for binding to Ras-escort proteins, and thereby inhibiting its signaling [55]. In addition to its

antitumor activity in mice and humans, FTS also exhibits anti-inflammatory activity [64, 99]. However, FTS has poor water solubility and limited oral bioavailability [66]. PEGylation was initially designed to improve its solubility. Interestingly, the PEG_{5k}-FTS_2 conjugate self-assembled to form small-sized micelles (20-30 nm) that were effective in solubilizing other hydrophobic drugs such as PTX. PEG_{5k}-FTS_2 differs from most drug carriers in that it shows an antitumor activity that is comparable to that of free FTS [67]. Additionally, PTX formulated in PEG_{5k}-FTS_2 micelles demonstrated a synergistic antitumor activity that was significantly higher than that of Taxol [67].

Most reported micellar systems including PEG_{5k}-FTS_2 are designed to load drugs through hydrophobic interactions. While working well for highly hydrophobic drugs, they only have limited effectiveness in formulating drugs that are either moderately hydrophobic or hydrophilic. The carrier/drug incompatibility will result in not only low drug loading capacity but also limited stability of the drug-loaded micelles [116]. Park's group has shown that inclusion of less hydrophobic and hydrogen bond-forming "hydrotropic motifs" into the hydrophobic domain of polymeric micelles significantly improved both drug loading capacity and the colloidal stability of drug-loaded micelles [68, 116, 117]. However, this concept has not been demonstrated in lipidic systems. We hypothesized that incorporation of a drug-interactive motif into a surfactant at the interfacial region will provide an additional carrier/drug interaction mechanism, which could enhance both drug-loading capacity and formulation stability [69, 110]. Among several motifs screened, the 9-Fluorenylmethoxycarbony (Fmoc) moiety, a functional group that is routinely used for amino acid protection, was demonstrated to be the most potent drug-interactive group [69]. We demonstrated that incorporation of Fmoc motifs into a PEG-

lipopeptide conjugate led to a significant improvement in loading of a number of therapeutic agents of diverse structures [70, 118].

Considering the significance of Fmoc as a novel "formulation chemophor" or a structural unit capable of interacting with many pharmaceutical agents, we hypothesized that incorporation of Fmoc will further improve the performance of our PEG_{5k}-FTS_2 delivery system. We report in this study the development and characterization of a new micellar carrier composed of an FTS-based hydrophobic domain, a PEG hydrophilic segment and a drug-interactive Fmoc motif (PEG_{5k}-Fmoc-FTS_2). Our data showed that inclusion of an Fmoc motif into PEG_{5k}-FTS_2 led to a significant improvement in drug loading capacity for both PTX and DOX. More importantly, delivery of PTX or DOX via PEG_{5k}-Fmoc-FTS_2 led to superior antitumor activity over other treatments including drugs formulated in PEG_{5k}-FTS_2 micelles in breast cancer and prostate cancer models.

4.3 EXPERIMENTAL PROCEDURE

4.3.1 Materials

Paclitaxel (98%) was purchased from AK Scientific Inc. (CA, USA). Doxorubicin (>99%) was purchased from LC Laboratories (MA, USA). 1,1'-dioctadecyl-3,3,3',3'-tetramethylindodicarbocyanine perchlorate, D-307 (DiD) were purchased from Invitrogen (NY, USA). *N*-hydroxysuccinimide (NHS) and dicyclohexylcarbodiimide (DCC) were purchased from Alfa Aesar (MA, USA). 4-(dimethylamino) pyridine (DMAP) was purchased from Calbiochem-

Novabiochem Corporation (CA, USA). FTS was synthesized and purified following a published literature [103].

4.3.2 Synthesis of PEG_{5K}-Fmoc-FTS_2 conjugate

PEG_{5K}-Fmoc-FTS_2 was synthesized via solution condensation reactions from poly(ethylene glycol) methyl ether (mPEG-OH, Mw=5000 Da) ($mPEG_{5K}$-OH) (**Figure 26**). $MPEG_{5K}$-OH was reacted with succinate anhydride (5 eq.) in CH_2Cl_2 overnight using DMAP (5 eq.) as a catalyst. The PEG derivative was precipitated with 10 volume of cold ether and washed with ether twice. Excess DMAP was removed by additional washes with cold ethanol (Yield = 91%). The carboxy-terminated mPEG ($mPEG_{5K}$-COOH) was then reacted with tris(hydroxymethyl)aminomethane (Tris) in the presence of NHS (3 eq.) and DCC (3 eq.) in CH_2Cl_2 for one day, followed by a similar purification step as described above (Yield = 92%). The two hydroxyl groups in the PEG-derivatized Tris were blocked by forming acetonide using p-Toluenesulfonic acid (TsOH) as a catalyst in acetone (Quantitative). Then, Fmoc group was coupled to the remaining OH of Tris via reaction with 9-fluorenylmethoxycarbonyl chloride (Fmoc-Cl) (2 eq.) and triethylamine (3 eq.) in CH_2Cl_2 overnight. PEGylated molecules were similarly purified as described above and acetonide group was removed by treatment with 1% TsOH in CH_2Cl_2 (Yield = 50%, 2 steps). Finally, FTS (4 eq.) was coupled onto the PEGylated molecules with DCC (4 eq.) and DMAP (0.4 eq.) as the coupling reagents. The reaction mixture was filtered and precipitated with ether and ethanol twice, and concentrated under vacuum (Yield = 85%). The powder was then dissolved in water and filtered through a filter with a pore size of 0.2 μm. The final product was obtained by lyophilizing the filtrate. PEG_{5K}-FTS_2 was synthesized following our reported method [67].

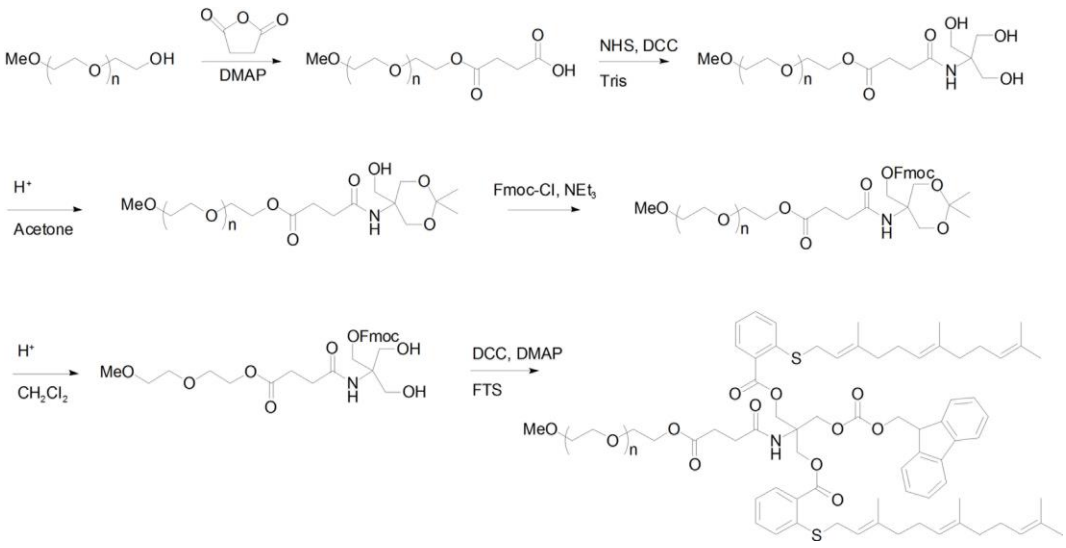

Figure 26. Synthesis scheme of PEG_{5K}-Fmoc-FTS_2 conjugate

4.3.3 Preparation and characterization of PTX- and DOX-loaded micelles

PTX (10 mM in chloroform) and PEG_{5K}-Fmoc-FTS_2 conjugate (10 mM in chloroform) were mixed with various carrier/drug ratios. After removing chloroform, a thin film of drug/carrier mixture was formed. PTX-loaded micelles were formed by adding DPBS to hydrate the thin film followed by gentle votexing. To load DOX into PEG_{5K}-Fmoc-FTS_2 micelle, DOX·HCl was first treated with triethylamine (3 eq.) in a mixture of chloroform ($CHCl_3$)/methanol (MeOH) (1:1, v/v) to remove HCl from DOX·HCl. DOX-loaded PEG_{5K}-Fmoc-FTS_2 micelles were then similarly prepared as described above. The PTX loading efficiency was quantified by high performance liquid chromatography (HPLC) as described before [67]. The DOX loading efficiency was examined by Waters Alliance 2695 Separations Module combined with Waters 2475 Fluorescence Detector (Excitation: 490 nm; Emission: 590 nm; Gain: 3; Sensitivity (FUFS): 10000). Hibar 250-4 LiChrosorb RP-8 (5 micron) column (Sorbent Lot no. L59040432) was used and the mobile phase consisted of acetonitrile/water (52.5:47.5, v/v) with 2.5 mM

CH_3COONH_4 and 0.05% (v/v) CH_3COOH. The flow rate of mobile phase was 1 mL/min and running time was 12 mins. Drug loading capacity (DLC) and drug loading efficiency (DLE) were calculated from the following equations:

$$\text{DLC (\%)} = [\text{weight of drug loaded}/(\text{weight of polymer + drug used})] \times 100\%$$

$$\text{DLE (\%)} = (\text{weight of loaded drug}/\text{weight of input drug}) \times 100\%$$

The mean diameter, morphology and size distribution of PEG_{5K}-Fmoc-FTS_2 micelles were assessed by dynamic light scattering (DLS) and transmission electron microscopy (TEM). The critical micelle concentration (CMC) of PEG_{5K}-Fmoc-FTS_2 micelles was determined using pyrene as a fluorescence probe [119]. The *in vitro* kinetics of DOX release from PEG_{5K}-Fmoc-FTS_2 micelles was examined by a dialysis method [120]. The hemolytic effect of PEG_{5K}-Fmoc-FTS_2 micelles was examined as described [102].

4.3.4 Cell culture and animals

4T1.2 (mouse metastatic breast cancer cell line), MCF-7 (human breast carcinoma cell line), and A549 (human lung adenocarcinoma epithelial cell line) were obtained from ATCC (VA, USA). HCT116 (human colon carcinoma cell line) was kindly provided by Dr. Lin Zhang (University of Pittsburgh Cancer Institute). All cell lines were cultured in DMEM containing 5% FBS and 1% penicillin-streptomycin at 37 ℃ in a humidified 5 % CO_2 atmosphere. Female BALB/c mice, 4-6 weeks in age, and CD-1 mice, 4-6 weeks in age, were purchased from Charles River (Davis, CA). Male nude mice, 6-8 weeks in age, were purchased from Harlan (Livermore, CA). All animals were housed under pathogen-free conditions according to AAALAC guidelines. All animal-related experiments were performed in full compliance with institutional guidelines and

approved by the Animal Use and Care Administrative Advisory Committee at the University of Pittsburgh.

4.3.5 *In vitro* cytotoxicity study

The cytotoxicity of drugs (PTX and DOX) formulated in PEG_{5K}-Fmoc-FTS_2 micelles was assessed with several cancer cell lines and compared to Taxol and free DOX, respectively, by MTT assay [67]. The cytotoxicity of free PEG_{5K}-FTS_2, PEG_{5K}-Fmoc-FTS_2 and FTS was also examined.

4.3.6 Maximum tolerated dose (MTD) studies

Groups of 4 female CD-1 mice were administered intravenously with free DOX (5, 10, 15, 20 mg DOX/kg), DOX-loaded PEG_{5K}-Fmoc-FTS_2 micelles (5, 10, 15, 20, 25, 30 mg DOX/kg), Taxol (15, 20, 25 mg PTX/kg), or PTX-loaded PEG_{5K}-Fmoc-FTS_2 micelles (50, 75, 100, 120, 140 mg PTX/kg), respectively. Changes in body weight and mouse survival were monitored daily for two weeks. The MTD was defined as the maximal dose that causes neither greater than 15% of body weight loss nor mouse mortality within two weeks after administration [102].

4.3.7 NIRF optical imaging

Nude mice bearing bilateral s.c. PC-3 xenografts were i.v. injected with 200 μL of DiD-loaded PEG_{5K}-Fmoc-FTS_2 at a concentration of 0.4 mg/mL. At indicated times (0.5 h, 6 h, 24 h, 48 h, 72 h and 96 h), the mice were scanned using a Carestream Molecular Imaging System, *In vivo*

Multispectral FX PRO, with the excitation at 630 nm and the emission at 700 nm using a 30 s exposure time. The mice were anesthetized by isoflurane inhalation before each imaging. After 96 h, the mice were euthanized by CO_2 overdose. The tumor and major organs were excised for *ex vivo* imaging.

4.3.8 Plasma pharmacokinetics and tissue distribution

DOX·HCl and DOX-loaded PEG_{5K}-Fmoc-FTS_2 micelles were injected into female BALB/c mice via tail vein at a dose of 5 mg DOX/kg. The blood samples were collected in heparinized tubes at different time points (3 min, 8 min, 15min, 30 min, 1 h, 2 h, 4 h, 8 h, and 12 h) post-injection. The blood was centrifuged (2500 rpm, 10 min) and plasma was collected for the analysis. DOX in plasma was extracted by extraction buffer (10% Triton X-100, deionized water, and isopropanol at a volumetric ratio of 1:2:15) [110]. DOX was examined by HPLC using fluorescence detection. Non-compartmental pharmacokinetic analysis was done by WinNonlin. For tissue biodistribution study, DOX·HCl and DOX-loaded PEG_{5K}-Fmoc-FTS_2 were injected into female BALB/c mice bearing 4T1.2 breast tumor at a dose of 5 mg DOX/kg, respectively. At day 1 post-injection, tumor tissues and major organs were collected from the mice. The tissues were weighed and homogenized using Homogenizer PowerGen 500 (Fisher Scientific). The tissue solutions were mixed with the extraction buffer and DOX was extracted overnight at -20 ℃. The solutions were centrifuged (2500 rpm, 10 min) and the supernatant was used for HPLC measurement. The concentrations of DOX in tissues were determined based on the standard curve of DOX in blood.

4.3.9 *In vivo* therapeutic study

Two tumor models (a syngeneic murine breast cancer model (4T1.2) and a human prostate cancer (PC-3) xenograft model) were used to assess the therapeutic activity of PTX or DOX formulated in PEG_{5K}-Fmoc-FTS_2 micelles. The breast cancer model was established by inoculation of 4T1.2 cells (1×10^5) in 200 μL PBS at the right flank of female BALB/c mice. Treatments were started when tumors achieved a volume of ~50 mm^3 and this day was designated as day 1. Then tumor-bearing mice were randomly divided into six groups (n=5) and administered i.v. with PBS (control), PEG_{5K}-Fmoc-FTS_2 micelles, Taxol (10 mg PTX/kg), PTX-loaded PEG_{5K}-Fmoc-FTS_2 micelles (10, 20 mg PTX/kg), and PTX-loaded PEG_{5K}-FTS_2 (10 mg PTX/kg), respectively on days 1, 3, 5, 8, 11 and 14. Free PEG_{5K}-Fmoc-FTS_2 micelles were given at the equivalent dosage of the carrier in the group of PTX-loaded PEG_{5K}-Fmoc-FTS_2 micelles (10 mg PTX/kg). The therapeutic effect of DOX-loaded PEG_{5K}-Fmoc-FTS_2 micelles (5, 10 mg DOX/kg) was similarly evaluated in 4T1.2 tumor model. Controls include PBS, PEG_{5K}-Fmoc-FTS_2 micelles, DOX·HCl (5 mg DOX/kg), liposomal DOX (5 mg DOX/kg), and DOX-loaded PEG_{5K}-FTS_2 (5 mg DOX/kg). Tumor sizes were measured with digital caliper three times per week and calculated as $V = (L \times W^2)/2$, L = the longest diameter, W = the shortest diameter (mm). Each group was compared by relative tumor volume (RTV) (where RTV equals to the tumor volume divided by the initial tumor volume before treatment). Mice were sacrificed when the tumors developed ulceration or reached 2000 mm^3. The body weights of all mice from different groups were monitored every three days. The antitumor activity of PTX-loaded PEG_{5K}-Fmoc-FTS_2 micelles was further evaluated in a human prostate cancer xenograft model, PC-3. Different groups were similarly treated as described above on days 1, 3, 6, 9 and 12. Tumor size and body weight were monitored as described above.

4.3.10 Statistical analysis

Data are presented as mean ± standard deviation (SD). Statistical analysis was performed by Student's t-test for comparison of two groups, and comparisons for multiple groups were made with one-way analysis of variance (ANOVA), followed by Newman-Keuls test if the overall $P < 0.05$. In all statistical analysis, the threshold of significance was defined as $P < 0.05$.

4.4 RESULTS AND DISCUSSION

4.4.1 Preparation and characterization of drug-loaded PEG_{5K}-Fmoc-FTS_2 micelles

PEG_{5K}-Fmoc-FTS_2 conjugate, containing one Fmoc motif and two molecules of FTS coupled to one molecule of PEG via a labile ester linkage, was synthesized via solution condensation reactions (**Figure 26 and 27**). ^{1}H NMR spectrum of PEG_{5K}-Fmoc-FTS_2 conjugate is shown in **Figure 28**, with signals at 3.63 ppm and 7-8 ppm attributable to the methylene protons of PEG and benzene ring protons of Fmoc motif, respectively. Carbon chain and benzene ring signals of FTS were located at 1.5-2.2 and 7-8 ppm, respectively. The molecular weight of the PEG_{5K}-Fmoc-FTS_2 conjugate measured by MALDI-TOF Mass Spectra is close to the theoretical value (6105) (**Figure 29**), indicating the successful synthesis of PEG_{5K}-Fmoc-FTS_2 conjugate.

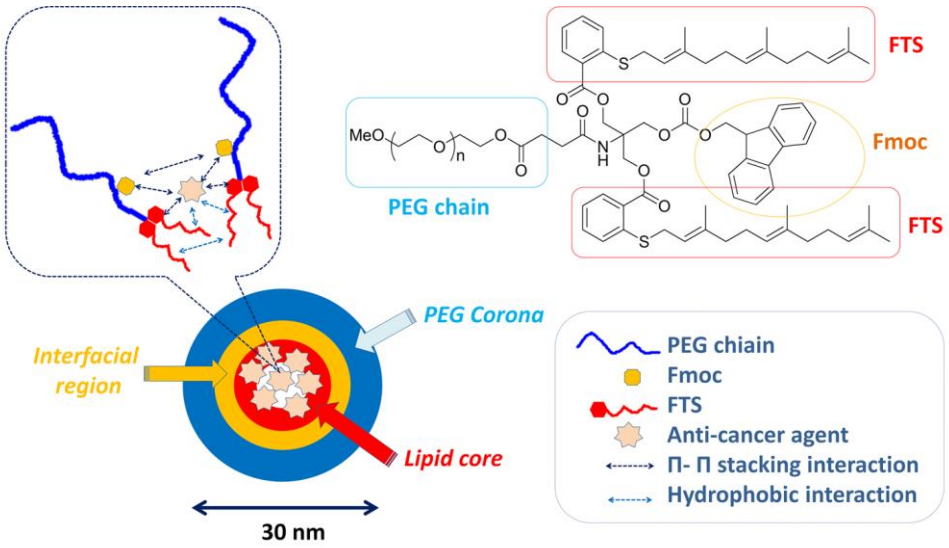

Figure 27. Chemical structure of PEG_{5K}-Fmoc-FTS_2 and the postulated model of carrier/drug interaction.

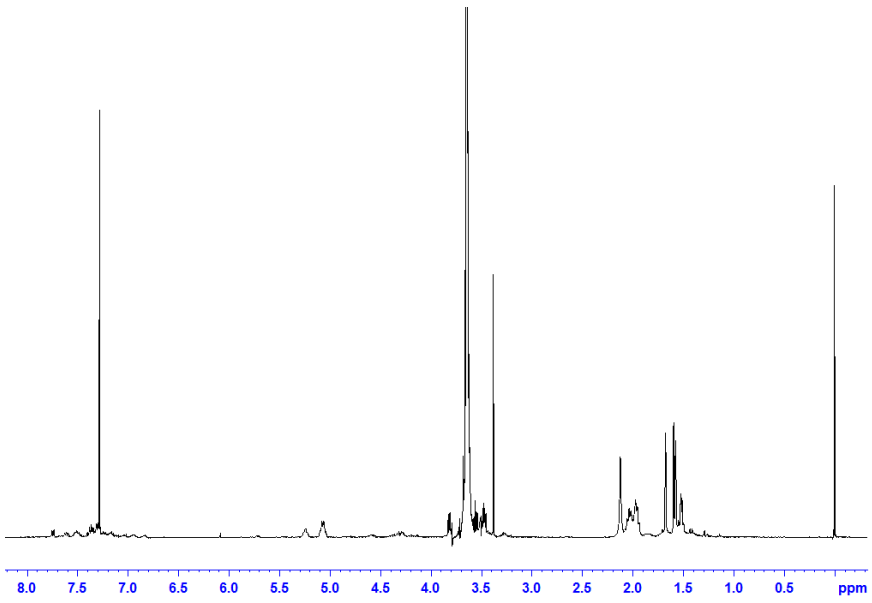

Figure 28. ^{1}HNMR spectra (400MHz) of PEG_{5K}-Fmoc-FTS_2 conjugate in $CDCl_3$.

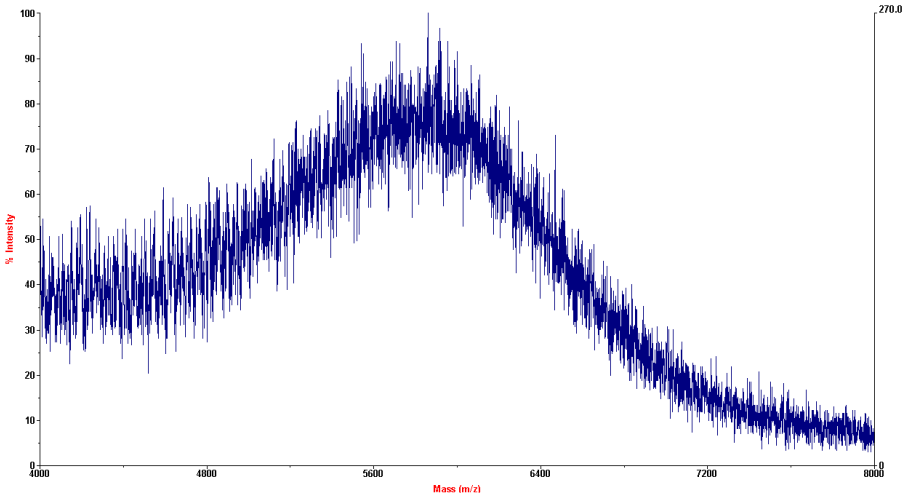

Figure 29. MADLI-TOF of PEG_{5K}-Fmoc-FTS_2 conjugate

Similar to PEG_{5K}-FTS_2 micellar system, the PEG_{5K}-Fmoc-FTS_2 conjugate readily formed micelles in aqueous solution (**Figure 30**). DLS measurements showed that PEG_{5K}-Fmoc-FTS_2 micelles had hydrodynamic sizes around 20 nm at the concentration of 20 mg/mL (**Figure 30A**). TEM showed spherical particles with a uniform size distribution (**Figure 30B**). PEG_{5K}-Fmoc-FTS_2 conjugate forms small-sized micelles that were highly effective in solubilizing various anticancer drugs such as PTX, DOX (**Tables 6 and 7**), and many others (data not shown). It has been demonstrated that the size of the particles needs to be within sub-100 nm range for them to efficiently reach the poorly vascularized tumors [32]. Such small sizes are also critical to enable the particles effective in deep penetration into the tumor tissues, especially the tumors with a tough tangle of collagen such as pancreatic and some breast cancers [98].

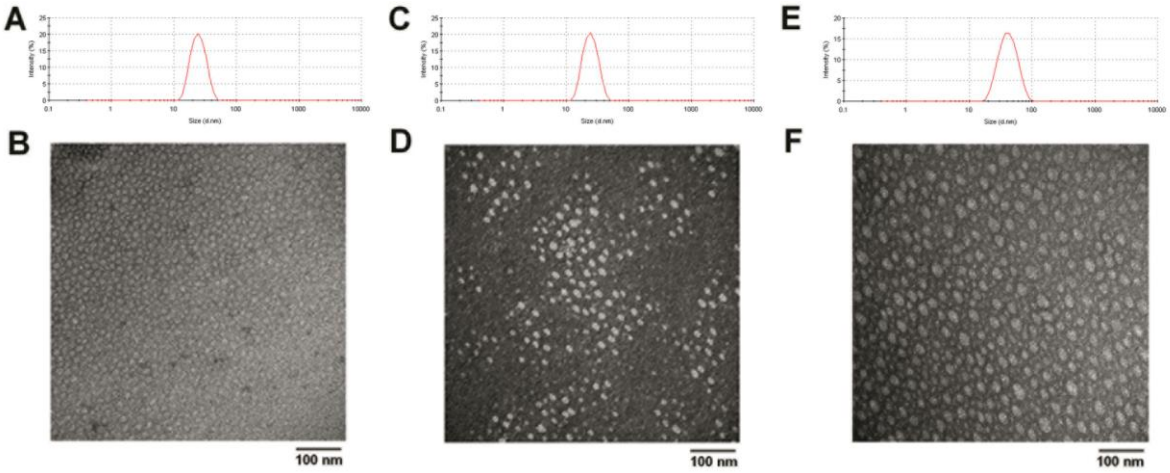

Figure 30. The size distribution and morphology of free drug PEG_{5K}-Fmoc-FTS_2 micelles (A, B), PTX-loaded PEG_{5K}-Fmoc-FTS_2 micelles (C, D) and DOX-loaded PEG_{5K}-Fmoc-FTS_2 micelles (E, F) measured by DLS and TEM, respectively.
Drug concentration in micelle was kept at 1 mg/mL. Blank micelle concentration was 20 mg/mL.

Table 6. Physicochemical characterization of drug-free and DOX-loaded PEG_{5k}-FTS_2 and PEG_{5k}-Fmoc-FTS_2 micelles.

Micelles	Molar Ratio	Conc. of DOX[a)] (mg/mL)	Size[b)] (nm)	PDI[c)]	DLC[d)] (%)	DLE[e)] (%)	Stability[f)] (hour)
PEG_{5K}-FTS_2	-	-	17.6	0.20	-	-	-
PEG_{5K}-FTS_2 : DOX	0.5 :1	1	100.9	0.37	10.2	65.5	30
PEG_{5K}-FTS_2 : DOX	1 :1	1	69.7	0.29	7.5	88.1	48
PEG_{5K}-FTS_2 : DOX	2.5 :1	1	24.2	0.27	3.2	90.2	120
PEG_{5K}-Fmoc-FTS_2	-	-	24.8	0.22	-	-	-
PEG_{5K}-Fmoc-FTS_2 : DOX	0.1 :1	1	130.4	0.29	32.8	69.7	20
PEG_{5K}-Fmoc-FTS_2 : DOX	0.25 :1	1	173.9	0.32	17	65.9	48
PEG_{5K}-Fmoc-FTS_2 : DOX	0.5 :1	1	120.0	0.33	10.2	67.8	120
PEG_{5K}-Fmoc-FTS_2 : DOX	1 :1	1	29.23	0.31	6.6	81.2	240
PEG_{5K}-Fmoc-FTS_2 : DOX	2.5 :1	1	25.67	0.21	3.1	91.2	336

[a)]DOX concentration in micelle was kept at 1 mg/mL. Blank micelle concentration was 20 mg/mL. Values reported are the mean ± SD for triplicate samples. [b)]Measured by dynamic light scattering particle sizer. [c)]PDI = polydispersity index. [d)]DLC = drug loading capacity. [e)]DLE = drug loading efficiency. [f)]Data means there was no noticeable size change during the follow-up period.

Table 7. Physicochemical characterization of drug-free and PTX-loaded PEG_{5k}-FTS_2 and PEG_{5k}-Fmoc-FTS_2 micelles.

Micelles	Molar Ratio	Conc. of PTX[a)] (mg/mL)	Size[b)] (nm)	PDI[c)]	DLC[d)] (%)	DLE[e)] (%)	Stability[f)] (hour)
PEG_{5K}-FTS_2	-	-	17.6	0.20	-	-	-
PEG_{5K}-FTS_2 : PTX	2.5 :1	1	24.9	0.35	4.5	81.2	2
PEG_{5K}-FTS_2 : PTX	5 :1	1	25.6	0.23	2.8	97.6	20
PEG_{5K}-Fmoc-FTS_2	-	-	24.8	0.22	-	-	-
PEG_{5K}-Fmoc-FTS_2 : PTX	0.5 :1	1	36.2	0.19	12.1	55.4	12
PEG_{5K}-Fmoc-FTS_2 : PTX	1 :1	1	29.4	0.11	9.0	73.2	15
PEG_{5K}-Fmoc-FTS_2 : PTX	2.5 :1	1	29.7	0.12	4.6	87.3	17
PEG_{5K}-Fmoc-FTS_2 : PTX	5 :1	1	25.9	0.27	2.6	96.0	48

[a)]PTX concentration in micelle was kept at 1 mg/mL. Blank micelle concentration was 20 mg/mL. Values reported are the mean ± SD for triplicate samples. [b)]Measured by dynamic light scattering particle sizer. [c)]PDI = polydispersity index. [d)]DLC = drug loading capacity. [e)]DLE = drug loading efficiency. [f)]Data means there was no noticeable size change during the follow-up period.

The size, DLC, DLE, and colloidal stability of drug-loaded PEG_{5K}-Fmoc-FTS_2 micelles were then examined and compared to those of the counterparts without an Fmoc motif. In general, incorporation of DOX or PTX led to an increase in the particle sizes for both micellar systems. However, the sizes gradually became close to the original size with the increase in carrier/drug molar ratio. For DOX, a minimal carrier/drug molar ratio of 0.5:1 was needed to formulate the drug in PEG_{5K}-FTS_2 micelles (**Table 6**). In contrast, DOX could be loaded into PEG_{5K}-Fmoc-FTS_2 micelles at a carrier/drug molar ratio as low as 0.1:1. The DLC for DOX/PEG_{5K}-Fmoc-FTS_2 mixed micelles at this carrier/drug ratio is 32.8%, which represents a 3.2-fold increase compared with the PEG_{5K}-FTS_2 formulation. In addition, DOX/PEG_{5K}-Fmoc-FTS_2 mixed micelles were significantly more stable than the counterparts without an Fmoc motif under all carrier/drug ratios examined (**Table 6**). Similarly, incorporation of an Fmoc motif

significantly improved the performance of PEG_{5K}-FTS_2 micelles in formulating PTX (**Table 7**). The DLC for PTX/PEG_{5K}-Fmoc-FTS_2 mixed micelles was 12.1%, which is a 2.7-fold increase compared with the counterpart without an Fmoc. The morphology and size uniformity were largely retained following loading of PTX (**Figures 30C and D**) or DOX (**Figures 30E and F**) at a respective molar ratio of 2.5:1 and 1:1. Incorporation of an Fmoc group into PEG_{5K}-FTS_2 system led to a significant improvement in drug loading capacity for PTX or DOX and the colloidal stability of the resulting drug-loaded micelles was also significantly improved (**Tables 6 and 7**). These improvements are likely due to an enhanced drug/carrier interaction. Fmoc group contains a bulky, fused fluorenylmethyl ring structure capable of providing strong hydrophobic interaction and forming π-π stacking with compounds carrying aromatic moieties (**Figure 27, unpublished data**).

The CMC of PEG_{5K}-Fmoc-FTS_2 micelles was examined using pyrene as a fluorescence probe (**Figure 31**). The CMC of the PEG_{5K}-Fmoc-FTS_2 micelles is 0.2 μM (**Figure 31**), which is lower than that of PEG_{5K}-FTS_2 micelles (0.68 μM) [67]. This is due to that Fmoc can not only enhance the carrier/drug interaction, but also facilitate the interaction among the carrier molecules. The reduced CMC will improve the stability of PEG_{5K}-Fmoc-FTS_2 micelles upon dilution *in vivo*.

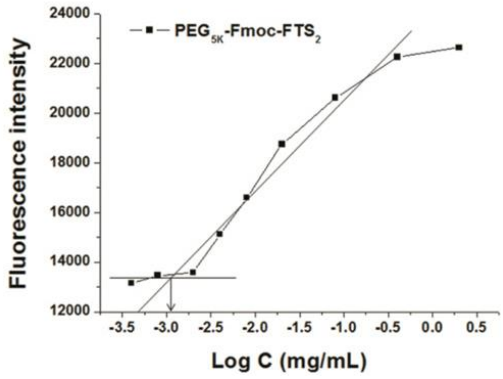

Figure 31. CMC of PEG_{5K}-Fmoc-FTS_2 micelles

4.4.2 *In vitro* drug release study

The profile of DOX release from PEG_{5K}-Fmoc-FTS_2 micelles was examined by a dialysis method and compared to that of DOX-loaded PEG_{5K}-FTS_2 micelles. For the initial 8 h, about 50.7 % of DOX was released from PEG_{5K}-FTS_2 formulation while only 38.3 % of DOX was released from DOX-loaded PEG_{5K}-Fmoc-FTS_2 micelles (**Figure 32**). Overall, DOX formulated in PEG_{5k}-Fmoc-FTS_2 micelles exhibited a slower relative rate of DOX release compared to the counterpart without an Fmoc motif.

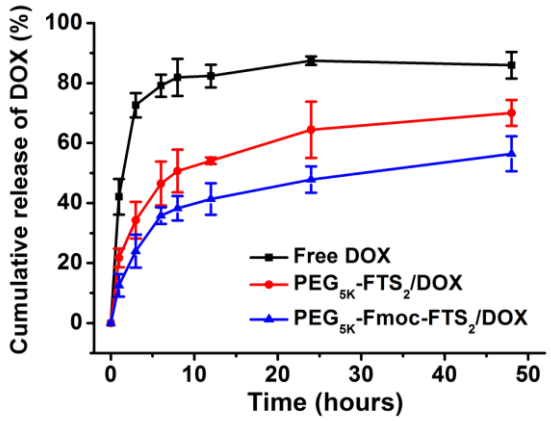

Figure 32. Cumulative DOX release profile from free DOX, DOX-loaded PEG_{5K}-FTS_2 and PEG_{5K}-Fmoc-FTS_2 micelles.DPBS (PH = 7.4) containing 0.5% (w/v) Tween 80 was used as the release medium. Values reported are the means ± SD for triplicate samples.

4.4.3 Hemolytic effect of micelles

Figure 33 shows the hemolytic activities of drug-free PEG_{5K}-Fmoc-FTS_2 micelles and polyethylenimine (PEI), a cationic polymer known to have significant hemolytic effect [86]. PEI induced hemolysis in a dose-dependent manner. In contrast, PEG_{5K}-Fmoc-FTS_2 micelles showed

only negligible levels of hemolytic activity at the same experimental concentrations, suggesting the safe profile of PEG_{5K}-Fmoc-FTS_2 micelles.

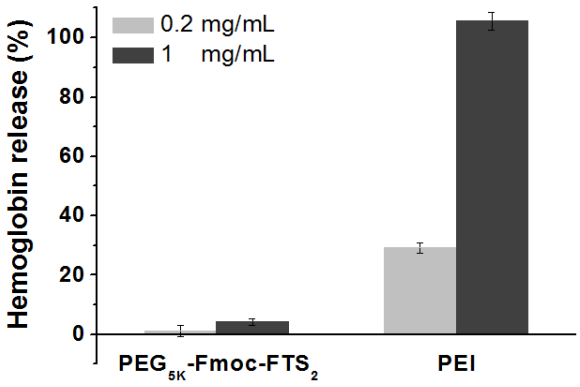

Figure 33. *In vitro* hemolysis assay of PEG_{5k}-Fmoc-FTS_2 micelles compared with PEI with two different concentrations (0.2, 1 mg/mL).
Values reported are the mean ± SD for triplicate samples.

4.4.4 *In vitro* cytotoxicity of free and drug-loaded micelles

The cytotoxicity of drug-free PEG_{5K}-Fmoc-FTS_2 and PEG_{5K}-FTS_2 micelles was examined in 4T1.2 and HCT-116 tumor cells and compared to free FTS (**Figures 34A and B**). Free FTS inhibited the tumor cell growth in a concentration-dependent manner. The two FTS conjugates were comparable but slightly less active than free FTS in cytotoxicity towards both 4T1.2 and HCT-116 tumor cells (**Figures 34A and B**). Cytotoxicity of PEG_{5K}-FTS_2 conjugate was well retained following the incorporation of an Fmoc motif (**Figures 34A and B**). The cytotoxicity of PEG_{5K}-Fmoc-FTS_2 is unlikely to be attributed to the surface activity since PEG-Fmoc-FTS_2 micelles showed minimal hemolytic activity at the concentrations that were much higher than those used in the cytotoxicity study (**Figure 33**). It is likely that the cytotoxicity of PEG-FTS comes from the released FTS following intracellular delivery. This is supported by the

observation that a PEG_{5K}-FTS_2 conjugate with a relatively labile ester linkage is more active than a similar conjugate with a relatively stable amide linkage [67].

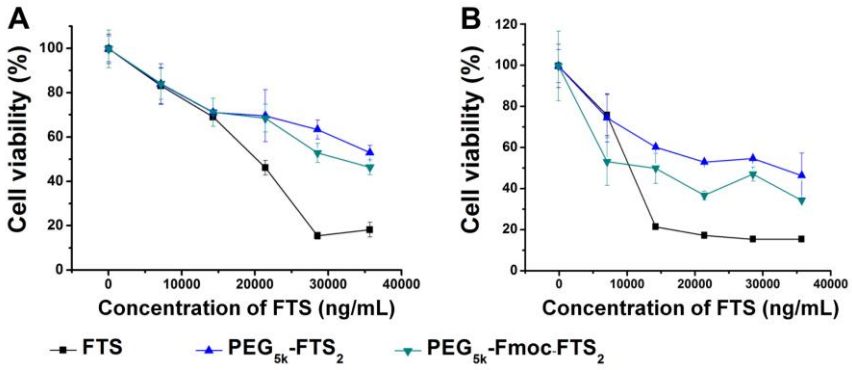

Figure 34. Cytotoxicity of drug-free PEG_{5k}-FTS_2 and PEG_{5k}-Fmoc-FTS_2 micelles compared to FTS against 4T1.2 mouse breast cancer cell line (A) and HCT-116 human colon carcinoma cell line (B).

Figures 35A-C show the cytotoxicity of Taxol and PTX formulated in PEG_{5K}-Fmoc-FTS_2 micelles in several cancer cell lines. Taxol inhibited the tumor cell growth in a concentration dependent manner. Delivery of PTX via PEG_{5K}-Fmoc-FTS_2 micelles led to a significant increase in the cytotoxicity at low concentrations. We also tested the cytotoxicity of DOX formulated in PEG_{5K}-Fmoc-FTS_2 micelles and compared to free DOX·HCl. Similarly, DOX-loaded PEG_{5K}-Fmoc-FTS_2 micelles showed more potent cytotoxicity than free DOX at the low concentration range (**Figures 35D~F**). When PTX or DOX was formulated into the PEG_{5K}-Fmoc-FTS_2 micelles, they showed better cytotoxicity to MCF-7, A549 and HCT-116 cancer cells compared with Taxol formulation or free DOX (**Figures 35A-F**), suggesting that PTX or DOX can be more effectively delivered into tumor cells by PEG_{5K}-Fmoc-FTS_2 micelles, resulting in enhanced tumor cell killing.

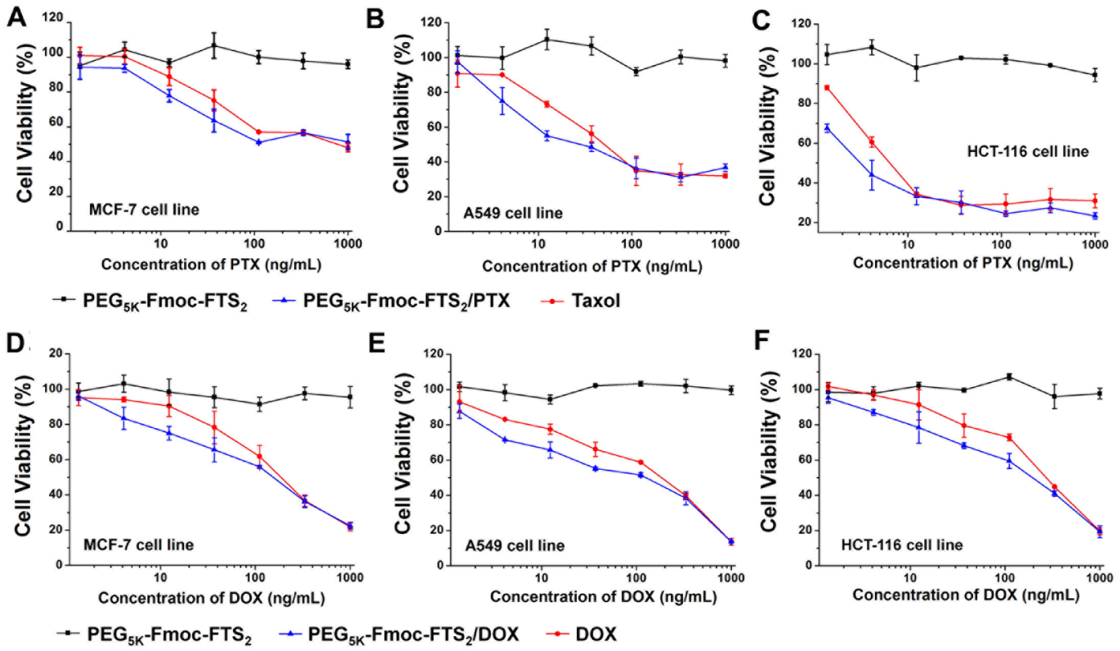

Figure 35. The anticancer effect of Taxol, drug-free and PTX/ PEG_{5k}-Fmoc-FTS_2 micelles. Performed on MCF-7 human breast carcinoma cell line (A), A549 human lung adenocarcinoma epithelial cell line (B) and HCT-116 human colon carcinoma cell line (C). Tumor cell killing of free DOX, drug-free and DOX-loaded PEG_{5k}-Fmoc-FTS_2 micelles was performed in MCF-7 human breast carcinoma cell line (D), A549 human lung adenocarcinoma epithelial cell line (E) and HCT-116 human colon carcinoma cell line (F). Cells were treated for 72 h and cytotoxicity was determined by MTT assay. Values reported are the means ± SD for triplicate samples.

4.4.5 Maximum tolerated dose (MTD) studies

Groups of 4 female CD-1 mice were administered intravenously with a single dose of either Taxol (15-25 mg PTX/kg) or PTX-loaded PEG_{5K}-Fmoc-FTS_2 micelles (50-140 mg PTX/kg). Taxol was well tolerated at the dose of 15 mg PTX/kg (**Table 8**). However, increasing the PTX dosage to 20 mg/kg resulted in the death of 1 out of the 4 treated mice (**Table 8**). For the mice treated with PTX-loaded PEG_{5K}-Fmoc-FTS_2 micelles, there was neither significant weight loss nor noticeable changes in normal activity at a PTX dosage as high as 140 mg/kg (**Table 8**). Therefore, the MTD for PTX/PEG_{5K}-Fmoc-FTS_2 is greater than 140 mg/kg, which is

significantly higher than that for Taxol (15-20 mg/kg). **Figure 36** shows the result of MTD study for DOX-loaded PEG_{5K}-Fmoc-FTS_2 micelles. There were no obvious body weight loss and other toxicity signs in the mice treated with DOX-loaded PEG_{5K}-Fmoc-FTS_2 micelles at the doses of 5-15 mg DOX/kg within two weeks. Only a moderate body weight loss (<10%) was found in mice treated with 20 mg/kg of DOX/PEG_{5K}-Fmoc-FTS_2 micelles on day 4, which was recovered on day 5. In contrast, although free DOX was well tolerated at the dose of 10 mg/kg, it caused a significant decrease (>15%) in the body weight, and eventually the death of all treated mice at a dose of 15 mg DOX/kg (**Table 8**). Thus, the MTD of DOX-loaded PEG_{5K}-Fmoc-FTS_2 micelles and free DOX is ~20 mg/kg and 10 mg/kg, respectively. Drug (DOX or PTX)-loaded PEG_{5K}-Fmoc-FTS_2 micelles demonstrated an excellent safety profile with a significantly higher MTD compared with free drug (**Table 8 and Figure 36**). This is likely due to a slow relative rate of drug release from the micelles before they reach the tumor site, leading to reduced drug uptake by normal tissues.

Table 8. Animal deaths in the MTD study

Formulation	Dose (mg/kg)	Animal death	Weight loss (%)
Taxol	15	0/4	-11.2*
Taxol	20	1/4	N/A
Taxol	25	3/4	N/A
PEG_{5K}-Fmoc-FTS_2/PTX	50	0/4	-13.1
PEG_{5K}-Fmoc-FTS_2/PTX	75	0/4	-10.8
PEG_{5K}-Fmoc-FTS_2/PTX	100	0/4	-8.3
PEG_{5K}-Fmoc-FTS_2/PTX	120	0/4	-4.5
PEG_{5K}-Fmoc-FTS_2/PTX	140	0/4	-1.6
Free DOX	5	0/4	-17.7
Free DOX	10	0/4	-11.0
Free DOX	15	4/4	N/A
Free DOX	20	4/4	N/A
PEG_{5K}-Fmoc-FTS_2/DOX	5	0/4	-24.2

PEG_{5K}-Fmoc-FTS_2/DOX	10	0/4	-21.2
PEG_{5K}-Fmoc-FTS_2/DOX	15	0/4	-15.2
PEG_{5K}-Fmoc-FTS_2/DOX	20	0/4	-6.4
PEG_{5K}-Fmoc-FTS_2/DOX	25	4/4	N/A
PEG_{5K}-Fmoc-FTS_2/DOX	30	4/4	N/A

* Negative values reflect the body weight increase.

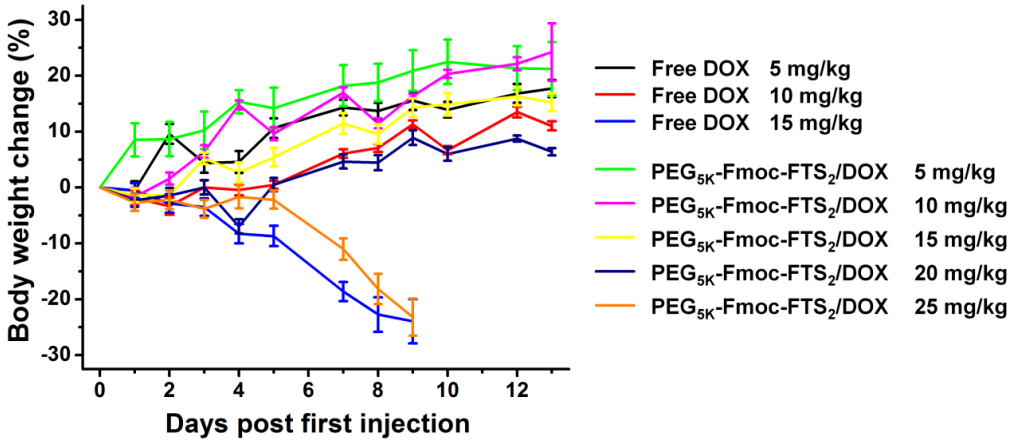

Figure 36. Body weight change of normal CD-1 mice (n = 4) administered intravenously with equivalent doses of free DOX or DOX-loaded PEG_{5k}-Fmoc-FTS_2 micelles in the MTD study.

4.4.6 NIRF optical imaging

Biodistribution and tumor-targeting efficiency of PEG_{5K}-Fmoc-FTS_2 micelles were tested in a human prostate cancer xenograft model (PC-3). DiD, a hydrophobic near infrared fluorescence (NIRF) dye with high penetration, low tissue absorption and scattering was loaded into the PEG_{5K}-Fmoc-FTS_2 micelles for tissue imaging. **Figure 37A** shows that DiD-loaded PEG_{5K}-Fmoc-FTS_2 micelles were able to accumulate at the tumor as early as 6 h post injection, and these micelles retained in the tumor at 96 h after injection. No obvious tumor accumulation was observed in the mice treated with free DiD dye [18]. After last imaging at 96 h post-injection, tumors and major organs were excised for *ex vivo* imaging. As shown in **Figure 37B & C**,

significantly higher levels of signal were observed in the tumor tissues compared with normal organs except the lung. The very small size of our micellar system may contribute significantly to the effective tumor localization (**Figure 37A**). Interestingly, little fluorescence signal was observed in liver and spleen, the two major internal organs that are involved in the nonspecific clearance of nanoparticles.

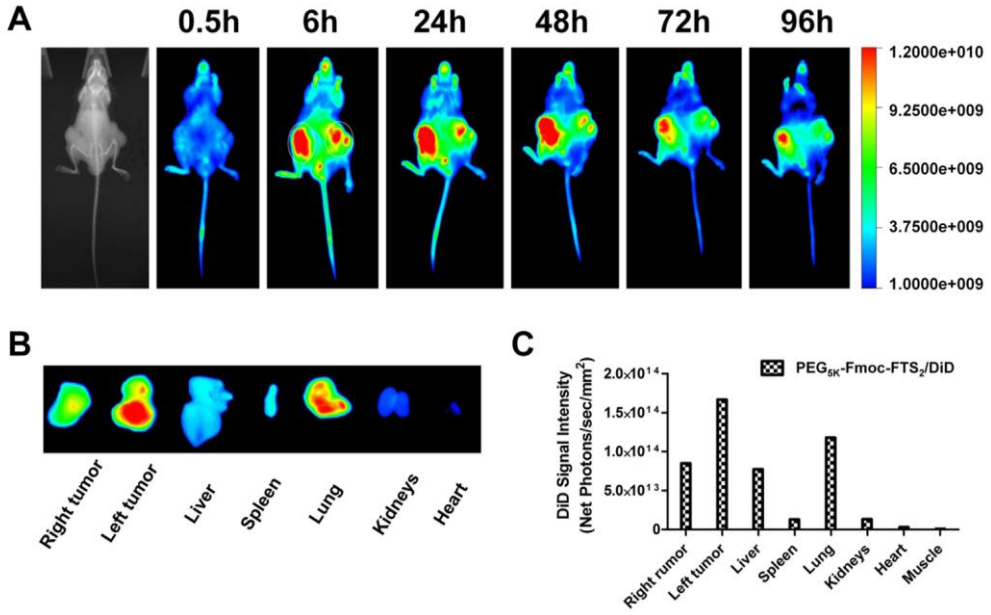

Figure 37. *In vivo* (A) and *ex vivo* (B) NIRF imaging of DiD-loaded PEG_{5k}-Fmoc-FTS_2 micelles in prostate cancer PC-3 xenograft-bearing mice. Quantitative fluorescence intensities of tumors and major organs from *ex vivo* images at 24 h (C).

4.4.7 Plasma pharmacokinetics and tissue distribution

Free DOX·HCl and DOX-loaded PEG_{5K}-Fmoc-FTS_2 micelles were injected to tumor-free mice at a dose of 5 mg/kg, and the DOX concentration in plasma was measured at different time points. **Figure 38A** shows the % of injected dose of DOX in the blood over time following i.v. administration. The pharmacokinetic parameters were calculated based on a non-compartment model and summarized in **Table 9**. The $T_{1/2}$ of DOX in DOX-loaded PEG_{5K}-Fmoc-FTS_2

micelles was 6.7-fold higher than that of free DOX. Furthermore, the plasma $AUC_{0\text{-}inf}$ of DOX for the micellar DOX was almost 19-fold higher than that of free DOX (64.8 vs 3.43 μg x h/mL). In contrast, the Vd of DOX for micellar DOX was significantly lower than that of free DOX (2.58 vs 7.34 L/kg), suggesting prolonged blood circulation of DOX-loaded PEG_{5K}-Fmoc-FTS_2 micelles.

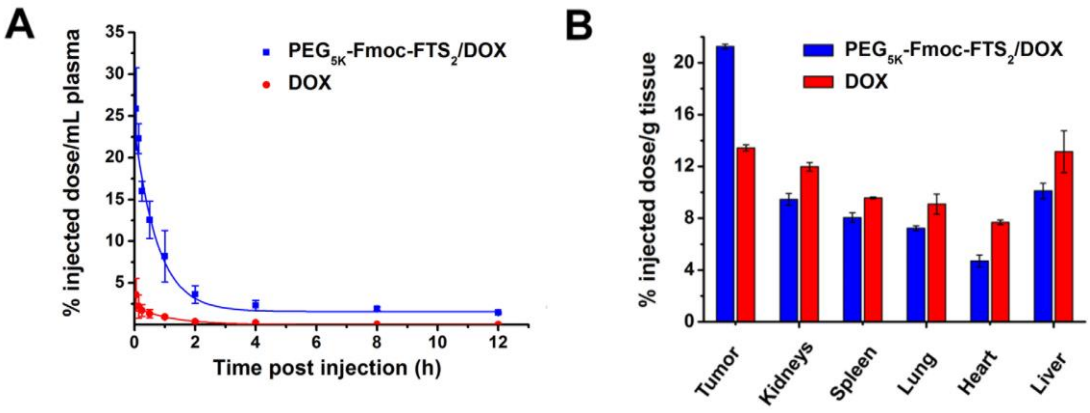

Figure 38. Blood retention kinetics of DOX·HCl and DOX-loaded PEG_{5k}-Fmoc-FTS_2 micelles in mice (A).
DOX·HCl and DOX- loaded PEG_{5K}-Fmoc-FTS_2 micelles were injected into female BALB/c mice via tail vein at a dose of 5 mg DOX/kg. Tissue distribution of DOX 1 day following the injection (B). DOX·HCl and DOX-loaded PEG_{5K}-Fmoc-FTS_2 were injected into female BALB/c mice bearing 4T1.2 breast tumor at the dose of 5 mg DOX/kg, respectively. Values are means ± SEM.

Table 9. Pharmacokinetic variables of free DOX and DOX-loaded PEG_{5k}-Fmoc-FTS_2 micelles

Groups	$T_{1/2}$ (h)	$AUC_{0\text{-}inf}$ (μg×h/mL)	Cmax (μg/mL)	CL (L/h/kg)	Vd (L/kg)
DOX	1.74	3.43	3.59	2.91	7.34
PEG_{5K}-Fmoc-FTS_2/DOX	11.60	64.80	25.84	0.15	2.58

The tissue distribution of DOX·HCl and DOX-loaded PEG_{5K}-Fmoc-FTS_2 micelles was also investigated in female BALB/c mice bearing 4T1.2 breast tumor. Free DOX·HCl and DOX-loaded PEG_{5K}-Fmoc-FTS_2 micelles were injected at the same DOX dose of 5 mg/kg. At 24h post-injection, major organs and tumors were excised for DOX determination. As shown in

Figure 38B, there was about 2-fold increase in the tumor uptake of DOX for DOX-loaded PEG_{5K}-Fmoc-FTS_2 micelles compared to free DOX. In addition, DOX-loaded PEG_{5K}-Fmoc-FTS_2 micelles were associated with a reduced DOX accumulation in normal organs such as heart compared to free DOX (**Figure 38B**). These findings showed that DOX-loaded PEG_{5K}-Fmoc-FTS_2 can not only increase the tumor-target efficacy of DOX, but also decrease DOX-associated cardiotoxicity.

4.4.8 *In vivo* therapeutic study

The antitumor activity of PTX- and DOX-loaded PEG_{5K}-Fmoc-FTS_2 micelles was first investigated in a syngeneic murine breast cancer model (4T1.2). As shown in **Figure 39A**, free PEG_{5K}-Fmoc-FTS_2 micelles alone showed no effects in inhibiting the tumor growth at the dose used. Taxol formulation showed a modest effect in inhibiting the tumor growth at a dose of 10 mg PTX/kg. In contrast, PTX formulated in PEG_{5K}-Fmoc-FTS_2 micelles showed a much more pronounced antitumor activity at the same dosage. It is also apparent that PTX/PEG_{5K}-Fmoc-FTS_2 mixed micelles were more active than the counterpart without an Fmoc motif ($P < 0.05$). Increasing the PTX dosage to 20 mg/kg resulted in a further improvement in the therapeutic effect.

Figure 39C shows the result of therapy study on DOX/PEG_{5K}-Fmoc-FTS_2 micelles in 4T1.2 tumor model. Both DOX/PEG_{5K}-FTS_2 and DOX/PEG_{5K}-Fmoc-FTS_2 were significantly more active than free DOX or liposomal DOX in inhibiting the tumor growth. There was also a trend of improvement in antitumor activity for DOX/PEG_{5K}-Fmoc-FTS_2 compared to DOX/PEG_{5K}-FTS_2 although it is not statistically significant ($P = 0.16$). No significant changes

were noticed in body weight in all treatment groups compared to PBS control group (**Figure 39B and D**).

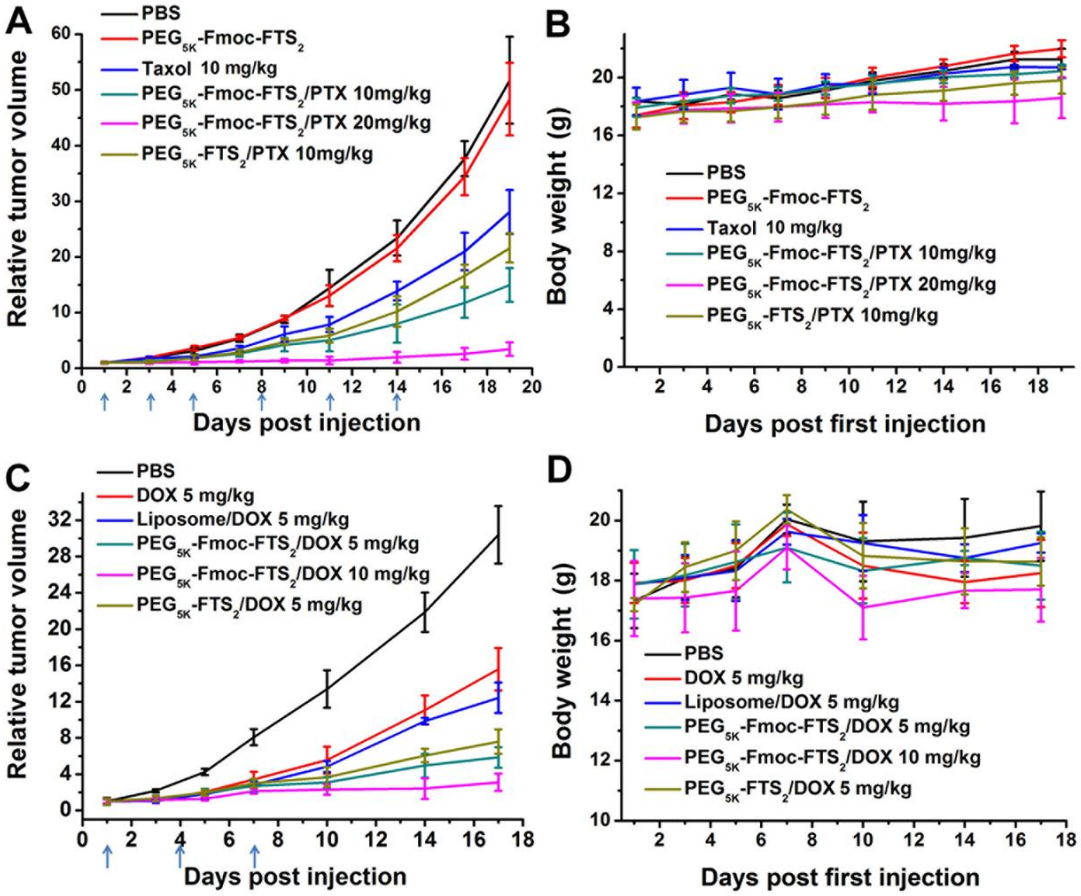

Figure 39. Enhanced antitumor activity of PTX formulated in PEG_{5K}-Fmoc-FTS_2 micelles in a syngeneic murine breast cancer model (4T1.2) (A). Changes of body weight in mice receiving different treatments (B).
$P < 0.01$ (10 mg PTX/kg PEG_{5K}-Fmoc-FTS_2 vs. Taxol), $P < 0.05$ (10 mg PTX/kg PEG_{5K}-Fmoc-FTS_2 vs. 10 mg PTX/kg PEG_{5K}-FTS_2). Enhanced antitumor activity of DOX formulated in PEG_{5K}-Fmoc-FTS_2 micelles in a syngeneic murine breast cancer model (4T1.2) compared to DOX·HCl and DOX-loaded liposome (C). Changes of body weight in mice receiving different treatments (D). $P < 0.01$ (5 mg DOX/kg PEG_{5K}-Fmoc-FTS_2 vs. DOX·HCl), $P < 0.01$ (5 mg DOX/kg PEG_{5K}-Fmoc-FTS_2 vs. 5 mg DOX/kg liposome).

The *in vivo* therapeutic activity of PTX formulated in PEG_{5K}-Fmoc-FTS_2 micelles was further evaluated in a human prostate cancer xenograft model (PC-3) (**Figure 40A**). PC-3 model has a

relatively slower growth rate than 4T1.2 tumor model and tumor growth was more effectively controlled by the different treatments in PC-3 model. Nonetheless, PTX/PEG_{5K}-Fmoc-FTS_2 mixed micelles were significantly more effective than either Taxol or PTX/PEG_{5K}-FTS_2 mixed micelles in inhibiting the tumor growth at the same dose of 10 mg PTX/kg. Figure 9C shows representative images of nude mice bearing PC-3 tumors treated with PBS and various PTX formulations by day 17 after initial treatment. By day 17, the RTV for PTX/PEG_{5K}-Fmoc-FTS_2 mixed micelles was 1.71, while the RTVs for mice treated with Taxol and PTX/PEG_{5K}-FTS_2 mixed micelles were 5.2, and 2.9, respectively. Increasing the dose of PTX to 20 mg PTX/kg led to a further improvement in antitumor activity, one out of the 5 mice in this group became tumor-free after day 38 without further treatment. No weight loss was observed in mice treated with all PTX formulations (**Figure 40B**), while consistent weight loss was shown in mice treated with PBS or carrier alone after day 9 (**Figure 40B**).

In vivo therapy study demonstrated that significant therapeutic effect can be achieved with minimal toxicity using our PEG_{5K}-Fmoc-FTS_2 micellar system (**Figures 39 and 40**) in both prostate and breast cancer models. The superior antitumor efficacy along with the minimal toxicity of the improved system could be ascribed to an enhanced stability, a decreased relative rate of drug release and an improved pharmacokinetic profile, leading to effective tumor targeting and reduced nonspecific uptake by normal tissues.

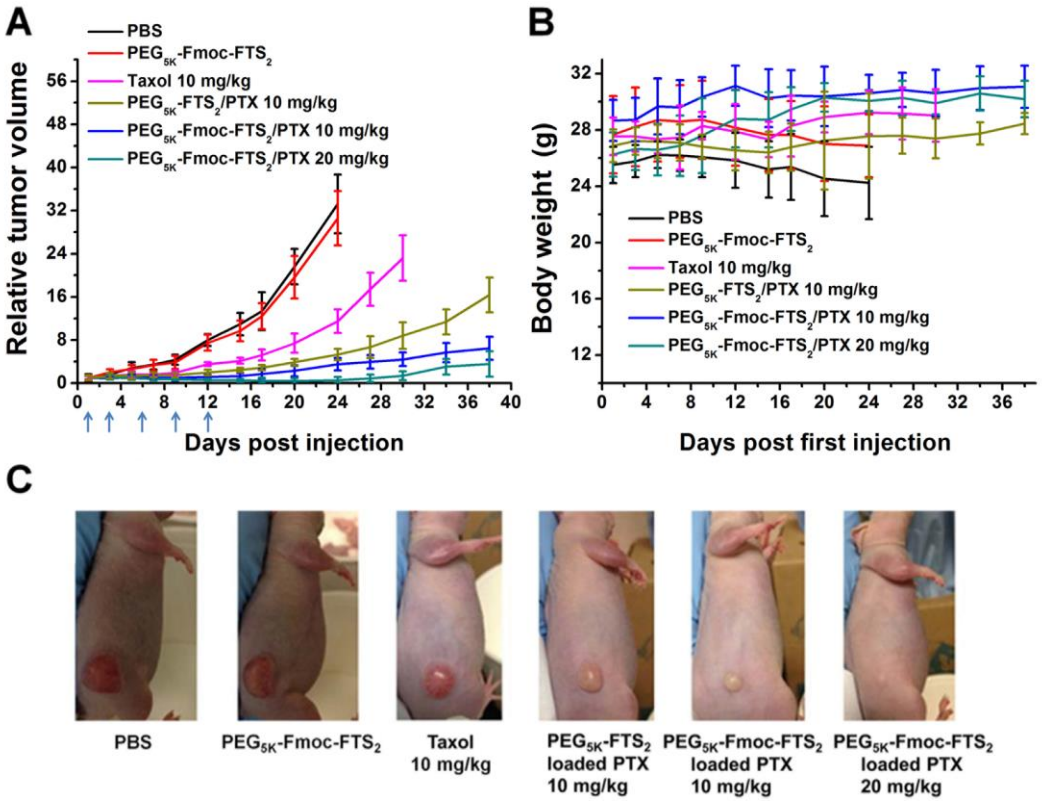

Figure 40. Enhanced antitumor activity of PTX formulated in PEG_{5K}-Fmoc-FTS_2 micelles in a human prostate cancer xenograft model (PC-3) (A). Changes of body weight in mice receiving different treatments (B).
$P < 0.01$ (10 mg PTX/kg PEG_{5K}-Fmoc-FTS_2 vs. Taxol), $P < 0.01$ (10 mg PTX/kg PEG_{5K}-Fmoc-FTS_2 vs. 10 mg PTX/kg PEG_{5K}-FTS_2). Photograph showing representative images of nude mice bearing PC-3 tumors treated with PBS and different PTX formulations by day 17 after initial treatment (C).

5.0 REDUCTION-SENSITIVE DUAL FUNCTIONAL NANOMICELLES FOR IMPROVED DELIVERY OF PACLITAXEL

5.1 ABSTRACT

We have developed a dual-functional nanocarrier composed of a hydrophilic polyethylene glycol (PEG) and a hydrophobic farnesylthiosalicylate (FTS, a nontoxic Ras antagonist), which is effective in delivery of hydrophobic anticancer drug, paclitaxel (PTX). To facilitate the retention of the therapeutic activity of the carrier, FTS was coupled to PEG via a reduction-sensitive disulfide linkage (PEG_{5k}-S-S-FTS_2). PEG_{5k}-S-S-FTS_2 conjugate formed uniform micelles with very small size (~30 nm) and the hydrophobic drug PTX could be readily incorporated into the micelles. Interestingly, inclusion of a disulfide linkage into the PEG_{5k}-FTS_2 micellar system resulted in a 4-fold decrease in the critical micelle concentration (CMC). In addition, the PTX loading capacity and colloidal stability of PTX-loaded micelles were improved. HPLC-MS showed that parent FTS could be more effectively released from PEG_{5k}-S-S-FTS_2 conjugate in tumor cells/tissues compared to PEG_{5k}-FTS_2 conjugate in vitro and in vivo. PEG_{5k}-S-S-FTS_2 exhibited a higher level of cytotoxicity toward tumor cells than PEG_{5k}-FTS_2 without a disulfide linkage. Furthermore, PTX-loaded PEG_{5k}-S-S-FTS_2 micelles were more effective in inhibiting the proliferation of cultured tumor cells compared to Taxol and PTX loaded in PEG_{5k}-FTS_2 micelles. More importantly, PTX-loaded PEG_{5k}-S-S-FTS_2 micelles demonstrated superior

antitumor activity compared to Taxol and PTX formulated in PEG_{5k}-FTS_2 micelles in an aggressive murine breast cancer model (4T1.2).

5.2 BACKGROUND

Polymeric micelles are an attractive delivery system due to their easy preparation, small sizes (10-100 nm), and their ability to solubilize hydrophobic drugs and accumulate preferentially within tumors [45, 97, 98, 102, 118]. We previously developed a nanocarrier based on polyethylene glycol (PEG)-derivatized farnesylthiosalicylate (FTS) [67]. PEG_{5k}-FTS_2 readily formed micelles (20~30 nm) that were highly efficient in loading hydrophobic anticancer drugs such as paclitaxel (PTX) [67]. More importantly, PTX-loaded PEG_{5k}-FTS_2 micelles achieved enhanced antitumor efficacy compared to Taxol formulation *in vivo* [67]. Different from most of the existing drug carriers that lack therapeutic effect, PEG_{5k}-FTS_2 itself exhibits antitumor activity [67]. FTS is a potent and especially nontoxic Ras antagonist [51, 103]. Ras gene mutations can be found in one-third of human cancers, with the highest incidence in adenocarcinomas of the pancreas (90%), colon (50%) and the lung (30%) tumor [52]. FTS can effectively inhibit the growth of many different types of tumors via inhibition of Ras-dependent signaling involved in tumor maintenance and progression [121]. The mechanism involves the dislodgement of Ras from the cell membrane and subsequent degradation of the protein [55, 84].

As a dual function carrier, the cleavability of the linkage between PEG and FTS in PEG_{5k}-FTS_2 conjugate is critical for its biological activity. In our previous study, we compared the antitumor activity of a conjugate with a labile ester linkage, PEG_{5K}-FTS_2(L), with that of a similar conjugate with a relatively stable amide linkage, PEG_{5K}-FTS_2(S) [67]. PEG_{5K}-FTS_2(L)

alone showed a significantly higher level of cytotoxicity towards tumor cells compared to PEG_{5K}-FTS_2(S) presumably due to a more readily release of FTS from PEG_{5K}-FTS_2(L) inside tumor cells [67]. In addition, delivery of PTX via PEG_{5K}-FTS_2(L) micelles led to an improved antitumor activity *in vivo* over PTX formulated in PEG_{5K}-FTS_2(S) micelles [67].

In this study, we propose to incorporate into PEG_{5K}-FTS_2(L) an additional cleavable linkage (disulfide bond) to further facilitate the release of FTS following intracellular delivery to tumor cells. We choose disulfide linkage because tumor cells have significantly higher concentrations of glutathione (GSH) than those in the extracellular fluids and disulfide linkage has been widely used to develop a reduction-sensitive delivery system to facilitate drug release at tumor sites [13, 49, 50, 110, 122-129]. Our data showed that incorporation into PEG_{5K}-FTS_2(L) a disulfide linkage led to an enhanced release of FTS inside tumor cells, which was associated with an improved cytotoxicity against tumor cells. Interestingly, the conjugate with a disulfide linkage (PEG_{5k}-S-S-FTS_2) exhibited a reduced critical micelle concentration (CMC) in addition to improved drug loading capacity and formulation stability. Finally, paclitaxel (PTX) formulated in PEG_{5k}-S-S-FTS_2 micelles was significantly more effective than the PEG_{5K}-FTS_2(L) formulation in inhibiting the tumor growth in a murine breast cancer model (4T1.2).

5.3 EXPERIMENTAL PROCEDURES

5.3.1 Materials

Paclitaxel (98%) was purchased from AK Scientific Inc. (CA, USA). FTS and PEG_{5K}-FTS_2 conjugate were synthesized according to published literature [67, 103]. Poly(ethylene glycol)

methyl ether (MeO-PEG-OH, MW=5000 kDa), dimethyl sulfoxide (DMSO), succinate anhydride, diethanolamine, trypsin-EDTA solution, Dulbecco's Modified Eagle's Medium (DMEM) and 3-(4,5-dimethylthiazol-2-yl)-2,5-diphenyl tetrazolium bromide (MTT) were all purchased from Sigma-Aldrich (MO, USA). Di-Boc-lysine, triethylamine (TEA) and trifluoroacetic acid (TFA) were obtained from Acros Organic (NJ, USA). Bis(2-hydroxyethyl) disulfide, dicyclohexylcarbodiimide (DCC) and *N*-hydroxysuccinimide (NHS) were purchased from Alfa Aesar (MA, USA). 4-(dimethylamino) pyridine (DMAP) was purchased from Calbiochem-Novabiochem Corporation (CA, USA). All solvents used in this study were HPLC grade.

5.3.2 Cell culture

MCF-7 is a human breast carcinoma cell line. 4T1.2 is a mouse metastatic breast cancer cell line. HCT-116 is a human colon carcinoma cell line. PC-3 and DU-145 are human prostate cancer cell lines. All cell lines were cultured in DMEM containing 5% FBS and 1% penicillin-streptomycin at 37 ℃ in a humidified 5 % CO_2 atmosphere.

5.3.3 Animals

Female BALB/c mice, 4-6 weeks in age, were purchased from Charles River (Davis, CA). All animals were housed under pathogen-free conditions according to AAALAC guidelines. All animal-related experiments were performed in full compliance with institutional guidelines and approved by the Animal Use and Care Administrative Advisory Committee at the University of Pittsburgh.

5.3.4 Synthesis of PEG_{5K}-S-S-FTS_2 conjugate

Figure 41 shows the synthesis route of PEG_{5K}-S-S-FTS_2 conjugate. Synthesis and structural characterizations are detailed below.

Compound **1:** Bis(2-hydroxyethyl) disulfide (1.54 g, 10 mmol) was added to a solution of FTS (3.58 g, 10 mmol), DCC (3.09 g, 15 mmol), DMAP (122 mg, 1 mmol) in CH_2Cl_2 (50 mL). The mixture was stirred at room temperature until TLC showed completion of reaction. The mixture was filtered through cotton and the filtrate was concentrated on a rotary evaporator. The residue was chromatographed (1:4 EtOAc/PE) on silica gel to afford the compound **1** (3.2 g, 6.5 mmol, 65%). ^{1}H NMR (400 MHz, $CDCl_3$) δ 7.99-7.97 (m, 1H), 7.45-7.41 (m, 1H), 7.32-7.28 (m, 1H), 7.17-7.13 (m, 1H), 5.36-5.32 (m, 1H), 5.10-5.07 (m, 2H), 4.59(t, *J* = 6.8 Hz, 2H), 3.88-3.87 (m, 2H), 3.58-3.56 (m, 2H), 3.06 (t, *J* = 6.8 Hz, 2H), 2.89 (t, *J* = 6 Hz, 2H), 2,.09-1.97(m, 8H), 1.73(s, 3H), 1.68(s, 3H), 1.60(s, 6H).

Compound **2:** Succinic anhydride (2 g, 20 mmol) was added to a solution of compound **1** (4.94 g, 10 mmol), DMAP (2.44 g, 20 mmol) in $CHCl_3$ (50 mL), and the mixture was refluxed until TLC showed completion of reaction. The mixture was concentrated on a rotary evaporator and the residue was chromatographed (1:1 EtOAc/PE) on silica gel to afford the compound **2** (5.8 g, 6.5 mmol, 97%). ^{1}H NMR (400 MHz, $CDCl_3$) δ 7.99-7.97 (m, 1H), 7.41-7.38 (m, 1H), 7.29-7.27 (m, 1H), 7.14-7.10 (m, 1H), 5.30-5.27 (m, 1H), 5.06-5.03 (m, 2H), 4.54(t, *J* = 6.8 Hz, 2H), 4.33(t, *J* = 6.8 Hz, 2H), 3.55-3.53 (m, 2H), 3.03 (t, *J* = 6.4 Hz, 2H), 2.89 (t, *J* = 6.4 Hz, 2H), 2.62-2.61 (m, 4H), 2.04-1.92(m, 8H), 1.69(s, 3H), 1.64(s, 3H), 1.55(s, 6H).

Compound **5:** Compound **5** was synthesized from compound **3** following a published method [67].

Compound **6:** DCC, DMAP, compound **2,** and compound **5** were dissolved in CH_2Cl_2 with a molar ratio of 1:6:3:0.3 and allowed to react overnight at room temperature. The solution was filtered and precipitated in diethyl ether and ethanol twice, respectively. The compound **6** was obtained by further drying under vacuum.

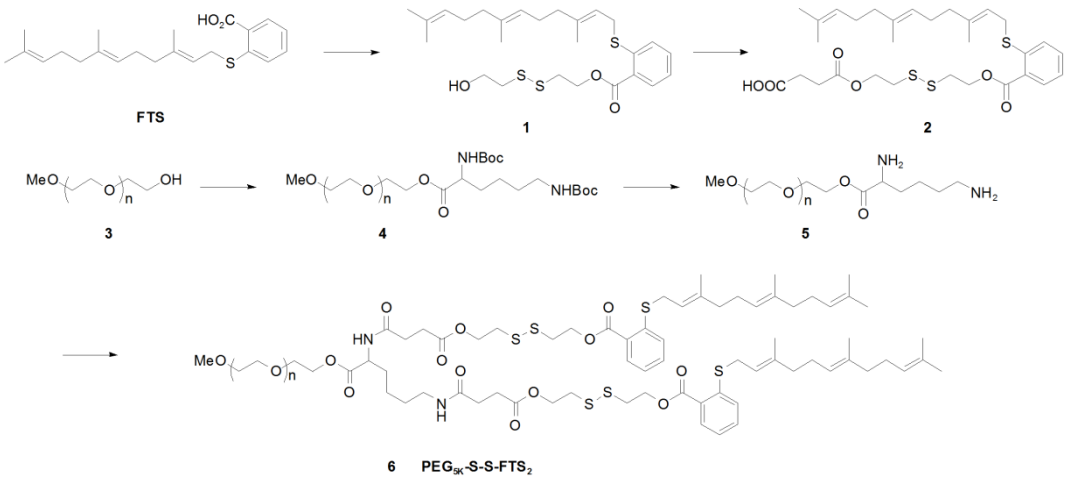

Figure 41. Synthesis scheme of PEG_{5k}-S-S-FTS_2 conjugate

5.3.5 Preparation and characterization of PTX-loaded PEG_{5K}-S-S-FTS_2 micelles

PTX-solubilized PEG_{5K}-S-S-FTS_2 micelles were prepared via a solvent evaporation method following our published protocol [13, 67]. Briefly, PTX (10 mM in chloroform) and PEG_{5K}-S-S-FTS_2 conjugate (10 mM in chloroform) were mixed with various carrier/drug ratios. A film of drug/carrier mixture was formed by removed the organic solvent and the film was further dried under vacuum. PTX-loaded micelles were formed by adding DPBS to hydrate the thin film followed by gentle vortexing. The PTX loading efficiency was measured by high performance liquid chromatography (HPLC) (Alliance 2695-2998 system) as described previously [67]. Drug

loading capacity (DLC) and drug loading efficiency (DLE) were calculated according to the following equation:

DLC (%) = [weight of drug used/(weight of polymer + drug used)] ×100%

DLE (%) = (weight of loaded drug/weight of input drug) ×100%

Morphology, micelle size, and size distribution were assessed by transmission electron microscopy (TEM) and dynamic light scattering (DLS) following our published protocol [118]. The critical micelle concentration (CMC) of PEG_{5K}-S-S-FTS_2 micelles was determined using pyrene as a fluorescence probe [80].

5.3.6 Release of FTS from the PEG_{5K}-S-S-FTS_2 and PEG_{5K}-FTS_2 conjugates

DU-145 and PC-3 cells were seeded in 6-well plates. After 24 h of incubation in DMEM with 5% FBS, the old medium was removed and the cells were incubated for 72 h in the presence of drug-free PEG_{5K}-S-S-FTS_2 or PEG_{5K}-FTS_2 micelles. The cells were washed with ice-cold PBS three times and solubilized via a mixture of MeOH and H_2O. The lysates were vortexed and then centrifuged at 14,000 rpm for 10 mins at 4 ℃. Supernatants were transferred to another set of 1.5-mL microtubes and stored at -80 ℃ for MS analysis. The amount of FTS in each sample was quantified by Waters' SYNAPT G2-S Mass Spectrometer according to the literature [87, 130]. Chromatographic separation of FTS was performed on an Acquity UPLC BEH C18 column (2.1 × 50 mm, 1.7 μm, Waters). The mobile phase A (MPA) was 0.1% formic acid in acetonitrile, and mobile phase B was 0.1% formic acid in water. The flow rate of mobile phase was 0.40 mL/min and the column temperature was maintained at 50 ℃. Data were processed using QuanLynx (v4.1, Waters). Extracted ion chromatograms (EICs) were extracted using a 20 mDa window centered on the expected *m/z* 357.189 for FTS.

Similarly, FTS release was examined with tumor tissues from female BALB/c mice bearing 4T1.2 tumor (~1 cm). Groups of 4 mice received i.v. injection of PEG_{5K}-FTS_2 or PEG_{5K}-S-S-FTS_2 conjugate at a dose of 58.5 μmol/kg. One day post injection, blood and tumors were collected. Samples were homogenized with PBS, and then mixed with 2 volumes of acetonitrile. The mixture was vortexed for 1 min, incubated for 5 mins and centrifuged at 14,000 rpm for 10 mins at 4 ℃. The supernatants were decanted from each sample into a clean centrifugation tube for MS analysis and FTS was then analyzed as described above.

5.3.7 *In vitro* cytotoxicity study

The cytotoxicity of PTX formulated in PEG_{5K}-S-S-FTS_2 micelles was assessed with several cancer cell lines and compared to Taxol and PTX loaded in PEG_{5K}-FTS_2 micelles, respectively. Briefly, MCF-7 cells (5000 cells/well) and HCT-116 cells (1000 cells/well) were seeded in 96-well plates. After incubation in DMEM with 5% FBS and 1% streptomycin-penicillin for 24 h, the old medium was removed and the cells were further incubated for 3 days in the presence of indicated concentrations of PTX formulated in Cremophor/EL, PEG_{5K}-S-S-FTS_2 or PEG_{5K}-FTS_2 micelles. Cell viability was then assessed by MTT assay following our published literature.[6] Similarly, the cytotoxicity of drug-free PEG_{5K}-S-S-FTS_2 micelles was examined and compared to free FTS and PEG_{5K}-FTS_2 micelles as described above.

5.3.8 *In vivo* therapeutic study

An aggressive murine breast cancer model (4T1.2) was used to examine the *in vivo* therapeutic effect of different formulations of PTX. Tumors were induced by inoculation of 4T1.2 cells (1 x

10^5) in 100 μL PBS at the right flank of female BALB/c mice. After tumors in the mice reached a tumor volume of ~ 40 mm^3, treatments were started and this day was designated as day 1. On the first day, tumor (4T1.2)-bearing mice were randomly divided into five groups (n=5) and administered i.v. with PBS (control), drug-free PEG_{5K}-S-S-FTS_2 micelles, Taxol (10 mg PTX/kg), PTX-loaded PEG_{5K}-FTS_2 and PEG_{5K}-S-S-FTS_2 micelles (10 mg PTX/kg), respectively on days 1, 3, 6, 8, 10 and 12. Tumor sizes were measured twice a week and tumor volumes were calculated by the formula: $(L \times W^2)/2$, where L and W represent the longest and shortest in tumor diameters (mm). Each group was compared by relative tumor volume (RTV) (where RTV equals to the tumor volume divided by the initial tumor volume before treatment). The body weights of all mice from each group were measured twice a week.

5.3.9 Statistical analysis

Data are presented as mean ± standard deviation (SD). Statistical analysis was performed by Student's t-test for comparison of two groups, and comparisons for multiple groups were made with one-way analysis of variance (ANOVA), followed by Newman-Keuls test if the overall $P < 0.05$. In all statistical analysis, the threshold of significance was defined as $P < 0.05$.

5.4 RESULTS

5.4.1 Synthesis of PEG_{5K}-S-S-FTS_2 conjugate

To facilitate the retention of the antitumor activity of FTS, a cleavable disulfide linkage was used to couple FTS to a hydrophilic PEG (PEG_{5K}-S-S-FTS_2). The chemical structure of PEG_{5K}-S-S-FTS_2 is shown in **Figure 41**. As shown in ^{1}H NMR spectra (**Figure 42**), the signals at 3.63 ppm and 7-8 ppm were attributed to the methylene protons located at the terminus of PEG and the benzene ring protons of FTS, respectively. Additionally, the chemical shift of -*CH*$_2$-S-S-*CH*$_2$- (2.9-3.1 ppm) could be observed, which confirmed the presence of a disulfide linkage (Figure S1). The molecular weight of PEG_{5K}-S-S-FTS_2 was determined by MALDI-TOF Mass Spectrometry (**Figure 43**), which is close to the theoretical value of PEG_{5K}-S-S-FTS_2. Both ^{1}H NMR and MALDI-TOF Mass spectra indicated the successful synthesis of PEG_{5K}-S-S-FTS_2 conjugate.

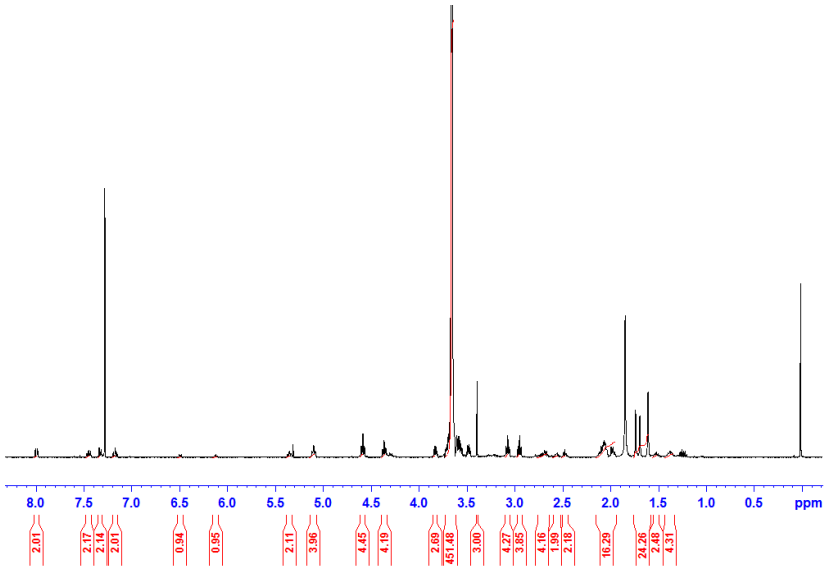

Figure 42. ^{1}H NMR spectra (400MHz) of PEG_{5K}-S-S-FTS_2 conjugate in $CDCl_3$

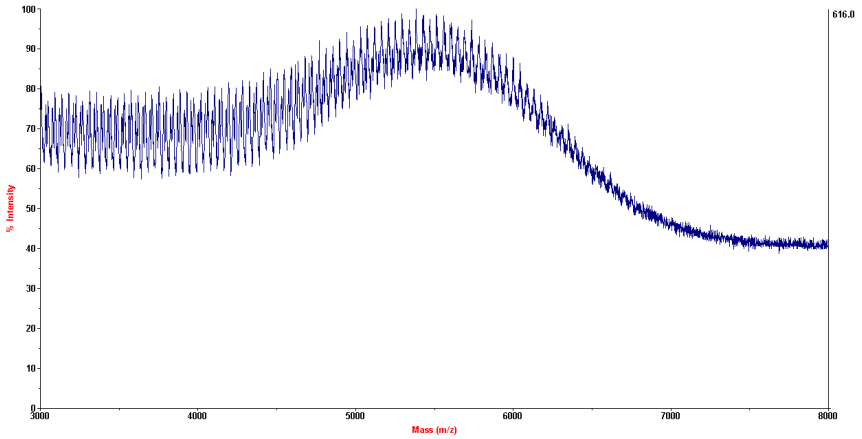

Figure 43. MADLI-TOF of PEG_{5K}-S-S-FTS_2 conjugate

5.4.2 Characterization of PTX-free and PTX/PEG_{5K}-S-S-FTS_2 micelles

PEG_{5K}-S-S-FTS_2 was soluble in aqueous solution and readily self-assembled to form micelles with size around 30 nm (**Figure 44A**). Figure 2C shows the TEM images of PEG_{5K}-S-S-FTS_2 micelles. Spherical particles of uniform size were observed and the sizes of the particles observed under TEM were consistent with those measured by DLS. **Figure 45** shows the CMCs of PEG_{5K}-FTS_2 and PEG_{5K}-S-S-FTS_2 micelles using pyrene as a fluorescence probe. It is interesting to notice that incorporation into PEG_{5K}-FTS_2 a disulfide linkage led to a ~4-fold decrease in CMC. PTX can be readily loaded into PEG_{5K}-S-S-FTS_2 micelles. The spherical shape and size of the micelles were well retained following incorporation of PTX (**Figures 44B and D**). We then evaluated the loading capacity and stability of PTX-loaded PEG_{5K}-S-S-FTS_2 micelles and compared to those of PEG_{5K}-FTS_2 formulation. As shown in **Table 10**, PTX could be loaded in PEG_{5K}-S-S-FTS_2 micelles at a carrier/drug molar ratio as low as 1/1. In contrast, a minimal carrier/drug molar ratio of 2.5/1 was needed to formulate PTX in PEG_{5K}-FTS_2 micelles.

Increasing the carrier/drug molar ratio was associated with an improvement in both drug loading efficiency (DLE) and the colloidal stability of PTX-loaded micelles (**Table 10**). In addition, PTX-loaded PEG_{5K}-S-S-FTS_2 micelles showed better colloidal stability than PEG_{5K}-FTS_2 formulation at all carrier/drug ratios examined (**Table 10).**

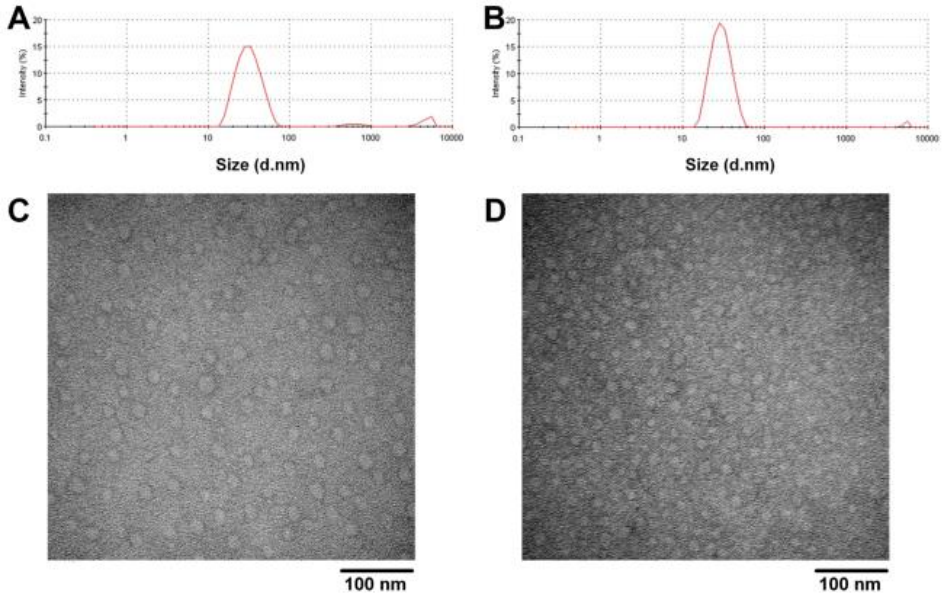

Figure 44. Particle size distribution of PTX-free PEG_{5K}-S-S-FTS_2 (A), and PTX-loaded PEG_{5K}-S-S-FTS_2 micelles (B). TEM images of PTX-free PEG_{5K}-S-S-FTS_2 (C), and PTX-loaded PEG_{5K}-S-S-FTS_2 micelles (D).

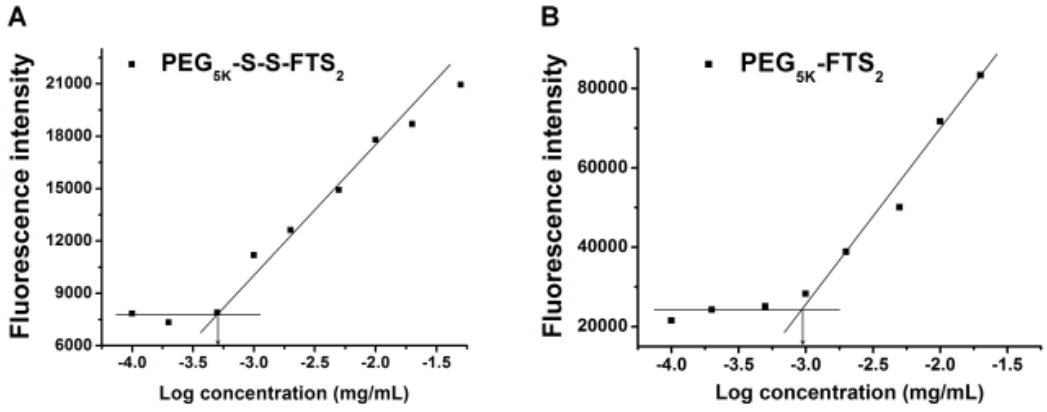

Figure 45. Critical micelle concentration (CMC) of PEG_{5K}-S-S-FTS_2 (A) and PEG_{5K}-FTS_2 (B) micelles.

Table 10. Physicochemical characterization of free drug and PTX-loaded PEG_{5k}-FTS_2 and PEG_{5k}-S-S-FTS_2 micelles.

Micelles	Molar ratio	Conc. of PTX [a] (mg/mL)	Size [b] (nm)	PDI[c]	DLC [d] (%)	DLE [e] (%)	Stability [f] (hour)
PEG_{5K}-FTS_2	-	-	17.6	0.20	-	-	-
PEG_{5K}-FTS_2 : PTX	2.5 :1	1	24.9	0.35	5.5	81.2	2
PEG_{5K}-FTS_2 : PTX	5 :1	1	25.6	0.23	2.8	97.6	20
PEG_{5K}-S-S-FTS_2	-	-	32.4	0.21	-	-	-
PEG_{5K}-S-S-FTS_2 : PTX	1 :1	1	28.5	0.22	12	85.2	1
PEG_{5K}-S-S-FTS_2 : PTX	2.5 :1	1	32.0	0.30	5.2	89.7	3.5
PEG_{5K}-S-S-FTS_2 : PTX	5 :1	1	30.2	0.35	2.6	94.8	30

[a]PTX concentration in micelle was kept at 1 mg/mL. Blank micelle concentration was 20 mg/mL. Values reported are the mean ± SD for triplicate samples. [b]Measured by dynamic light scattering particle sizer. [c]PDI = polydispersity index. [d]DLC = drug loading capacity. [e]DLE = drug loading efficiency. [f]Data means there was no noticeable size change during the follow-up period.

5.4.3 *In vitro* cytotoxicity of drug-free micelles

The antitumor activities of two PTX-free micelles, PEG_{5K}-S-S-FTS_2 and PEG_{5K}-FTS_2, were tested in HCT-116 and DU-145 cancer cell lines and compared to free FTS (**Figure 46**). PEG_{5K}-FTS_2 conjugate with an ester linkage was used as a reduction-insensitive control. As shown in **Figure 46A,** free FTS inhibited the HCT-116 cell growth in a concentration-dependent manner. PEG_{5K}-FTS_2 with a reduction-insensitive ester linkage was less active than free FTS in cytotoxicity (**Figure 46A**). Interestingly, incorporation into PEG_{5K}-FTS_2 an additional disulfide linkage led to a significant improvement in cytotoxicity compared to both free FTS and PEG_{5K}-FTS_2 (**Figure 46A**). Similar result was observed in DU-145 cell line (**Figure 46B**).

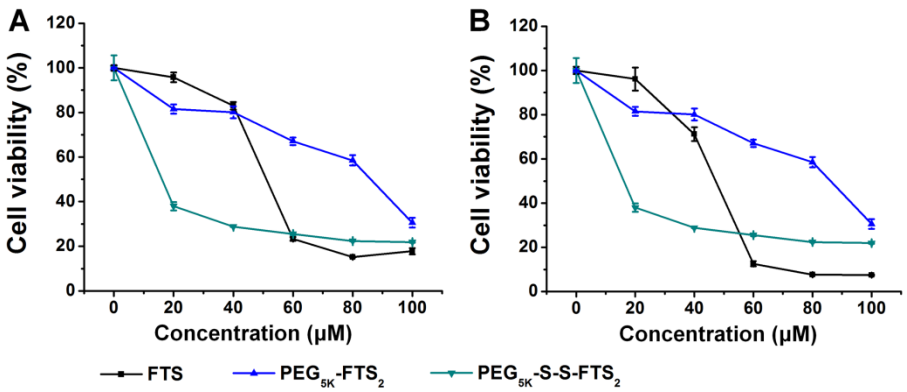

Figure 46. Cytotoxicity of drug free PEG_{5k}-FTS_2 and PEG_{5K}-S-S-FTS_2 micelles in comparison to free FTS in HCT-116 human colon carcinoma cell line (A) and DU-145 human prostate cancer cell line (B).
Cells were treated for 72 h and cytotoxicity was determined by MTT assay.

5.4.4 Release of FTS from the PEG_{5K}-S-S-FTS_2 and PEG_{5K}-FTS_2 conjugates

To investigate whether the improved cytotoxicity of PEG_{5K}-S-S-FTS_2 over PEG_{5K}-FTS_2 is attributed to a more effective release of FTS, HPLC-MS was employed to analyze FTS release inside PC-3 or DU-145 human prostate cancer cells 72 h following treatment with PEG_{5K}-FTS_2 or PEG_{5K}-S-S-FTS_2 micelles. We focused on the detection of the signal of parent FTS. The FTS extraction protocol had minimal impact on the integrity of PEG_{5K}-S-S-FTS_2 as demonstrated in a preliminary study (data not shown). **Figure 47A** shows that incorporation into PEG_{5K}-FTS_2 a disulfide linkage led to a 2 to 3-fold increase in the amounts of free FTS detected in PC-3 cells (**Figure 47A**). Similar result was observed in DU-145 cell line (**Figure 47B**). We also conducted a preliminary study on the release of FTS in tumor tissues *in vivo*. Female BALB/c mice bearing 4T1.2 tumor (~1 cm) received i.v. injection of PEG_{5K}-S-S-FTS_2 and PEG_{5K}-FTS_2 micelles at the same dose and the amounts of free FTS in the tumor tissues were examined 24 h later. As shown in **Figure 48**, a strong signal of FTS was detected in the tumor tissues while very little FTS signal was found in the blood. It is also apparent that significantly greater amounts of free FTS

were found in the tumors treated with PEG_{5K}-S-S-FTS_2 compared to the PEG_{5K}-FTS_2-treated tumors (**Figure 48**), implicating that FTS is more readily cleaved from PEG_{5K}-S-S-FTS_2 micelles at the tumor sites.

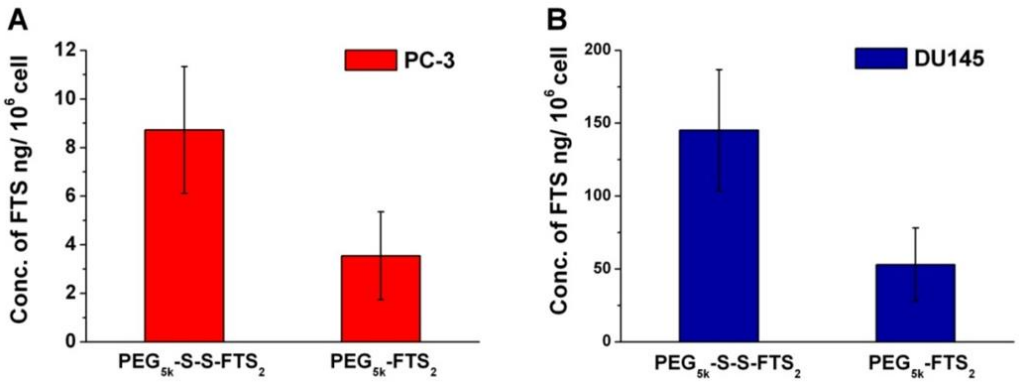

Figure 47. HPLC analysis of the amounts of released free FTS in PC-3 or DU-145 prostate cancer cells 72 h following treatment with PEG_{5K}-S-S-FTS_2 or PEG_{5K}-FTS_2 at a FTS concentration of 20 μM.

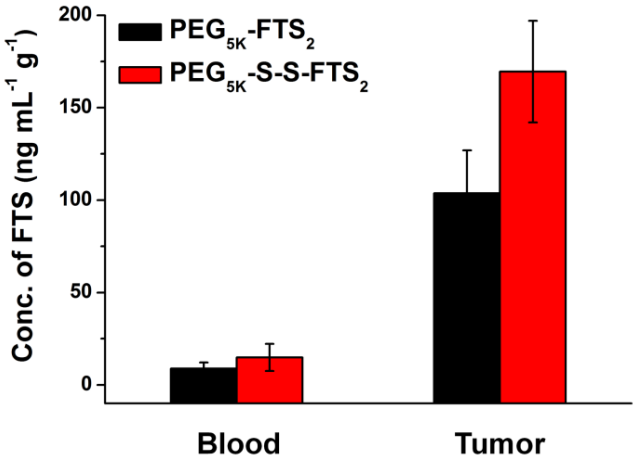

Figure 48. HPLC-MS analysis of FTS in blood and tumors 24 h following i.v. administration of PEG_{5K}-FTS_2 and PEG_{5K}-S-S-FTS_2.

5.4.5 *In vitro* cytotoxicity of drug-loaded micelles

Figure 49 shows the *in vitro* cytotoxicity of PTX formulated in PEG_{5K}-FTS_2 or PEG_{5K}-S-S-FTS_2 micelles, in comparison with Taxol formulation in MCF-7 and HCT-116 cells. Taxol inhibited the proliferation of MCF-7 breast cancer cells in a concentration dependent manner (**Figure 49A**). Delivery of PTX via PEG_{5K}-FTS_2 micelles led to a slight increase in cytotoxicity against MCF-7 tumor cells. More importantly, PTX formulated in PEG_{5K}-S-S-FTS_2 micelles were more active than both Taxol formulation and PTX-loaded PEG_{5K}-FTS_2 micelles in inhibiting the tumor cell growth, particularly at low PTX concentrations (**Figure 49A**). Similar result was observed in a colon carcinoma cell line, HCT-116 (**Figure 49B**).

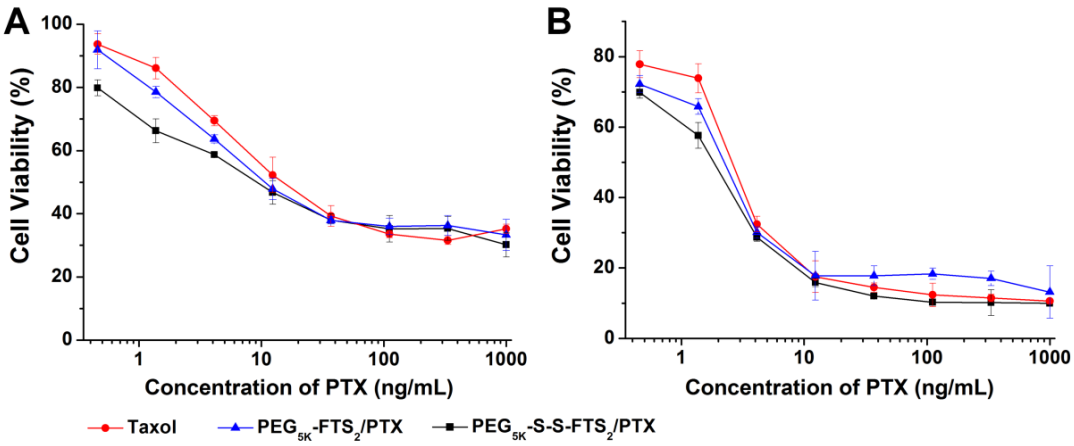

Figure 49. Cytotoxicity of PTX-loaded PEG_{5k}-FTS_2 and PEG_{5k}-S-S-FTS_2 micelles in comparison to Taxol formulation in MCF-7 human breast carcinoma cell line (A) and HCT-116 human colon carcinoma cell line (B). Cells were treated for 72 h and cytotoxicity was determined by MTT assay.

5.4.6 *In vivo* therapeutic study

Figure 50 shows the *in vivo* therapeutic activity of PTX formulated in PEG_{5K}-S-S-FTS in an aggressive murine breast cancer model (4T1.2). PEG_{5K}-S-S-FTS_2 micelles alone showed no effects in inhibiting the tumor growth at the concentration used. This is due to a relatively low concentration of FTS in this group. Taxol formulation showed a modest tumor growth inhibition at a dose of 10 mg PTX/kg (**Figure 50A**). In contrast, both PTX-loaded PEG_{5K}-FTS_2 and PEG_{5K}-S-S-FTS_2 micelles were more effective than Taxol formulation at the same dose (**Figure 50A**). More importantly, PTX formulated in PEG_{5K}-S-S-FTS_2 micelles exhibited even more potent tumor growth inhibition than PTX-loaded PEG_{5K}-FTS_2 micelles ($P < 0.05$) (**Figure 50A**). No significant changes in body weight were detected in all treatment groups compared to PBS control group (**Figure 50B**).

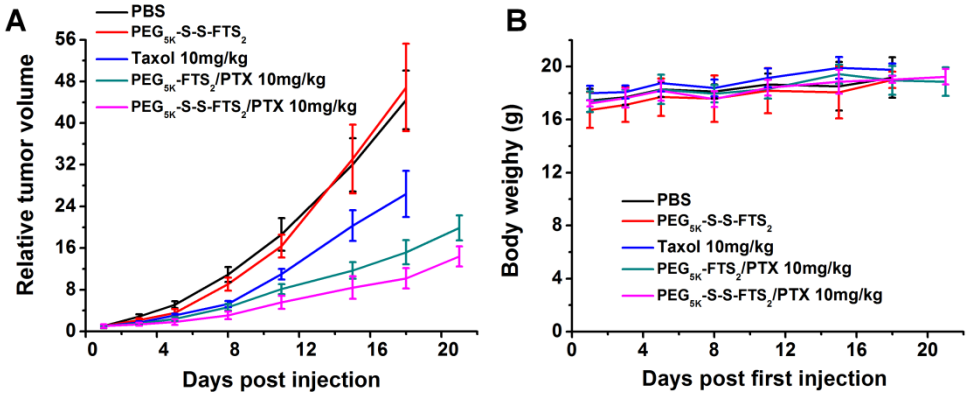

Figure 50. Antitumor activity of PTX formulated in PEG_{5K}-S-S-FTS_2 micelles in a syngeneic murine breast cancer model (4T1.2) (A). Changes of body weight in mice receiving different treatments (B).
$P < 0.05$ (PTX/ PEG_{5K}-S-S-FTS_2 vs. PTX/ PEG_{5K}-FTS_2). N = 5.

5.5 DISCUSSION

We have previously reported that PTX-loaded PEG_{5K}-FTS_2(L) micelles showed better antitumor activity than Taxol formulation, which could be ascribed to their preferential tumor accumulation and a possible synergistic effect between PEG_{5K}-FTS_2(L) carrier and loaded PTX [67]. In this study, we have shown that inclusion of a disulfide linkage led to a further improvement in the therapeutic activity compared to PTX formulated in PEG_{5k}-FTS_2(L) micelles and Taxol *in vivo* (**Figure 49**).

Similar to PEG_{5K}-FTS_2(L), PEG_{5K}-S-S-FTS_2 readily self-assembled to form micelles in aqueous solution with relatively small size (~30 nm) (**Table 10)**. Such small size shall enable the carrier to be highly effective in passive accumulation and deep penetration into solid tumors, including poorly vascularized tumors [32, 98]. Interestingly, inclusion of a disulfide linkage led to an improvement in both PTX loading capacity and the colloidal stability of PTX-loaded micelles (**Table 10**). We further noticed that incorporation into PEG_{5K}-FTS_2(L) a disulfide linkage resulted in a 4-fold decrease in CMC (**Figure 45**). A lower CMC will enable the micelles more stable in the blood circulation following systemic administration [131]. This is likely due to an improved cooperation in both carrier/carrier and carrier/drug interactions following incorporation of a flexible disulfide linkage into the lipid motif of the carrier. The increase in the chain length of lipid motif following inclusion of a disulfide linkage may also contribute to the improved PTX loading capacity and formulation stability.

HPLC-MS analysis showed that parent FTS can be detected from cultured cancer cells following treatment with PEG_{5K}-FTS_2(L) micelles (**Figure 47**), suggesting that FTS can be released from the conjugate via intracellular esterases. It is also apparent that significantly higher levels of parent FTS were found in tumor cells treated with PEG_{5K}-S-S-FTS_2 conjugate (**Figure**

47). A similar result was found in tumor tissues (**Figure 48**) in tumor-bearing mice receiving i.v. administration of PEG_{5K}-FTS_2(L) or PEG_{5K}-S-S-FTS_2 conjugate. FTS can be released from the PEG_{5K}-S-S-FTS_2 conjugate via two different mechanisms: one is direct cleavage of the ester linkage adjacent to FTS to generate the parent FTS, the other one involves reduction of the disulfide linkage first, followed by cleavage of the ester linkage to generate the parent FTS (**Figure 51**). The fact that significantly greater amounts of parent FTS were released from cells treated with PEG_{5K}-S-S-FTS_2 would suggest that the latter is the major mechanism for FTS release (**Figure 51**). This is probably because direct release of FTS from PEG_{5K}-FTS_2(L) by intracellular esterases is relatively ineffective due to the steric hindrance imposed by PEG. On the other hand, cleavage of disulfide linkage is a more effective process inside tumor cells due to the significantly increased GSH levels in tumor cells [49, 124]. Once released from the conjugate, the small molecule intermediate can be effectively hydrolyzed by the intracellular esterases to generate the parent FTS (**Figure 51**).

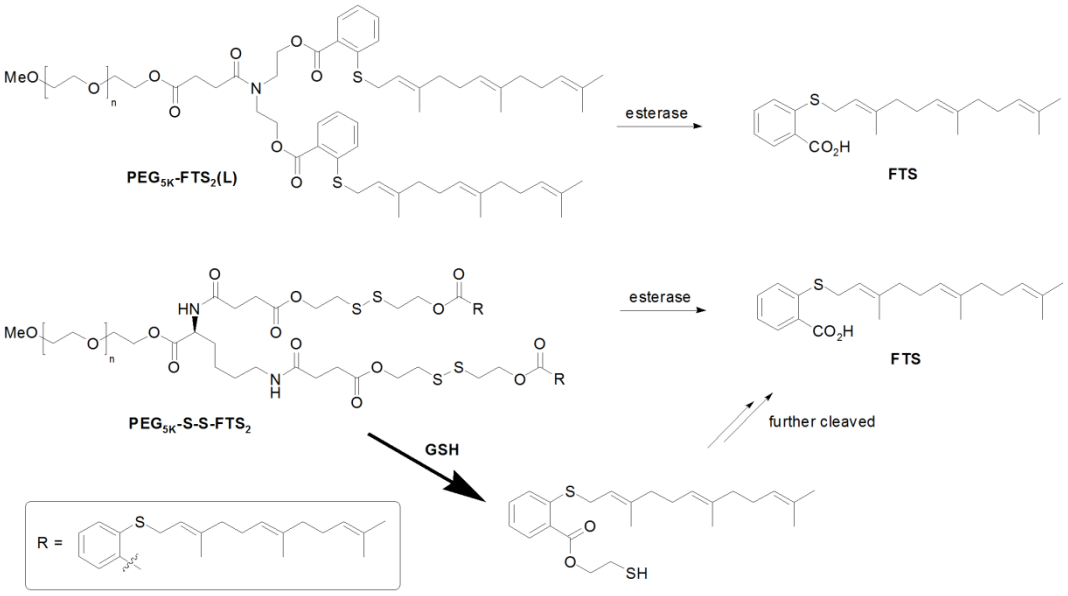

Figure 51. Proposed mechanism for the release of FTS from PEG_{5K}-FTS_2 and PEG_{5K}-S-S-FTS_2 conjugates following intracellular delivery to tumor cells.

In vitro cytotoxicity showed that PEG_{5K}-S-S-FTS_2 conjugate was significantly more effective in inhibiting the proliferation of cultured tumor cells compared to PEG_{5K}-FTS_2(L) conjugate (**Figure 46**). The increased cytotoxicity of PEG_{5K}-S-S-FTS_2 is most likely due to a facilitated release of FTS following inclusion of an additional cleavable disulfide linkage. It is interesting to note that PEG_{5K}-SS-FTS_2 also exhibited higher levels of cytotoxicity than free FTS at low concentrations (**Figure 46**). This is unlikely due to the surfactant activity of the conjugate as PEG_{5K}-SS-FTS_2 showed minimal hemolytic activity at even much higher concentrations (data not shown). It is possible that PEG_{5K}-SS-FTS_2 is more effectively taken up by tumor cells than free FTS, which will be further examined in the future. PEG_{5K}-S-S-FTS_2 not only retained the biological activity well, but also served as an efficient carrier to deliver hydrophobic drug PTX. PTX formulated in PEG_{5K}-S-S-FTS_2 micelles showed a level of cytotoxicity that was higher than that of either Taxol or PTX formulated in PEG_{5K}-FTS_2(L) micelles (**Figure 48**), particularly at low PTX concentrations.

In vivo antitumor study showed that PTX formulated in PEG_{5K}-FTS_2(L) micelles were significantly more effective than Taxol formulation in a syngeneic murine breast cancer model (Figure 8), which is consistent with our previous report [67]. It is also apparent that inclusion of a disulfide linkage in PEG_{5K}-FTS_2(L) micellar system led to a further improvement in antitumor activity (**Figure 49**). The improved performance is likely attributed to a more effective cleavage of FTS from the conjugate in the tumor tissue, which shall lead to not only enhanced intracellular delivery of FTS but also facilitated release of loaded drug following disassembly of micelles. It remains to be investigated whether the improved carrier/drug interaction and the reduced CMC of the PEG_{5K}-S-S-FTS_2 micellar system also contribute to the overall improvement in antitumor activity.

6.0 SUMMARY AND PERSPECTIVES

Chemotherapy is the most commonly used cancer treatment. However, the traditional anticancer agents are limited by their undesirable properties such as low aqueous solubility and low tumor selectivity. Upon intravenous administration, these small molecule drugs are rapidly degraded or cleared from systemic circulation. Simultaneously, they are nonselectively widely distributed to normal tissues and tumors, causing severe systemic toxicity. Nanomedicines can avoid this problem by achieving targeted delivery of anticancer agents to tumor tissues, which is based on the exploitation of enhanced permeability and retention (EPR) effect. EPR effect was discovered by Maeda and his colleagues about 30 years ago, which is the most important strategy for enhancing the delivery of small molecule anti-cancer drugs to tumors. Due to solid tumors tend to present with a poorly differentiated vasculature, nanocarriers with a certain size can selectively go to tumor tissues. Together with the fact that tumor tissues usually lack functional lymphatics and therefore are unable to eliminate extravasated nanocarriers, this allows for nanocarriers to accumulate in the tumor tissue. Development of effective nanocarriers will be important and beneficial to deliver therapeutic agents in a safer and more efficient manner. They can encapsulate water insoluble drugs, protect them from biodegradation and alter their blood pharmacokinetic behavior and biodistribution. Currently, a wide range of macromolecular delivery systems such as long-circulating liposomes, nanoparticles, polymers and micelles have been employed for the development of new cancer therapies. Some of them did present with

quite promising therapeutic efficacy and are approved for clinical use, including Doxil (liposomal doxorubicin (DOX)), Abraxane (albumin-based nanoparticle containing paclitaxel (PTX)), Oncaspar (polyethylene glycol (PEG)-L-asparaginase), Genexol-PM (micellar paclitaxel) and so on.

Among the many studied delivery systems, polymeric micelles have attracted an increasing interest because of their simplicity, small sizes, and their ability to solubilize water-insoluble drugs and accumulate specifically in tumors. For conventional chemotherapy, various approaches to achieve dual delivery of small-molecular drugs. The co-delivery of multiple agents to tumors could achieve combinatorial effects to enhance therapeutic efficacy and lower the risk of resistance by affecting multiple pathways involved in cancer. The development of polymeric micelles possessing both biological activities by themselves and the ability to deliver other anticancer drugs offers a feasible solution for drug combination cancer therapies. The design of polymeric micelles that exhibit antitumor activity can either reduce the side effects caused by the encapsulated drug or simultaneously provide a synergistic activity with the loaded drug.

During my graduate study, I worked on several cohesive projects to develop dual functional nanomicellar carriers for the targeted delivery of anticancer drugs for cancer. First, we developed PEG-derivatized FTS conjugates, which retained the biological activity of FTS and formed small-sized micelles that effectively solubilize a PTX. PTX formulated in this micellar system showed a PTX release kinetics that was significantly slower than that of the Taxol. PTX formulated in PEG_{5K}-FTS_2(L) micelles was more cytotoxic than free PTX *in vitro*. *In vivo*, PTX/PEG_{5K}-FTS_2(L) showed antitumor activity that was more potent than that of Taxol or PTX/PEG_{5K}-FTS_2(S). PEG_{5K}-FTS_2(L) may represent a promising micellar system that could

effectively deliver anticancer agents to tumors. Furthermore, it may potentially synergize with the co-delivered drugs to enhance overall antitumor activity.

In addition, efforts were also made to systematically study the SAR of a PEG-FTS based dual functional carrier. A structure activity relationship (SAR) study was conducted in four PEG-FTS conjugates that vary in the molecular weight of PEG (PEG_{2K} vs PEG_{5K}) and the molar ratio of PEG/FTS (1/2 vs 1/4). We demonstrated that PEG_{5K}-FTS_4 formed the most stable mixed micelles with PTX among the four PEG-FTS conjugates. *In vivo*, PTX-loaded PEG_{5K}-FTS_4 led to an improved tumor growth inhibitory effect in comparison to PTX formulated in PEG_{2K}-FTS_2, PEG_{2K}-FTS_4, and PEG_{5K}-FTS_2 as well as Taxol in a syngeneic mouse model of breast cancer (4T1.2).

In order to further improve the performance of the PEG-FTS-based dual functional carrier, a drug-interactive Fmoc motif was introduced into this system. We demonstrated that both drug loading capacity and formulation stability were significantly improved by inclusion of a drug-interactive Fmoc motif. Pharmacokinetics and biodistribution studies showed that DOX-loaded PEG_{5K}-Fmoc-FTS_2 micelles were able to retain DOX in the bloodstream for a prolonged period of time and were highly effective in targeted delivery of DOX to tumors. More importantly, PTX- or DOX-loaded PEG_{5K}-Fmoc-FTS_2 micelles led to a superior antitumor activity over other treatments including drugs formulated in PEG_{5K}-FTS_2 micelles in both breast cancer and prostate cancer models. PEG_{5K}-Fmoc-FTS_2 may represent a promising micellar system for effective delivery of anticancer agents to tumors.

As a dual function carrier, the cleavability of the linkage between PEG and FTS in PEG_{5K}-FTS2 conjugate is critical for its biological activity. An improved dual-functional micellar carrier composed of a PEG shell and FTS core via a disulfide linkage (PEG_{5k}-S-S-FTS_2)

was developed. PEG_{5k}-S-S-FTS_2 retained the FTS biological activity well, which was attributed to an effective release of FTS from the conjugate following intracellular uptake. In addition, PEG_{5k}-S-S-FTS_2 readily self-assembled into small-sized micelles and formed stable mixed micelles with PTX. More importantly, PTX-loaded PEG_{5k}-S-S-FTS_2 micelles demonstrated more effective therapeutic effects *in vivo* over Taxol formulation and PTX-loaded PEG_{5k}-FTS_2 micelles.

PEG-FTS-based micellar systems demonstrated potential as effective and dual-functional carriers for poorly water soluble anticancer agents. Despite the promising data, particularly the data on *in vivo* therapeutic efficacy, much remains to be done to further demonstrate their potential, particularly more toxicity and pharmacokinetics study. In addition, more systematic studies on the structure-activity relationship of polymeric micellar systems are needed to better understand the mechanism of drug-carrier interaction and establish a stable micellar system with a high drug loading capacity. These studies shall lead to the development of effective delivery system for anticancer drug with potential for rapid translation into clinical study.

BIBLIOGRAPHY

[1] Torre LA, Bray F, Siegel RL, Ferlay J, Lortet-Tieulent J, Jemal A. Global cancer statistics, 2012. CA: a cancer journal for clinicians. 2015;65:87-108.

[2] Rawat M, Singh D, Saraf S, Saraf S. Nanocarriers: promising vehicle for bioactive drugs. Biological & pharmaceutical bulletin. 2006;29:1790-8.

[3] Lipinski CA, Lombardo F, Dominy BW, Feeney PJ. Experimental and computational approaches to estimate solubility and permeability in drug discovery and development settings. Advanced drug delivery reviews. 2001;46:3-26.

[4] Wiernik PH, Schwartz EL, Strauman JJ, Dutcher JP, Lipton RB, Paietta E. Phase I clinical and pharmacokinetic study of taxol. Cancer research. 1987;47:2486-93.

[5] Torchilin VP. Micellar nanocarriers: pharmaceutical perspectives. Pharmaceutical research. 2007;24:1-16.

[6] Brigger I, Dubernet C, Couvreur P. Nanoparticles in cancer therapy and diagnosis. Advanced drug delivery reviews. 2002;54:631-51.

[7] Haag R, Kratz F. Polymer therapeutics: concepts and applications. Angewandte Chemie. 2006;45:1198-215.

[8] Mi Y, Liu Y, Feng SS. Formulation of Docetaxel by folic acid-conjugated d-alpha-tocopheryl polyethylene glycol succinate 2000 (Vitamin E TPGS(2k)) micelles for targeted and synergistic chemotherapy. Biomaterials. 2011;32:4058-66.

[9] Gong J, Chen M, Zheng Y, Wang S, Wang Y. Polymeric micelles drug delivery system in oncology. Journal of controlled release : official journal of the Controlled Release Society. 2012;159:312-23.

[10] Oerlemans C, Bult W, Bos M, Storm G, Nijsen JF, Hennink WE. Polymeric micelles in anticancer therapy: targeting, imaging and triggered release. Pharmaceutical research. 2010;27:2569-89.

[11] Torchilin VP. Multifunctional nanocarriers. Advanced drug delivery reviews. 2006;58:1532-55.

[12] Zhang Y, Zhuo RX. Synthesis and in vitro drug release behavior of amphiphilic triblock copolymer nanoparticles based on poly (ethylene glycol) and polycaprolactone. Biomaterials. 2005;26:6736-42.

[13] Duan K, Zhang X, Tang X, Yu J, Liu S, Wang D, et al. Fabrication of cationic nanomicelle from chitosan-graft-polycaprolactone as the carrier of 7-ethyl-10-hydroxy-camptothecin. Colloids and surfaces B, Biointerfaces. 2010;76:475-82.

[14] Avgoustakis K, Beletsi A, Panagi Z, Klepetsanis P, Livaniou E, Evangelatos G, et al. Effect of copolymer composition on the physicochemical characteristics, in vitro stability, and biodistribution of PLGA-mPEG nanoparticles. International journal of pharmaceutics. 2003;259:115-27.

[15] Xiao K, Luo J, Fowler WL, Li Y, Lee JS, Xing L, et al. A self-assembling nanoparticle for paclitaxel delivery in ovarian cancer. Biomaterials. 2009;30:6006-16.
[16] Li Y, Xiao K, Luo J, Lee J, Pan S, Lam KS. A novel size-tunable nanocarrier system for targeted anticancer drug delivery. Journal of controlled release : official journal of the Controlled Release Society. 2010;144:314-23.
[17] Luo J, Xiao K, Li Y, Lee JS, Shi L, Tan YH, et al. Well-defined, size-tunable, multifunctional micelles for efficient paclitaxel delivery for cancer treatment. Bioconjugate chemistry. 2010;21:1216-24.
[18] Xiao K, Luo J, Li Y, Lee JS, Fung G, Lam KS. PEG-oligocholic acid telodendrimer micelles for the targeted delivery of doxorubicin to B-cell lymphoma. Journal of controlled release : official journal of the Controlled Release Society. 2011;155:272-81.
[19] Lukyanov AN, Hartner WC, Torchilin VP. Increased accumulation of PEG-PE micelles in the area of experimental myocardial infarction in rabbits. Journal of controlled release : official journal of the Controlled Release Society. 2004;94:187-93.
[20] Sawant RR, Torchilin VP. Multifunctionality of lipid-core micelles for drug delivery and tumour targeting. Molecular membrane biology. 2010;27:232-46.
[21] Knop K, Hoogenboom R, Fischer D, Schubert US. Poly(ethylene glycol) in drug delivery: pros and cons as well as potential alternatives. Angewandte Chemie. 2010;49:6288-308.
[22] Torchilin VP, Trubetskoy VS, Whiteman KR, Caliceti P, Ferruti P, Veronese FM. New synthetic amphiphilic polymers for steric protection of liposomes in vivo. Journal of pharmaceutical sciences. 1995;84:1049-53.
[23] Takeuchi H, Kojima H, Toyoda T, Yamamoto H, Hino T, Kawashima Y. Prolonged circulation time of doxorubicin-loaded liposomes coated with a modified polyvinyl alcohol after intravenous injection in rats. European journal of pharmaceutics and biopharmaceutics : official journal of Arbeitsgemeinschaft fur Pharmazeutische Verfahrenstechnik eV. 1999;48:123-9.
[24] Liang XJ, Chen C, Zhao Y, Wang PC. Circumventing tumor resistance to chemotherapy by nanotechnology. Methods in molecular biology. 2010;596:467-88.
[25] Goel S, Duda DG, Xu L, Munn LL, Boucher Y, Fukumura D, et al. Normalization of the vasculature for treatment of cancer and other diseases. Physiological reviews. 2011;91:1071-121.
[26] Bertrand N, Wu J, Xu X, Kamaly N, Farokhzad OC. Cancer nanotechnology: the impact of passive and active targeting in the era of modern cancer biology. Advanced drug delivery reviews. 2014;66:2-25.
[27] Strong LE, West JL. Optically modulated cancer therapeutic delivery: past, present and future. Therapeutic delivery. 2015;6:545-58.
[28] Matsumura Y, Maeda H. A new concept for macromolecular therapeutics in cancer chemotherapy: mechanism of tumoritropic accumulation of proteins and the antitumor agent smancs. Cancer research. 1986;46:6387-92.
[29] Maeda H, Wu J, Sawa T, Matsumura Y, Hori K. Tumor vascular permeability and the EPR effect in macromolecular therapeutics: a review. Journal of controlled release : official journal of the Controlled Release Society. 2000;65:271-84.
[30] Trubetskoy VS. Polymeric micelles as carriers of diagnostic agents. Advanced drug delivery reviews. 1999;37:81-8.
[31] Moghimi SM, Davis SS. Innovations in avoiding particle clearance from blood by Kupffer cells: cause for reflection. Critical reviews in therapeutic drug carrier systems. 1994;11:31-59.

[32] Cabral H, Matsumoto Y, Mizuno K, Chen Q, Murakami M, Kimura M, et al. Accumulation of sub-100 nm polymeric micelles in poorly permeable tumours depends on size. Nature nanotechnology. 2011;6:815-23.
[33] Gref R, Minamitake Y, Peracchia MT, Trubetskoy V, Torchilin V, Langer R. Biodegradable long-circulating polymeric nanospheres. Science. 1994;263:1600-3.
[34] Yu B, Tai HC, Xue W, Lee LJ, Lee RJ. Receptor-targeted nanocarriers for therapeutic delivery to cancer. Molecular membrane biology. 2010;27:286-98.
[35] Sawant RR, Jhaveri AM, Torchilin VP. Immunomicelles for advancing personalized therapy. Advanced drug delivery reviews. 2012;64:1436-46.
[36] Sawant RR, Sawant RM, Torchilin VP. Mixed PEG-PE/vitamin E tumor-targeted immunomicelles as carriers for poorly soluble anti-cancer drugs: improved drug solubilization and enhanced in vitro cytotoxicity. European journal of pharmaceutics and biopharmaceutics : official journal of Arbeitsgemeinschaft fur Pharmazeutische Verfahrenstechnik eV. 2008;70:51-7.
[37] Lee ES, Na K, Bae YH. Polymeric micelle for tumor pH and folate-mediated targeting. Journal of controlled release : official journal of the Controlled Release Society. 2003;91:103-13.
[38] Xu W, Siddiqui IA, Nihal M, Pilla S, Rosenthal K, Mukhtar H, et al. Aptamer-conjugated and doxorubicin-loaded unimolecular micelles for targeted therapy of prostate cancer. Biomaterials. 2013;34:5244-53.
[39] Maurice T, Su TP. The pharmacology of sigma-1 receptors. Pharmacology & therapeutics. 2009;124:195-206.
[40] Xiao K, Li Y, Lee JS, Gonik AM, Dong T, Fung G, et al. "OA02" peptide facilitates the precise targeting of paclitaxel-loaded micellar nanoparticles to ovarian cancer in vivo. Cancer research. 2012;72:2100-10.
[41] Sawant RR, Jhaveri AM, Koshkaryev A, Qureshi F, Torchilin VP. The effect of dual ligand-targeted micelles on the delivery and efficacy of poorly soluble drug for cancer therapy. Journal of drug targeting. 2013;21:630-8.
[42] Probert HM, Gibson GR. Investigating the prebiotic and gas-generating effects of selected carbohydrates on the human colonic microflora. Letters in applied microbiology. 2002;35:473-80.
[43] Toncheva V, Schacht E, Ng SY, Barr J, Heller J. Use of block copolymers of poly(ortho esters) and poly (ethylene glycol) micellar carriers as potential tumour targeting systems. Journal of drug targeting. 2003;11:345-53.
[44] Bae Y, Fukushima S, Harada A, Kataoka K. Design of environment-sensitive supramolecular assemblies for intracellular drug delivery: polymeric micelles that are responsive to intracellular pH change. Angewandte Chemie. 2003;42:4640-3.
[45] Torchilin V. Multifunctional and stimuli-sensitive pharmaceutical nanocarriers. European journal of pharmaceutics and biopharmaceutics : official journal of Arbeitsgemeinschaft fur Pharmazeutische Verfahrenstechnik eV. 2009;71:431-44.
[46] Lee HJ, Ponta A, Bae Y. Polymer nanoassemblies for cancer treatment and imaging. Therapeutic delivery. 2010;1:803-17.
[47] Bae Y, Nishiyama N, Fukushima S, Koyama H, Yasuhiro M, Kataoka K. Preparation and biological characterization of polymeric micelle drug carriers with intracellular pH-triggered drug release property: tumor permeability, controlled subcellular drug distribution, and enhanced in vivo antitumor efficacy. Bioconjugate chemistry. 2005;16:122-30.

[48] Hu J, Miura S, Na K, Bae YH. pH-responsive and charge shielded cationic micelle of poly(L-histidine)-block-short branched PEI for acidic cancer treatment. Journal of controlled release : official journal of the Controlled Release Society. 2013;172:69-76.
[49] Wu G, Fang YZ, Yang S, Lupton JR, Turner ND. Glutathione metabolism and its implications for health. The Journal of nutrition. 2004;134:489-92.
[50] Huang H, Zhang X, Yu J, Zeng J, Chang PR, Xu H, et al. Fabrication and reduction-sensitive behavior of polyion complex nano-micelles based on PEG-conjugated polymer containing disulfide bonds as a potential carrier of anti-tumor paclitaxel. Colloids and surfaces B, Biointerfaces. 2013;110:59-65.
[51] Haklai R, Weisz MG, Elad G, Paz A, Marciano D, Egozi Y, et al. Dislodgment and accelerated degradation of Ras. Biochemistry. 1998;37:1306-14.
[52] Bos JL. ras oncogenes in human cancer: a review. Cancer research. 1989;49:4682-9.
[53] Cox AD, Der CJ. Ras family signaling: therapeutic targeting. Cancer biology & therapy. 2002;1:599-606.
[54] Pylayeva-Gupta Y, Grabocka E, Bar-Sagi D. RAS oncogenes: weaving a tumorigenic web. Nature reviews Cancer. 2011;11:761-74.
[55] Rotblat B, Ehrlich M, Haklai R, Kloog Y. The Ras inhibitor farnesylthiosalicylic acid (Salirasib) disrupts the spatiotemporal localization of active Ras: a potential treatment for cancer. Methods in enzymology. 2008;439:467-89.
[56] Jansen B, Schlagbauer-Wadl H, Kahr H, Heere-Ress E, Mayer BX, Eichler H, et al. Novel Ras antagonist blocks human melanoma growth. Proceedings of the National Academy of Sciences of the United States of America. 1999;96:14019-24.
[57] Niv H, Gutman O, Henis YI, Kloog Y. Membrane interactions of a constitutively active GFP-Ki-Ras 4B and their role in signaling. Evidence from lateral mobility studies. The Journal of biological chemistry. 1999;274:1606-13.
[58] Kloog Y, Cox AD, Sinensky M. Concepts in Ras-directed therapy. Expert opinion on investigational drugs. 1999;8:2121-40.
[59] Laheru D, Shah P, Rajeshkumar NV, McAllister F, Taylor G, Goldsweig H, et al. Integrated preclinical and clinical development of S-trans, trans-Farnesylthiosalicylic Acid (FTS, Salirasib) in pancreatic cancer. Investigational new drugs. 2012;30:2391-9.
[60] Goldberg L, Israeli R, Kloog Y. FTS and 2-DG induce pancreatic cancer cell death and tumor shrinkage in mice. Cell death & disease. 2012;3:e284.
[61] Biran A, Brownstein M, Haklai R, Kloog Y. Downregulation of survivin and aurora A by histone deacetylase and RAS inhibitors: a new drug combination for cancer therapy. International journal of cancer Journal international du cancer. 2011;128:691-701.
[62] Gana-Weisz M, Halaschek-Wiener J, Jansen B, Elad G, Haklai R, Kloog Y. The Ras inhibitor S-trans,trans-farnesylthiosalicylic acid chemosensitizes human tumor cells without causing resistance. Clinical cancer research : an official journal of the American Association for Cancer Research. 2002;8:555-65.
[63] Aizman E, Mor A, Levy A, George J, Kloog Y. Ras inhibition by FTS attenuates brain tumor growth in mice by direct antitumor activity and enhanced reactivity of cytotoxic lymphocytes. Oncotarget. 2012;3:144-57.
[64] Mor A, Aizman E, Kloog Y. Celecoxib enhances the anti-inflammatory effects of farnesylthiosalicylic acid on T cells independent of prostaglandin E(2) production. Inflammation. 2012;35:1706-14.

[65] Chen Y, Zhang X, Lu J, Huang Y, Li J, Li S. Targeted delivery of curcumin to tumors via PEG-derivatized FTS-based micellar system. The AAPS journal. 2014;16:600-8.
[66] Kraitzer A, Kloog Y, Haklai R, Zilberman M. Composite fiber structures with antiproliferative agents exhibit advantageous drug delivery and cell growth inhibition in vitro. Journal of pharmaceutical sciences. 2011;100:133-49.
[67] Zhang X, Lu J, Huang Y, Zhao W, Chen Y, Li J, et al. PEG-farnesylthiosalicylate conjugate as a nanomicellar carrier for delivery of paclitaxel. Bioconjugate chemistry. 2013;24:464-72.
[68] Kim JY, Kim S, Pinal R, Park K. Hydrotropic polymer micelles as versatile vehicles for delivery of poorly water-soluble drugs. Journal of controlled release : official journal of the Controlled Release Society. 2011;152:13-20.
[69] Gao X, Huang Y, Makhov AM, Epperly M, Lu J, Grab S, et al. Nanoassembly of surfactants with interfacial drug-interactive motifs as tailor-designed drug carriers. Molecular pharmaceutics. 2013;10:187-98.
[70] Zhang P, Huang Y, Liu H, Marquez RT, Lu J, Zhao W, et al. A PEG-Fmoc conjugate as a nanocarrier for paclitaxel. Biomaterials. 2014;35:7146-56.
[71] Zhang X, Huang Y, Zhao W, Liu H, Marquez R, Lu J, et al. Targeted delivery of anticancer agents via a dual function nanocarrier with an interfacial drug-interactive motif. Biomacromolecules. 2014;15:4326-35.
[72] Goldspiel BR. Clinical overview of the taxanes. Pharmacotherapy. 1997;17:110S-25S.
[73] Xie Z, Guan H, Chen X, Lu C, Chen L, Hu X, et al. A novel polymer-paclitaxel conjugate based on amphiphilic triblock copolymer. Journal of controlled release : official journal of the Controlled Release Society. 2007;117:210-6.
[74] Harding SE. The macrostructure of mucus glycoproteins in solution. Advances in carbohydrate chemistry and biochemistry. 1989;47:345-81.
[75] Prencipe G, Tabakman SM, Welsher K, Liu Z, Goodwin AP, Zhang L, et al. PEG branched polymer for functionalization of nanomaterials with ultralong blood circulation. Journal of the American Chemical Society. 2009;131:4783-7.
[76] Croy SR, Kwon GS. Polymeric micelles for drug delivery. Current pharmaceutical design. 2006;12:4669-84.
[77] Zhang Z, Feng SS. Nanoparticles of poly(lactide)/vitamin E TPGS copolymer for cancer chemotherapy: synthesis, formulation, characterization and in vitro drug release. Biomaterials. 2006;27:262-70.
[78] Zhang Z, Lee SH, Gan CW, Feng SS. In vitro and in vivo investigation on PLA-TPGS nanoparticles for controlled and sustained small molecule chemotherapy. Pharmaceutical research. 2008;25:1925-35.
[79] Prashant C, Dipak M, Yang CT, Chuang KH, Jun D, Feng SS. Superparamagnetic iron oxide--loaded poly(lactic acid)-D-alpha-tocopherol polyethylene glycol 1000 succinate copolymer nanoparticles as MRI contrast agent. Biomaterials. 2010;31:5588-97.
[80] Huang Y, Lu J, Gao X, Li J, Zhao W, Sun M, et al. PEG-derivatized embelin as a dual functional carrier for the delivery of paclitaxel. Bioconjugate chemistry. 2012;23:1443-51.
[81] Nikolovska-Coleska Z, Xu L, Hu Z, Tomita Y, Li P, Roller PP, et al. Discovery of embelin as a cell-permeable, small-molecular weight inhibitor of XIAP through structure-based computational screening of a traditional herbal medicine three-dimensional structure database. Journal of medicinal chemistry. 2004;47:2430-40.
[82] Kloog Y, Cox AD. RAS inhibitors: potential for cancer therapeutics. Molecular medicine today. 2000;6:398-402.

[83] Blum R, Kloog Y. Tailoring Ras-pathway--inhibitor combinations for cancer therapy. Drug resistance updates : reviews and commentaries in antimicrobial and anticancer chemotherapy. 2005;8:369-80.
[84] Paz A, Haklai R, Elad-Sfadia G, Ballan E, Kloog Y. Galectin-1 binds oncogenic H-Ras to mediate Ras membrane anchorage and cell transformation. Oncogene. 2001;20:7486-93.
[85] Marom M, Haklai R, Ben-Baruch G, Marciano D, Egozi Y, Kloog Y. Selective inhibition of Ras-dependent cell growth by farnesylthiosalisylic acid. The Journal of biological chemistry. 1995;270:22263-70.
[86] Reul R, Nguyen J, Kissel T. Amine-modified hyperbranched polyesters as non-toxic, biodegradable gene delivery systems. Biomaterials. 2009;30:5815-24.
[87] Haklai R, Elad-Sfadia G, Egozi Y, Kloog Y. Orally administered FTS (salirasib) inhibits human pancreatic tumor growth in nude mice. Cancer chemotherapy and pharmacology. 2008;61:89-96.
[88] Maeda H. The enhanced permeability and retention (EPR) effect in tumor vasculature: the key role of tumor-selective macromolecular drug targeting. Advances in enzyme regulation. 2001;41:189-207.
[89] Jain RK. Vascular and interstitial barriers to delivery of therapeutic agents in tumors. Cancer metastasis reviews. 1990;9:253-66.
[90] Clarke HC, Kocher HM, Khwaja A, Kloog Y, Cook HT, Hendry BM. Ras antagonist farnesylthiosalicylic acid (FTS) reduces glomerular cellular proliferation and macrophage number in rat thy-1 nephritis. Journal of the American Society of Nephrology : JASN. 2003;14:848-54.
[91] Weisz B, Giehl K, Gana-Weisz M, Egozi Y, Ben-Baruch G, Marciano D, et al. A new functional Ras antagonist inhibits human pancreatic tumor growth in nude mice. Oncogene. 1999;18:2579-88.
[92] Kumar N. Taxol-induced polymerization of purified tubulin. Mechanism of action. The Journal of biological chemistry. 1981;256:10435-41.
[93] Weiss RB, Donehower RC, Wiernik PH, Ohnuma T, Gralla RJ, Trump DL, et al. Hypersensitivity reactions from taxol. Journal of clinical oncology : official journal of the American Society of Clinical Oncology. 1990;8:1263-8.
[94] Nishiyama N, Kataoka K. Current state, achievements, and future prospects of polymeric micelles as nanocarriers for drug and gene delivery. Pharmacology & therapeutics. 2006;112:630-48.
[95] Kataoka K, Harada A, Nagasaki Y. Block copolymer micelles for drug delivery: design, characterization and biological significance. Advanced drug delivery reviews. 2001;47:113-31.
[96] Perrault SD, Walkey C, Jennings T, Fischer HC, Chan WC. Mediating tumor targeting efficiency of nanoparticles through design. Nano letters. 2009;9:1909-15.
[97] Zhang X, Huang Y, Li S. Nanomicellar carriers for targeted delivery of anticancer agents. Therapeutic delivery. 2014;5:53-68.
[98] Bourzac K. Nanotechnology: Carrying drugs. Nature. 2012;491:S58-60.
[99] Mor A, Aizman E, Chapman J, Kloog Y. Immunomodulatory properties of farnesoids: the new steroids? Current medicinal chemistry. 2013;20:1218-24.
[100] Lu J, Huang Y, Zhao W, Chen Y, Li J, Gao X, et al. Design and characterization of PEG-derivatized vitamin E as a nanomicellar formulation for delivery of paclitaxel. Molecular pharmaceutics. 2013;10:2880-90.

[101] Wang J, Sun J, Chen Q, Gao Y, Li L, Li H, et al. Star-shape copolymer of lysine-linked di-tocopherol polyethylene glycol 2000 succinate for doxorubicin delivery with reversal of multidrug resistance. Biomaterials. 2012;33:6877-88.
[102] Lu J, Huang Y, Zhao W, Marquez RT, Meng X, Li J, et al. PEG-derivatized embelin as a nanomicellar carrier for delivery of paclitaxel to breast and prostate cancers. Biomaterials. 2013;34:1591-600.
[103] Marciano D, Ben-Baruch G, Marom M, Egozi Y, Haklai R, Kloog Y. Farnesyl derivatives of rigid carboxylic acids-inhibitors of ras-dependent cell growth. Journal of medicinal chemistry. 1995;38:1267-72.
[104] Baines AT, Xu D, Der CJ. Inhibition of Ras for cancer treatment: the search continues. Future medicinal chemistry. 2011;3:1787-808.
[105] Xiao K, Li Y, Luo J, Lee JS, Xiao W, Gonik AM, et al. The effect of surface charge on in vivo biodistribution of PEG-oligocholic acid based micellar nanoparticles. Biomaterials. 2011;32:3435-46.
[106] Dreher MR, Liu W, Michelich CR, Dewhirst MW, Yuan F, Chilkoti A. Tumor vascular permeability, accumulation, and penetration of macromolecular drug carriers. Journal of the National Cancer Institute. 2006;98:335-44.
[107] Serajuddin AT. Salt formation to improve drug solubility. Advanced drug delivery reviews. 2007;59:603-16.
[108] El-Rayes BF, Ibrahim D, Shields AF, LoRusso PM, Zalupski MM, Philip PA. Phase I study of liposomal doxorubicin (Doxil) and cyclophosphamide in solid tumors. Investigational new drugs. 2005;23:57-62.
[109] Lukyanov AN, Torchilin VP. Micelles from lipid derivatives of water-soluble polymers as delivery systems for poorly soluble drugs. Advanced drug delivery reviews. 2004;56:1273-89.
[110] Lee SY, Kim S, Tyler JY, Park K, Cheng JX. Blood-stable, tumor-adaptable disulfide bonded mPEG-(Cys)4-PDLLA micelles for chemotherapy. Biomaterials. 2013;34:552-61.
[111] Bae Y, Kataoka K. Intelligent polymeric micelles from functional poly(ethylene glycol)-poly(amino acid) block copolymers. Advanced drug delivery reviews. 2009;61:768-84.
[112] Zhang X, Liu K, Huang Y, Xu J, Li J, Ma X, et al. Reduction-Sensitive Dual Functional Nanomicelles for Improved Delivery of Paclitaxel. Bioconjugate chemistry. 2014.
[113] Zhang X, Huang Y, Zhao W, Chen Y, Zhang P, Li J, et al. PEG-Farnesyl Thiosalicylic Acid Telodendrimer Micelles as an Improved Formulation for Targeted Delivery of Paclitaxel. Molecular pharmaceutics. 2014;11:2807-14.
[114] Downward J. Targeting RAS signalling pathways in cancer therapy. Nature reviews Cancer. 2003;3:11-22.
[115] Asher WM, Parvin S, Virgillo RW, Haber K. Echographic evaluation of splenic injury after blunt trauma. Radiology. 1976;118:411-5.
[116] Huh KM, Lee SC, Cho YW, Lee J, Jeong JH, Park K. Hydrotropic polymer micelle system for delivery of paclitaxel. Journal of controlled release : official journal of the Controlled Release Society. 2005;101:59-68.
[117] Saravanakumar G, Min KH, Min DS, Kim AY, Lee CM, Cho YW, et al. Hydrotropic oligomer-conjugated glycol chitosan as a carrier of paclitaxel: synthesis, characterization, and in vivo biodistribution. Journal of controlled release : official journal of the Controlled Release Society. 2009;140:210-7.

[118] Zhang P, Lu J, Huang Y, Zhao W, Zhang Y, Zhang X, et al. Design and evaluation of a PEGylated lipopeptide equipped with drug-interactive motifs as an improved drug carrier. The AAPS journal. 2014;16:114-24.
[119] La SB, Okano T, Kataoka K. Preparation and characterization of the micelle-forming polymeric drug indomethacin-incorporated poly(ethylene oxide)-poly(beta-benzyl L-aspartate) block copolymer micelles. Journal of pharmaceutical sciences. 1996;85:85-90.
[120] Xiong XB, Huang Y, Lu WL, Zhang X, Zhang H, Nagai T, et al. Enhanced intracellular delivery and improved antitumor efficacy of doxorubicin by sterically stabilized liposomes modified with a synthetic RGD mimetic. Journal of controlled release : official journal of the Controlled Release Society. 2005;107:262-75.
[121] Goldberg L, Haklai R, Bauer V, Heiss A, Kloog Y. New derivatives of farnesylthiosalicylic acid (salirasib) for cancer treatment: farnesylthiosalicylamide inhibits tumor growth in nude mice models. Journal of medicinal chemistry. 2009;52:197-205.
[122] McCarley RL. Redox-responsive delivery systems. Annual review of analytical chemistry. 2012;5:391-411.
[123] Saito G, Swanson JA, Lee KD. Drug delivery strategy utilizing conjugation via reversible disulfide linkages: role and site of cellular reducing activities. Advanced drug delivery reviews. 2003;55:199-215.
[124] Meng F, Hennink WE, Zhong Z. Reduction-sensitive polymers and bioconjugates for biomedical applications. Biomaterials. 2009;30:2180-98.
[125] Li Y, Xiao K, Luo J, Xiao W, Lee JS, Gonik AM, et al. Well-defined, reversible disulfide cross-linked micelles for on-demand paclitaxel delivery. Biomaterials. 2011;32:6633-45.
[126] Wang H, Tang L, Tu C, Song Z, Yin Q, Yin L, et al. Redox-responsive, core-cross-linked micelles capable of on-demand, concurrent drug release and structure disassembly. Biomacromolecules. 2013;14:3706-12.
[127] Koo AN, Min KH, Lee HJ, Lee SU, Kim K, Kwon IC, et al. Tumor accumulation and antitumor efficacy of docetaxel-loaded core-shell-corona micelles with shell-specific redox-responsive cross-links. Biomaterials. 2012;33:1489-99.
[128] Lee SY, Tyler JY, Kim S, Park K, Cheng JX. FRET Imaging Reveals Different Cellular Entry Routes of Self-Assembled and Disulfide Bonded Polymeric Micelles. Molecular pharmaceutics. 2013;10:3497-506.
[129] Zhang MZ, Ishii A, Nishiyama N, Matsumoto S, Ishii T, Yamasaki Y, et al. PEGylated Calcium Phosphate Nanocomposites as Smart Environment-Sensitive Carriers for siRNA Delivery. Adv Mater. 2009;21:3520-+.
[130] Zhao M, He P, Xu L, Hidalgo M, Laheru D, Rudek MA. Determination of salirasib (S-trans,trans-farnesylthiosalicylic acid) in human plasma using liquid chromatography-tandem mass spectrometry. Journal of chromatography B, Analytical technologies in the biomedical and life sciences. 2008;869:142-5.
[131] Yokoyama M. Block copolymers as drug carriers. Critical reviews in therapeutic drug carrier systems. 1992;9:213-48.